New Approach in Prediction of Soil Liquefaction

To the Faculty of Geosciences, Geo-Engineering and Mining
of the Technische Universität Bergakademie Freiberg
approved

THESIS

to attain the academic degree of
Doktor-Ingenieur
Dr.-Ing.

submitted

by M.Sc. Abbas Daftari

born on the 1982 in Ghaemshahr, Iran.

Reviewers: Prof. Dr.-Ing. Wolfram Kudla, TU Freiberg.
Prof. Dr. Ing. Stravros Savidis, TU Berlin.
Prof. Dr. Ing. habil. Heinz Konietzky, TU Freiberg.

Date of the award 23.11.2015

Abstract

Liquefaction is the phenomena when there is loss of strength in saturated and cohesion-less soils because of increased pore water pressures and hence reduced effective stresses due to dynamic loading. It is a phenomenon in which the strength and stiffness of a soil is reduced by earthquake shaking or other rapid loading.

In this study, after the short review of liquefaction definition, the models of prediction and estimation of liquefaction were considered. Application of numerical modelling with two major software (FLAC & PLAXIS) for the Wildlife site liquefaction, under superstition earthquake in 1987 were compared and analysed.

Third step was started with introduction of Fuzzy logic and neural network as two common intelligent mathematical methods. These two patterns for prediction of soil liquefaction were combined. The "Neural network- Fuzzy logic-Liquefaction- Prediction" (NFLP) was applied for liquefaction prediction in Wildlife site. The results show the powerful prediction of liquefaction happening with high degree of accuracy in this case.

Keywords: Liquefaction, Numerical modelling, Finn-Byrne, UBC3D-PLM, Neural network, Fuzzy logic

Acknowlwdgments

First of all, I wish to express my deep gratitude to my supervisor "**Prof. Dr. Ing. Wolfram Kudla**" for the support and the encouragement provided during the period of my research work. I would like also to thank him for the opportunity he gave me to work together with the Mining and special underground structure Engineering institute of the department of Geotechnics and mining Engineering, mining technical University of Freiberg.

I sincerely wish to express my deep appreciation to members of Mining and special underground structure Engineering institute special "**Dr. Ing. Sebastian Szczyrba**" for their brotherly and useful suggestions, comments during this research.

I want to thank my parents who provided the best environment growing up, provided encouragement throughout my education.

Appreciation is expressed to my beautiful wife, "**Aida**". I would have been impossible to complete this work without her love, understanding, patience and sacrifices.

I also want to thank my family and friends for their support and motivation.

Table of Contents

Chapter 1. Introduction

List of Figures

List of tables

1. Overview

In this chapter the liquefaction phenomena will be introduced. After that, the kind of liquefaction will be considered. In continue the modelling of liquefaction will be presented and the difference process of them will become clear. Simultaneously literatures review investigates the results and methodologies of papers and researches which presented liquefaction modelling briefly. In this chapter overall structure of this thesis will be noted.

2. Introduction of Liquefaction Phenomenon

Liquefaction is one of the significant, remarkable, and complex themes in geotechnical earthquake engineering. Liquefaction induced failure has been and continues to be a major cause of destruction during earthquakes. The direct and indirect costs related with ground failure may far exceed the damage caused by other type of failures such as structural collapses. Its devastating effects sprang to the attention of geotechnical engineering in 1964 when the Alaska earthquake was followed by the Niigata earthquake in Japan (Figure 1.1). Both earthquakes produced severe damage to buildings, foundation of structures and natural slopes due to liquefaction. After that soil liquefaction has been received lot of considerations and the corresponding technologies to analyze and prevent liquefaction have significantly improved over the years. A qualitative understanding of sand liquefaction and its effects under cyclic loading was first presented by Casagrande (Casagrande, 1936). The term liquefaction was originally coined by Mogami and Kubo (Mogami & Kubo, 1953). The cause of liquefaction of sands has been understood for many years. A more specific definition of soil liquefaction is given by Sladen et al:

> "Liquefaction is a phenomenon wherein a mass of soil lose a large percentage of its shear resistance, when subjected to monotonic, cyclic, or shock loading, and flows in a manner resembling a liquid until the shear stresses acting on the mass are as low as the reduced shear resistance (Sladen et al, 1985)".

The one of newest definition has presented with Idriss and Boulanger:

> "Loose cohesionless soils tend to contract during cyclic loading, which can transfer normal stress from the soil skeleton to pore water, if the soil is saturated and largely unable to drain during shaking. The result is a reduction in effective confining stress within the soil and an associated loss of strength and stiffness that contributes to deformations of the soil deposit. This loss of strength and stiffness due to increasing pore pressures is called liquefaction (Idriss & Boulanger, 2008)."

Following the principle of effective stress states, effective stress equals to total stress minus the pore water pressure:

$$\sigma' = \sigma - u \tag{1-1}$$

σ' = effective stress
σ = total stress
u = pore water pressure

If the quantity of σ remains constant, as the pore water pressure u slowly increases, the effective stress σ' gradually decreased. If the pore water pressure builds up to the point at which it is equal to the total stress, the effective stress becomes zero. As the stiffness and strength of a soil depends on the magnitude of effective stress, the soil loses its strength completely when the effective stress becomes zero and the soil is in a liquefaction state (Seed & Lee, 1966).

The term of liquefaction has actually been used to describe some related phenomena. Because the phenomena can have similar effects, it can be problematic to distinguish between them. However the mechanisms causing them are different. Figure 1.2 shows intergranular contact before and after liquefaction. These phenomena can be divided into two main categories: flow liquefaction and cyclic mobility.

Figure 1.1 Tilting of Apartment Buildings at Kawagishi-Cho, Produced by 1964 Niigata Earthquake (www.ce.washington.edu)

2.1. Flow Liquefaction

Flow liquefaction can occur when the shear stress required for static equilibrium of a soil mass is greater than the shear strength of the soil in its liquefaction state. Once triggered, the large deformations produced by flow liquefaction are actually driven by static shear stresses. In contrast to flow liquefaction, cyclic mobility occurs when static shear stress is less than the shear strength of the liquefaction soil. The deformation produced by cyclic mobility failures develop incrementally during earthquake shaking (Kramer, 1995). Failures caused by flow liquefaction are often characterized by large and rapid movements which can produce the type of disastrous effects. In figure 1.3 these kind of liquefaction has been presented.

2.2 Cyclic mobility

Cyclic mobility is a liquefaction occurrence, generated by cyclic loading, occurring in soil deposits with static shear stresses lower than the soil strength. Deformations due to cyclic mobility develop incrementally because of static and dynamic stresses that exist during an earthquake. Lateral spreading, a common result of cyclic mobility, can occur on gently sloping and on flat ground close to rivers and lakes (Figure 1.4).

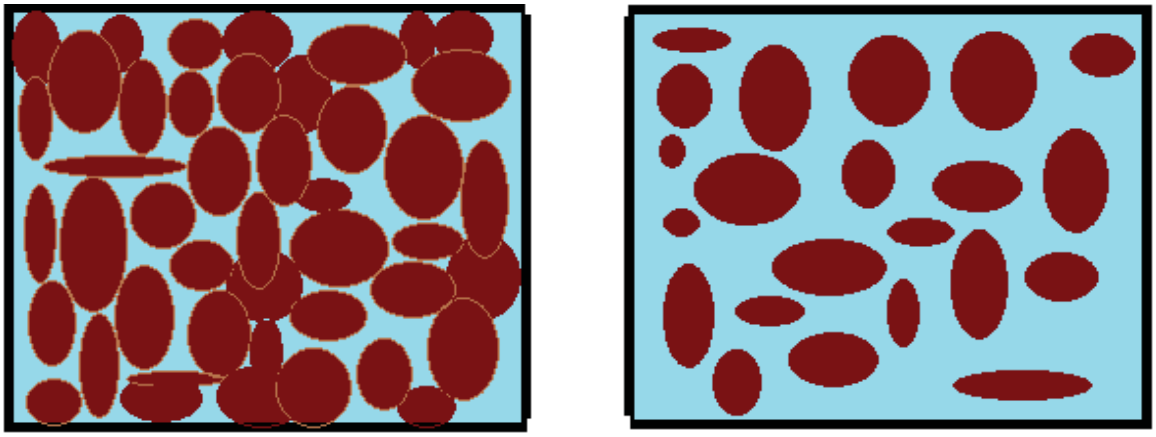

Soil grains before liquefaction Soil grains after liquefaction

Figure 1.2 Intergranular contacts before and after liquefaction

As mentioned before, these two kinds of liquefaction have similar effects in the field; the term liquefaction will be taken to include both flow liquefaction and cyclic mobility in this dissertation. In figure 1.5, the differences between cyclic mobility and flow liquefaction‘s reaction under shear loading has been illustrated.

(a) (b)

Figure 1.3 Flow Liquefaction damage. (www.ce.washington.edu)

a: Alaska Earthquake, 1964, b: Santa Barbara Earthquake, 1925.

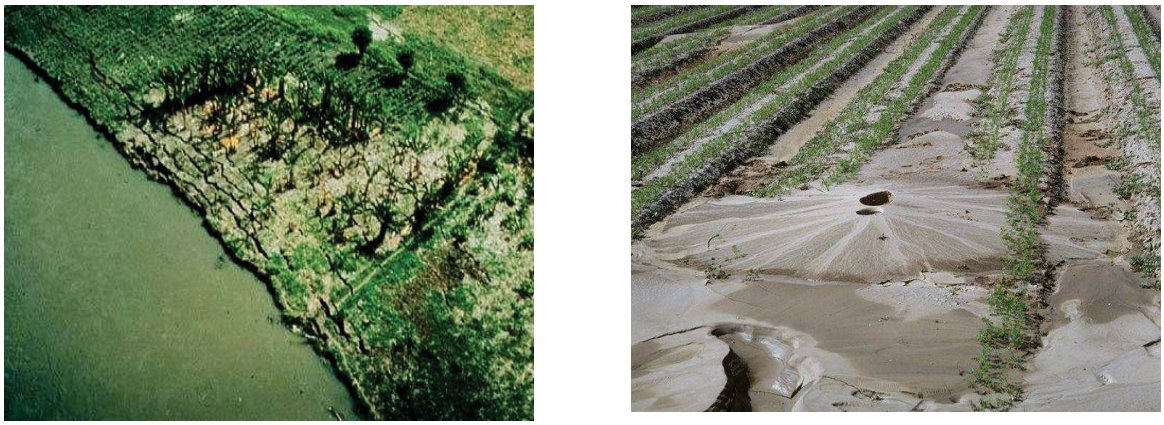

(a) (b)

Figure 1.4 Liquefaction damage from cyclic mobility. (www.ce.washington.edu)

a: Guatemala earthquake 1976. b: El Centro earthquake 1979.

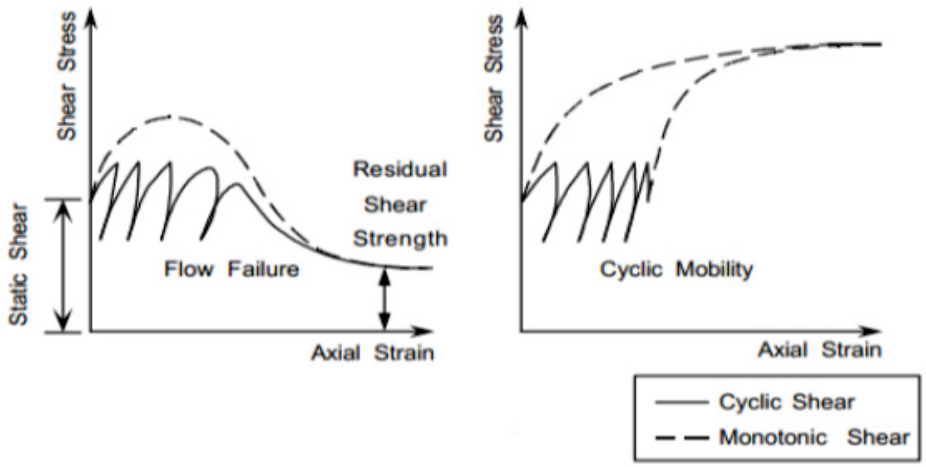

Figure 1.5 Reaction of soils under shear loading in cyclic mobility and flow liquefaction (Rauch, 1997)

3. Method in evaluating liquefaction potential of soils

Many researchers have shown that loose sandy soil is susceptible to liquefaction (Kramer, 1996; Youd et. al., 2001; Groot et. al., 2006). Many factors related to the property of the soil can influence liquefaction potential. In fact, these phenomena determined by a combination of soil properties, Geological and historical factors and characteristics of the loading (cyclic such as earthquake). Some of the main factors include the following:

Soil properties:

Dynamic shear modulus,

Damping characteristic,

Unit weight,

Grain size characteristics,

Relative density,

Soil structure,

Geological and historical factors:

Method of soil formation,
Aging and Cementation,
Lateral earth pressure coefficient,
Depth of water table,
Effective confining pressure,
Rate of Saturation,
Anisotropy,

Loading characteristics:

Frequency and amplitude of ground loading (shaking),
Duration of ground waving (shaking).

Some of these factors cannot be determined directly, but their effects can be included in the evaluation procedure by performing cyclic loading tests on undisturbed samples or by measuring the liquefaction characteristics of the soil by means of some in-situ tests.

Generally, 6 main groups have been presented for evaluation of soil liquefaction. These models will be investigated in the next sections. These methods are:

Field methods,
Laboratory methods,
Analytical methods,
Numerical methods,
Geographic information system (GIS) methods,
Intelligent mathematical methods (fuzzy logic, neural network, etc.).

3.1. Field methods

Using of insitu testing is the principal method in common engineering practice for assessable evaluation of liquefaction potential. Calculation of two variables is required for evaluation of liquefaction resistance of soils. They are as follows:

The cyclic demand on a soil layer, expressed in terms of CSR and
The capacity of the soil to resist liquefaction, expressed in terms of *CRR*.

The models proposed by Seed and Idriss (1971), Seed and Peacock (1971), Iwasaki (1978) and Robertson and Wride (1998) methods are extensively used for predicting liquefaction potential using field data. Youd et al. (2001) reviewed in detail the available field methods available for the evaluation of liquefaction potential of soils.

3.1.1. SPT based methods

Standard penetration test is widely used as an economical, quick and convenient method for investigating the penetration resistance of non-cohesive soils. This test is an indirect means to obtain important design parameters for non-cohesive soils. The typical SPT dimension tool has been illustrated in figure 1.6. The count is normalized to an over burden pressure of approximately 100KPa and hammer energy ration or hammer efficiency of 60%. If the sample has a fine content more than 5%, $(N1)_{60}$ should be corrected for the influence of fines content. Correlation of $(N1)_{60}$ to an equivalent clean sand value, $(N1)_{60cs}$ according to Youd and Idriss, (2001) is given by:

$$(N_1)_{60cs} = \alpha + \beta(N_1)_{60} \quad (1\text{-}2)$$

$\alpha = 0$ for $FC \leq 5\%$
$\alpha = \text{Exp}\,(1.76-(190/FC^2))$ for $5\% < FC < 35\%$
$\alpha = 5$ for $FC \geq 35\%$

$\beta = 1$ for $FC \leq 5\%$

$\beta = (0.99 + (FC1.5/1000))$ for $5\% < FC < 35\%$

$\beta = 1.2$ for $FC \geq 35\%$

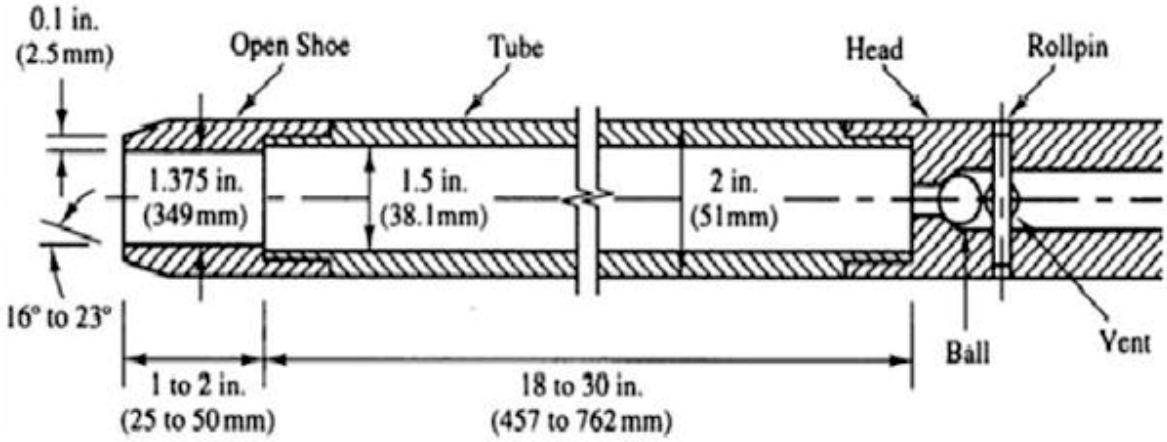

Figure 1.6 Typical SPT dimension (www.eeg.geoscienceworld.org)

3.1.1.1. Seed and Idriss method

The initial approach for estimating behavior of soils in the field during dynamic loading was developed by Seed and Idriss (1971). The process is referred to as the simplified procedure, and involves the comparison of the seismic stresses imparted onto a soil mass during an earthquake (Cyclic Stress Ratio, CSR) to the resistance of the soil to large magnitude strain and strength loss (Cyclic Resistance Ratio, CRR). The CSR estimation is based on the estimated ground accelerations produced by an earthquake, the stress conditions present in the soil, and correction factors accounting for the flexibility of the soil mass (Youd & Idriss 1997). Seed and Idriss developed this empirical method by combining the data on earthquake characteristics and in-situ properties of soil deposits, which is widely used all over the world for the assessment of liquefaction hazard (Figure 1.7).

3.1.1.2. Seed and Peacock method

In the Seed and Peacock (1971) method, the average shear stress τ_{av} will be calculated same as in Seed and Idriss method. Using corrected SPT 'N' value and the proposed chart by Seed and

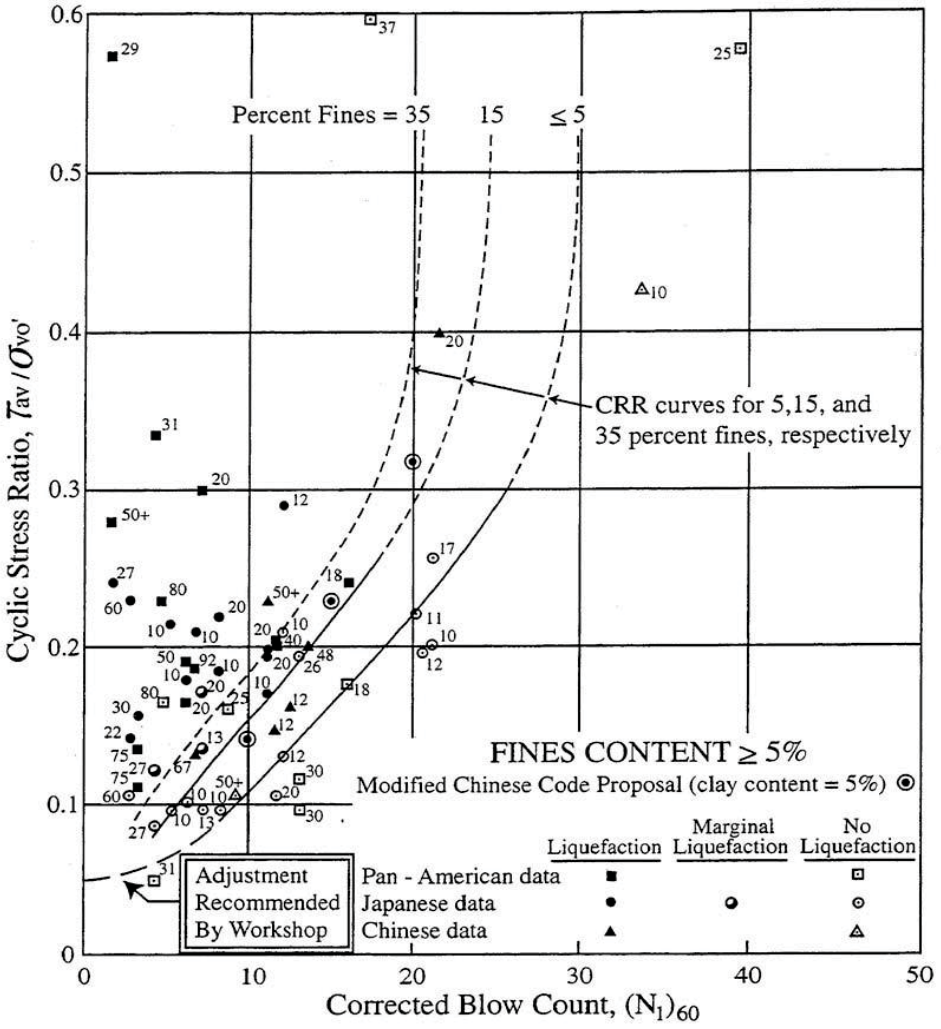

Figure 1.7 Curves recommended for calculation of CRR from SPT data

(Youd & Idriss, 1997; Youd et al., 2001)

Peacock, τ_Z can be calculated at the chosen depth of the soil strata. If $\tau_{av} > \tau_Z$ then soil will liquefy at that zone.

3.1.1.3. Iwasaki et al. method

Iwasaki et al. (1982) proposed a simple geotechnical method as in the Japanese Bridge Code. In this method, soil liquefaction capability factor R, is calculated along with a dynamic load L, and induced in a soil element by the seismic motion. The ratio of both is defined as 'liquefaction resistance'. The soil liquefaction capacity is designed by the three factors:

Account the overburden pressure,
Grain size,
Fine content.

In this method it is presumed that the severity of liquefaction should be relative to the thickness of the liquefied layer, closeness of the liquefied layer to the surface, and the factor of safety of the liquefied layer (Figure 1.8).

3.1.2. CPT based methods

The CPT -Cone Penetration Test- gains improvement over SPT for its easiness, repeatability, truthfulness and continuous record. Using electronic transducers, it's possible to record real time measurement of cone resistance (q_c), sleeve friction (f_s), and pore pressure (u) during penetration of the probe. Having a continuous soil profile allows for a more detailed definition of soil layer (Figure 1.9).

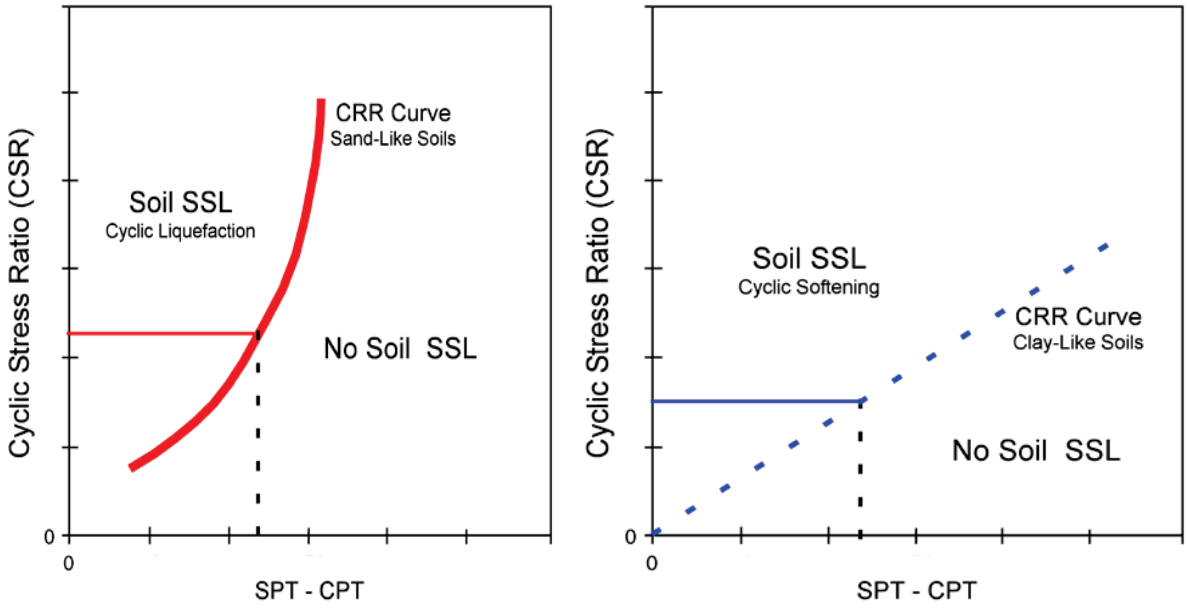

CRR curve sand-like soils CRR curve clay-like soils

Figure 1.8 Typical CRR curve (Geotechnical seismic hazards, 2010)

3.1.2.1. Robertson and Wride method

A method to evaluation cyclic shear resistance (CSR) was developed by Seed and Idriss (1971) based on maximum ground acceleration at the site as under:

$$CSR = \tau_{av} / \sigma_{o'} = 0.65\ (MWF)\ (\sigma_o / \sigma_{o'})\ (a_{max} / g)\ r_d \quad (1\text{-}3)$$

$$MWF = (M)^{2.56} / 173 \quad (1\text{-}4)$$

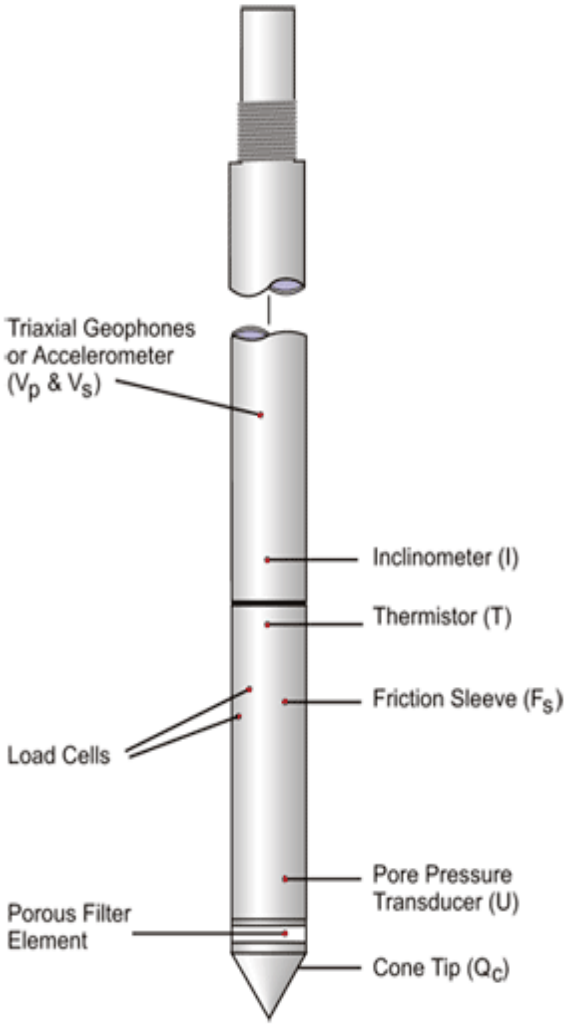

Figure 1.9 Typical CPT equipment (www.eeg.geoscienceworld.org)

Where:

MWF: the magnitude weighting factor.

M: the earthquake magnitude (M = 7.5).

r_d: the shear stress reduction factor.

a_{max}: peak ground acceleration.

g: gravity of earth.

Seed et al. (1985) also developed a method to estimate the cyclic resistance ratio (CRR) for clean sands and silty sands based on the CPT using normalized penetration resistance. The cone penetration resistance q_c can be normalized as:

$$q_{c1N} = C_q (q_c / p_a) \quad (1\text{-}5)$$

$$c_q = (p_a / \sigma_o')^n \quad (1\text{-}6)$$

c_q: normalized factor for cone penetration resistance.
p_a: atmosphere of pressure.
n: an exponent that varies with soil type (= 0.5 for sands and 1 for clays).
q_c: field cone penetration resistance.
σ_o': effective overburden stress.

The normalized penetration resistance (q_{c1N}) for silty sands is corrected to an equivalent clean sand value $(q_{c1N})_{CS}$ as:

$$(q_{c1N})_{CS} = K_C \, q_{c1N} \quad (1\text{-}7)$$

K_C: correction factor for grain characteristic.

K_C is defined as below by Robertson and Wride (1998):

$$K_C = 1.0 \qquad \text{for } I_C \leq 1.64 \quad (1\text{-}8)$$

$$K_C = -0.403 I_C^4 + 5.581 I_C^3 - 21.63 I_C^2 + 33.75 I_C - 17.88 \qquad \text{for } I_C > 1.64 \quad (1\text{-}9)$$

If $I_C > 2.6$, the soil in this range are likely to clay rich or plastic to liquefy. I_C is the soil behavior type index and is calculated as:

$$I_C = [(3.47 - \log q)^2 + (1.22 + \log f)^2]^{0.5} \quad (1\text{-}10)$$

q: normalized penetration resistance.

$$q= [(q_c-\sigma_o)/p_a][\ p_a/\ \sigma_o\ ]^n \quad (1\text{-}11)$$

$$F = [f_s / (q_c- \sigma_o)]* 100 \quad (1\text{-}12)$$

f_s: being the sleeve friction stress.

$$CRR_{7.5} = 0.833[\frac{(qc\ 1N)\ cs}{1000}] +0.05 \quad \text{if } (q_{c1N})_{cs} <50 \quad (1\text{-}13)$$

$$CRR_{7.5} = 93[\frac{(qc\ 1N)\ cs}{1000}]^3 +0.08 \quad \text{if } 50 \leq (q_{c1N})_{cs} <160 \quad (1\text{-}14)$$

$(q_{c1N})_{cs}$: clean sand cone penetration resistance normalized to approximately 100 kPa .

Then, by using the equivalent clean sand normalized penetration resistance $(q_{c1N})cs$, CRR can be estimated from the Figure 1.10.

3.1.2.2. Other research

The CPT based liquefaction relationship was reevaluated by Idriss and Boulanger (2004) using case history data compiled by Shibata and Teparaksa (1988), Kayen et al. (1992), Boulanger (2003) and Moss (2003).

Moss (2003) has provided a most comprehensive compilation of field data and associated interpretations. He used friction ratio R_f instead of the parameter I_C, soil behavior type index and examined for the cohesion less soils with fines content greater than or equal to 35%.

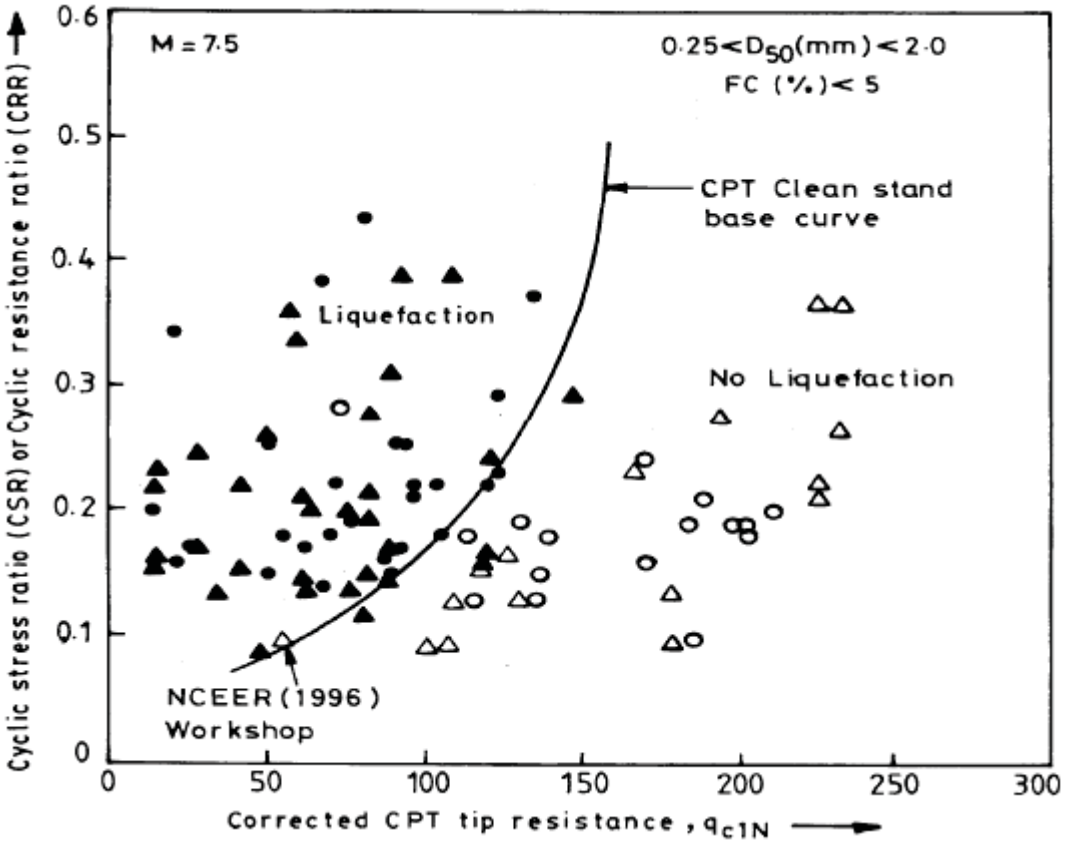

Figure 1.10 Calculation of CRR frome CPT q_{c1n} (Youd et al., 2001)

3.1.3. Shear wave velocity based methods

The shear wave velocity (v_s) based procedure has advanced significantly in recent years, with improved correlations and more databases as summarized by Andrus and Stokoe (2000). Shear wave velocity can be determined either by subsurface geophysical method or by surface geophysical method as explained earlier Liquefaction potential can be evaluated from the shear wave velocity (v_s) using the following three methods. These procedures can be useful particularly for sites where it is difficult to penetrate or sample soils.

3.1.3.1. Andrus and Stokoe method

Andrus and Stokoe have carried general research into the use of shear wave velocity as an index of liquefaction resistance. Several researchers have developed relationships between shear wave velocity and liquefaction resistance.

Andrus and Stokoe (2000) developed liquefaction resistance criteria from field measurements of shear wave velocity v_s. This method form the origin for the currently accepted shear wave velocity criteria for liquefaction potential assessment.

Shear wave velocity v_s is corrected similar to SPT 'N' value using the atmospheric pressure p_a and initial effective vertical stress, σ_o'. The cyclic resistance ratio (CRR) is determined empirically at different depths using the correlation developed between CRR and the shear wave velocity for the liquefaction assessment.

3.1.3.2. Hatanaka, Uchida and Ohara method

Hatanaka et al. (1997) made a systematic research relating the undrained cyclic shear strength of high quality undisturbed gravel samples to the shear wave velocity measured insitu v_{S1} is used for correcting the effect of effective confining stress on v_S by using the following equation.

$$v_{s1} = \frac{Vs}{\left(\frac{\sigma v'}{98}\right)3/8} \quad (1\text{-}15)$$

3.1.3.3. Tokimatsu, Yamazaki, and Yoshimi method

This method is proposed by Tokimatsu et al. (1986). The working principle in this procedure is that the liquefaction strength has a good correlation with elastic shear modulus for a given soil under a given confining pressure. Tsurumaki et al. (2003) verified the simplified procedure using new data

for different kinds of gravelly soils by undrained cyclic triaxial tests on undisturbed sample of gravelly soils obtained by the in-situ freezing sampling method.

3.2. Laboratory methods

3.2.1. Cyclic triaxial test

The cyclic triaxial test is the most commonly used test for the measurement of dynamic soil properties at high strain levels (Figure 1.11). This test simulates the liquefaction phenomenon during earthquakes by applying cyclic shear to the saturated sandy soil under undrained condition.

Seed and Lee (1966) were the first to reproduce liquefaction in a cyclic load triaxial test on loose and dense sands and concluded that liquefaction occurs more easily in sandy soils having higher void ratios and void ratio remaining constant, lower the effective confining pressure higher the liquefaction susceptibility. Numerous test results were reported by researchers, Lee and Seed (1967), Castro (1969), Castro and Poulos (1977), Castro et al. (1982), Seed (1983), Vaid and Chern

(1983), Mohamad and Dobry (1986), Vasquez-Herrera and Dobry (1989), Konrad and Wang (1993).

3.2.2. Cyclic direct simple shear test

The cyclic direct simple shear test is capable of reproducing earthquake stress conditions much more accurately than the cyclic triaxial test (Figure 1.12). It is most commonly used for liquefaction testing. In this test, a short cylindrical specimen is restrained against lateral expansion by rigid boundary platens, a wire reinforced membrane or with a series of stacked rings. By applying cyclic horizontal shear stresses to the top or bottom of the specimen, the test sample is deformed in the same way as an element of soil subjected to vertically propagating S waves.

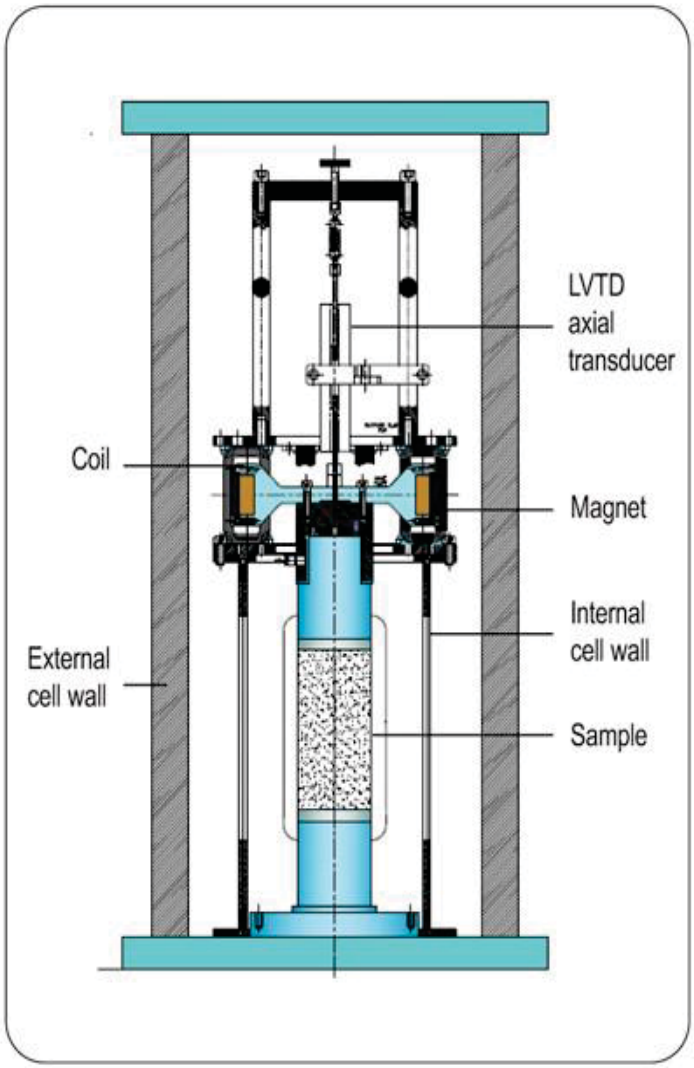

Figure 1.11 Typical cyclic triaxial test equipment (www.onlinemanuals.txdot.gov)

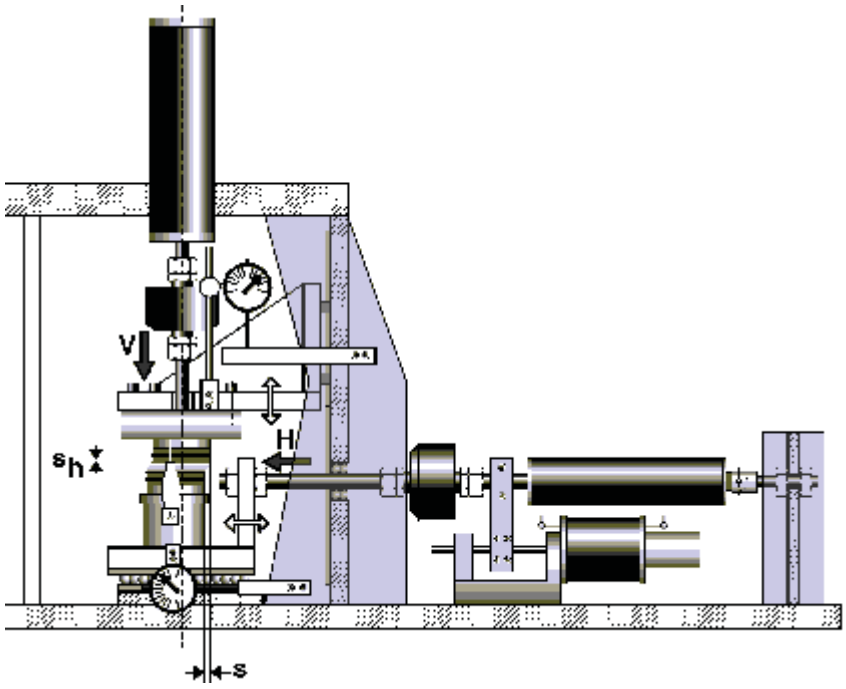

Figure 1.12 Typical Cyclic direct simple shear test equipment (www.ucl-sites.uclouvain.be)

Recognizing the difference between field and lab conditions, Peacoch and Seed (1968) used cyclic simple shear tests to study liquefaction problems. Subsequently, Seed and Peacoch (1971), Finn (1971, 1985), Pickering (1973), Martin et al. (1975) performed considerable cyclic simple shear tests to study liquefaction problem.

In recent years, simple shear devices that allow independent control of vertical and horizontal stresses have been developed. By the way, to better simulate actual earthquake conditions, Pyke (1979) used a large-scale simple shear apparatus.

3.2.3. Centrifuge modeling

The other type of laboratory test is model test. Model test usually attempt to reproduce the boundary condition and material property in the field by a small-scale physical model. It may be used to

evaluate the performance of a prototype or verify predictive theories. Model test is a useful method for studying dynamic behavior of earth structure and foundation.

The idea of performing experiments on small scale models in the centrifuge may have been presented for the first time in 1869 by E. Philips, in France. Centrifuge modeling of seismically-induced liquefaction, started at Cambridge University in England in the late 1970s, has proven to be a particularly useful tool in that respect.

A centrifuge is any device that spins and generates centrifugal forces to achieve some practical purpose. It produces what is essentially an artificial gravitational field that is higher than the earth's lg field. In geotechnical centrifuge, one small-scale soil or soil-structure model has subjected to a centrifugal acceleration typically somewhere between 30g and 200g (figure 1.13).

Unfortunately, if researchers make small-scale model of a system using the same soil as in the prototype, the confining stresses will be too small and the stress-strain behavior of the model will be quite different from that of the real system. To get the stresses back up to their correct values, they increase the g-level by putting the model on a centrifuge (Figure 1.14).

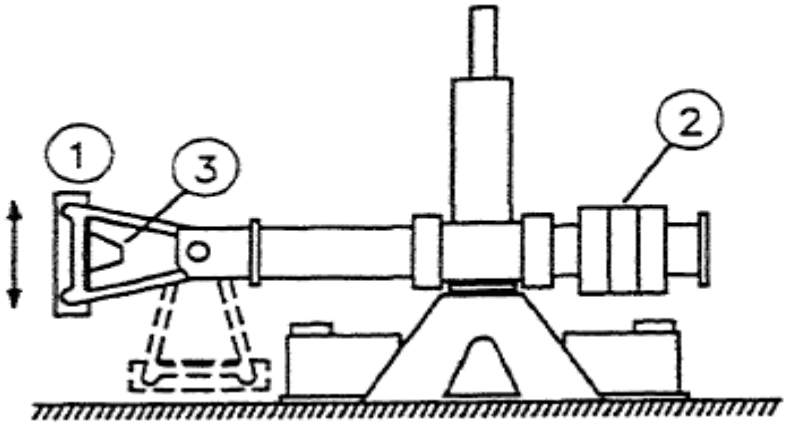

Figure 1.13 Sketch of RPI geotechnical centrifuge (www.homepages.rpi.edu)
(1. Platform, 2. Counterweights, 3. Model)

Figure 1.14 centrifuge device (www.gsl.erdc.usace.army.mil)

3.2.4. Shake table test

Shake table tests of many sizes are being used for liquefaction studies on saturated soil samples prepared in a container, fixed to a shaking platform and vibrated at the desired frequency for a prescribed time (Figure 1.15). A surcharge is placed on the sample to provide the confining pressure. The measurements of acceleration pore water pressure and settlements are made during the test. Shaking tables utilize a single horizontal translation degree of freedom, but shake table with multiple degrees of freedom have also been developed. Kokusho (1987) developed a numerical model based on shake table test.

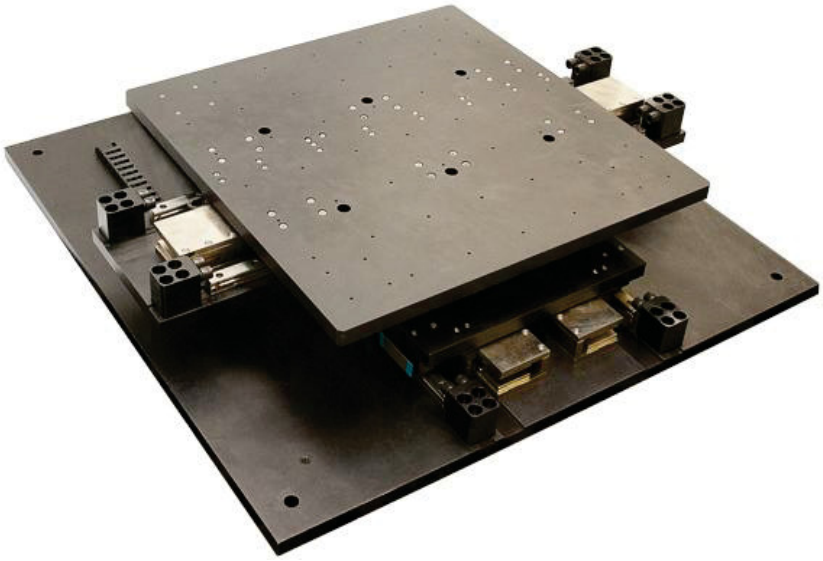

Figure 1.15 Normal shaking table equipment (www.quanser.blogspot.de)

3.3. Analytical methods

Several analytical approaches have been proposed to model liquefaction-induced ground deformation (Hamada, 1986; Youd & perkins, 1987; Yegian et al. 1991; Byrne 1991; Baziar et al. 1992; Bartlett & Youd, 1992-1995; Jibson 1994; Towhata et al. 1996-1997; Rauch, 1997; Youd et al., 1999). These analytical models are capable of explaining a few, but not all aspects of

liquefaction-induced deformations. Most analytical models require numerous parameters for predicting liquefaction-induced deformation, and are therefore impractical to apply over the large areas covered by lifeline networks. The empirical methods based on case histories of Liquefaction-induced deformation are alternate approaches readily applicable for assessing damage to lifeline networks after earthquakes.

3.3.1. Hamada et al. model

Hamada et al. (1986) calculate the amplitude of horizontal ground deformation only in terms of slope and thickness of liquefied layer:

$$D = 0.75H^{0.5}\theta^{0.33} \quad (1\text{-}17)$$

D: horizontal displacement (m).
θ: slope (%) of ground surface or base of liquefied soil.
H: thickness (m) of liquefied soil.

Base on equation 1-17 the Hamada model is only based on topographic and geotechnical parameters without any seismic parameters.

3.3.2. Youd & perkins model

The Liquefaction Severity Index (LSI) model (Youd & Perkins, 1987) has resemblances to attenuation curves for peak ground acceleration. It relates the amplitude of ground deformations, distance, and earthquake magnitude as follows:

$$\log LSI = 3.49 - 1.86 \log R + 0.98 M \quad (1\text{-}16)$$

LSI: general maximum amplitude of ground failure displacement (inch),

R: epicentered distance (km),

M: earthquake moment magnitude.

LSI cannot exceed 100 (Youd and Perkins 1987). Figure 1.16 compares the measured displacements and those calculated using Equation 1-16.

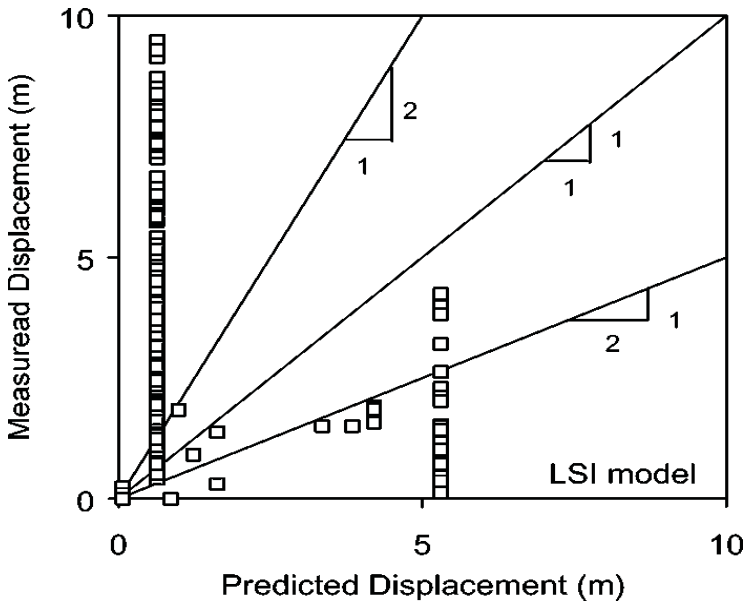

Figure 1.16 LSI model and measured versus predicted liquefaction induced lateral displacement (Bartlett & Youd ,1992)

3.3.3. Bartlett & Youd model

Bartlett and Youd (1992) proposed the following relation for predicting the amplitude of liquefaction-induced ground deformation:

$$\text{Log}(D+0.01) = b_0 + b_{off} + b_1 M + b_2 \log(R) + b_3 R + b_4 \log(W) + b_5 \log(S) + b_6 \log(T_{15}) + b_7 \log(100-F_{15}) + b_8 D50_{15} \quad (1\text{-}17)$$

D: horizontal displacement (m).

M: moment magnitude.

R: epicentered distance (km).

S: slope (%) of ground surface.

W: free-face ratio (%).

T_{15}: thickness (m) of saturated cohesionless soils.

F_{15}: average fine content (% finer than 75 μm).

$D50_{15}$: average D50 grain size (mm) in T_{15}.

The values of the ten constant coefficients b_0, b_{off}, and b_1 to b_8 are given in Table 1.1.

Table 1.1 Values of coefficients and adjusted R^2 (Bartlett and Youd, 1992)

Coefficient	**Original**	**F_{15}=13% $D50_{15}$=0.292 mm**
B_0	-15.787	-7.274
B_{off}	-0.579	-0.579
B_1	1.178	1.178
B_2	-0.927	-0.927
B_3	-0.013	-0.013
B_4	0.657	0.657
B_5	0.429	0.429
B_6	0.348	0.348
B_7	4.527	-
B_8	-0.922	-
R^2 adjusted	82.60%	61.00%
Number of data	467	467

3.4. Numerical methods

A numerical model is a mathematical simulation of a actual physical procedure. Not like to other engineering, in Geotechnical engineering it is not possible to choose a specific material type or geometry which one would like to work with. One has to face the fact that it is a must to work with what environment has to provide and make sure that it is well understood. For this reason it is wise to turn complex physical idea in to some mathematical systems and understand risk and uncertainties related.

Therefor it is the role of numerical modeling to assist researchers in developing correct mathematical concept and make it possible for them to base our design. The role of modeling in geotechnical engineering composed of three major components (Burland, 1987):

- Establishing the ground profile, insitu test and field measurement.
- Defining ground behavior, defining and describing the site condition.
- Modeling can be conceptual, analytical or physical and all are interlinked and supported by experience consisting of empiricism and precedent (Figure 1.17).

Normally, researchers are using the numeral modelling to analyze the problem. But for a comprehensive and a high level viewpoint the reason for modeling can be explained as:

- Make quantifiable estimates.
- Compare another possibility.
- Classify principal parameters.
- Understand physical procedure.

Researchers have presented several constitutive models for sand behaviors and soil liquefaction such as: FINN, UBCSAND, UBC3D-PLM, HYPOPLASTICITY, HYPERBOLIC and BOUNDING SURFACE models. Most of these models have been defined base on complicated

mathematic formulations. Although, these complex model could not satisfy the liquefaction process (Daftari & Kudla, 2014).

A constitutive model of a soil describes its stress-strain behavior. The stress-strain behavior of a soil depends on many factors such as the type of soil, stress-strain history, mode of deposition, anisotropy, and stress level dependency of stiffness (Brinkgreve, 2005; Schweiger, 2008).

Bounding surface plasticity was first developed for metals by Dafalias and Popov (1975). It was later applied to clays by Dafalias and Herrmann (1985), to pavement base materials by McVay and Taesiri (1985), to concrete by Yang et al. (1985), and to sands by Aboim and Roth (1982) and Bardet (1983, 1986a, 1986b, 1987).

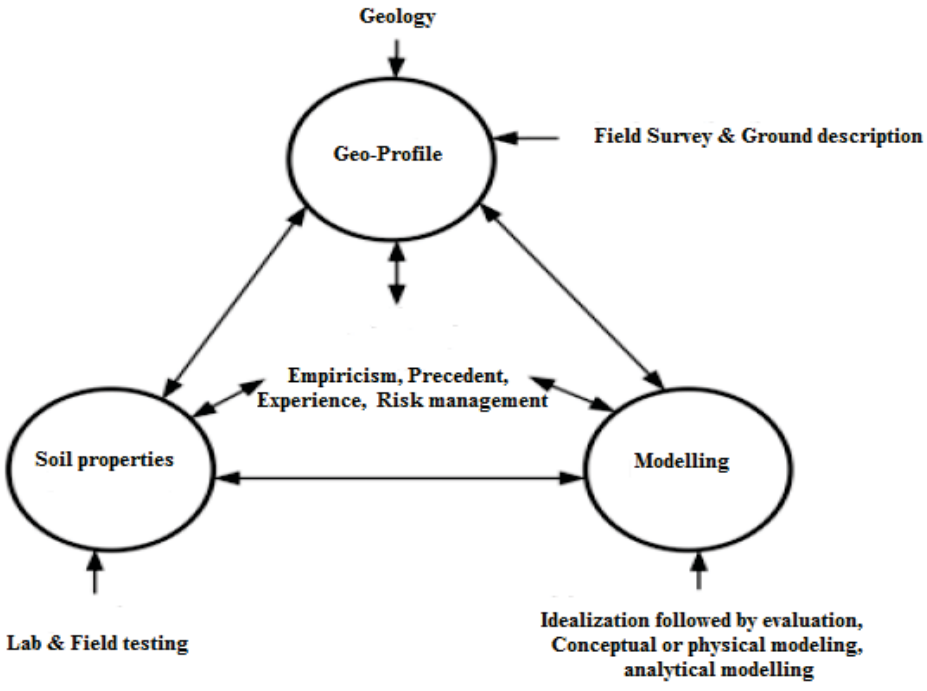

Figure 1.17 Expanded Burland triangle roles

Hashigushi (1980), independently, introduced the concept of bounding surface plasticity to obtain a continuous transition between elastic and elastoplastic responses. Dafalias (1986) coined the name of hypoplasticity to designate a particular type of bounding surface plasticity with a vanishing elastic domain (Bardet, 1990).

After that Kolymbas (1991) in University of Karlsruhe presented the outline of hypoplasticity model for sand. Then some researcher tried to develop and used this model for sand behavior (Wu & Bauer, 1994-1995; Kolymbas et al., 1996; Bauer, 1996; Gudehus, 1996; von Wolffersdorff, 1996). In next chapter FINN, UBCSAND and UBC3D-PLM models were complete explained.

3.5. GIS mapping methods

In liquefaction the failures took place due to liquefaction induced soil movement spread over few square km area continuously. Hence this is a problem where spatial variation involves and to represent this spatial variation Geographic Information System (GIS) is very useful in decision making about the area subjected to liquefaction.

Geographic Information System (GIS) is a computer based information system capable of capturing, storing, analyzing, and displaying geographically referenced information; data identified according to the location. The basic of this technique is classification and analysis of field geometries data, soil properties and other useful data in some maps and layers with using GIS software. For this reason this method is useful for special and individual case study.

For example some of these researches were listed:

- The Earthquake Hazard in Christchurch: A Detailed Evaluation (Elder et al., 1991),
- Geology of the Christchurch urban area (Brown & Weeber, 1992),
- Risks and Realities (Christchurch Engineering Lifelines Group, 1997),
- Liquefaction assessment of Waimakariri District (Beca, 2000),

- Liquefaction assessment of Christchurch City (Beca, 2002–2005),
- Earthquake hazard assessment for Selwyn District (Yetton & McCahon, 2006),
- Earthquake hazard assessment for Waimakariri District (Yetton & McCahon, 2009),
- Christchurch liquefaction studies update (Beca, 2012).

3.6. Intelligent mathematical methods

These methods present a powerful individual or hybrid intelligent system based on fuzzy logic, neural networks, genetic algorithms and other intelligent techniques. The correlation developed using straight methods are based on limited investigational data and do not provide stable and accurate predictions. The main disadvantage of these calculations is that they do not reproduce the complex structure of the soils and liquefaction. Whereas the soils have fairly complex structures, indefinite physical properties and spatial variability associated with the formation of them.

Therefore, their mechanical and dynamic characteristics exhibit the uncertain and spatial behavior in contrasts to most of the other engineering materials (Jaksa, 1995). The soft computing approaches such as GEP, Neural-network groups which allows developing spatially a model for the complex systems have recently emerged as promising approaches (Baykasoglu et al.,2008; Kayadelen, 2008; Kayadelen et al., 2009; Shahin et al., 2003; Tutmez & Tercan, 2007).

The probability of the liquefaction triggering was studied by Christian and Swiger (1975) using discriminant analysis with SPT data. Similar studies based on logistic regression, artificial neural networks (ANN) and Bayesian analysis were conducted by Youd and Gilstrap (1999), Juang et al. (2000) and Moss et al. (2003). Goh (1995) used back propagation neural network to develop the model for the liquefaction. Although the number of the data used in his study was limited.

The other basic of ‘soft computing’ is ‘fuzzy logic’, which is an estimated reasoning method to decrease with the uncertainties. This provides a systematic way of distributing with the inaccurate and ambiguous information on input data, their effects on the system, and the response of the

system (output). Fuzzy logic-based liquefaction models have been developed by various authors (Chen, 1997; Zahaby & Rahman, 1996). In chapter 3 basics and modeling of Neural-networks, Fuzzy logic and Hybrid of them were complete presented.

4. Organization of the Thesis

The thesis is organized into four chapters, as follows:

Chapter 1: Introduction of liquefaction and its types, consideration of previous liquefaction modelling and organization of the thesis.

Chapter 2: Explanation of 3 constitution models (FINN, UBCSAND and UBC3D-PLM), Information of case study (Wildlife site, California) and results of liquefaction modelling for case study.

Chapter 3: introduction of Neural-networks and Fuzzy logic, constructing and testing the liquefaction prediction engine base of Neural-networks and Fuzzy logic.

Chapter 4: Comparison of results, discussion and conclusion.

1. Overview

The significance of an accurate planned and executed experimental modelling has not been doubted. Nevertheless, experimental working can be expensive and time-consuming and normally used only for high-cost and high-risk projects. For regular projects, site investigation is doing in combination with laboratory testing to obtain soil parameters as accurate as possible. Then these parameters are used as input to either limit equilibrium based programs (slope stability, bearing capacity, etc.) to predict failure loads (ultimate limit state) or a numerical analysis program (finite element method, finite difference method, etc.) to predict the deformation under loading conditions (serviceability limit state).

This chapter will focus on two of the most popular numerical analysis technique used in geotechnical engineering, finite element method or FEM & Finite difference method or FDM). The emphasis of this chapter is on the application and not on the formulation of the FEM and FDM.

2. Introduction of numerical modelling

There are several different techniques of finding solutions to a geotechnical engineering problem. This section will focus on the numerical methods. One of the specific features of the numerical methods is that they usually involve solving a set of simultaneous partial differential equations (PDEs). Since soil is essentially a non-linear elasto-viscoplastic, three-phase material, direct solution of the set of PDEs is regularly impossible. Therefore, an iterative numerical approach is used. There are five major types of numerical methods used in geotechnical engineering; the finite element, the finite difference, the boundary element, the discrete element and the combined boundary/finite element. The way the PDEs are formulated and solved differs for each of these methods.

FLAC (Fast Lagrangian Analysis of Continua) and PLAXIS are the most commonly used by advanced geotechnical researchers. The other well-known software that work in this category are:

- ABAQUS (FEM) (General FEM with some geotechnical relations),
- ANSYS (FEM) (Mechanical/Structural),
- SIGMA/W (FEM) (Geotechnical),
- SEEP/W (FEM) (Seepage Analysis),
- MODFLOW (FEM) (Groundwater Modeling).

Modeling of real structures takes a fundamental understanding of how the system will function or perform. There is a need to simplify the real situation so that one can reasonable arrangement with the geometries and properties in the numerical scheme. The original steps of numerical modelling are:

- Selection of representative cross-section:
  Idealize the field conditions into a design X-section,
  Plane strain or axisymmetric models.

- Choice of numerical scheme and constitutive relationship:
  FEM or FDM or other formulations,
  Elastic or Mohr-Coulomb or Elastoplastic or other models.

- Characterization of material properties for use in models:
  Strength,
  Stiffness,
  Stress - Strain Relationships.

- Grid generation:
  Discretize the Design X-section into nodes or elements.

- Assign of materials properties to grid.
- Assigning boundary conditions.
- Calculate initial conditions.
- Determine loading or modeling sequence.

- Run the model.
- Obtain results.
- Interpret of results.

Before introducing the concept of the FEM and DEM, the difference between a discrete and a continuous system will be explored.

3. Discrete and a continuous system

In discrete system, a sufficient solution can be obtained using a finite number of well-defined components. Such problems can be readily solved even with rather large number of components, for example the analysis of a building frame consisting of beams, columns and slabs (Figure 2.1). For a continuous system, such as a soil layer, the sub-division is continued infinitely so that the problem can only be defined using the mathematical fiction of infinitesimal. Depending on the level of complexity involved, there are two ways of solving such a problem. Simple, linear problems can be solved easily by mathematical manipulation. Solution of complex, non-linear problems involves discretization of the problem into components of finite dimensions (Figure 2.1) and then using a numerical method such as the FEM and FDM.

4. Finite difference method

This method is the oldest and simplest technique. Normally this method requires the knowledge of initial values and boundary conditions. The other principal characteristic properties of finite difference method were listed below:

- Derivatives in the governing equation replaced by algebraic expression in terms of field variables:
  Stress or pressure,
  Displacement,
  Velocity.

- Field variables described at discrete points in space (i.e., nodes).
- Field variables are not defined between the nodes (are not defined by elements).
- No matrix operations are required.
- Explicit method generally used:

  Solution is done by time stepping using small intervals of time,

  Grid values generated at each time step,

  Good method for dynamics and large deformations.

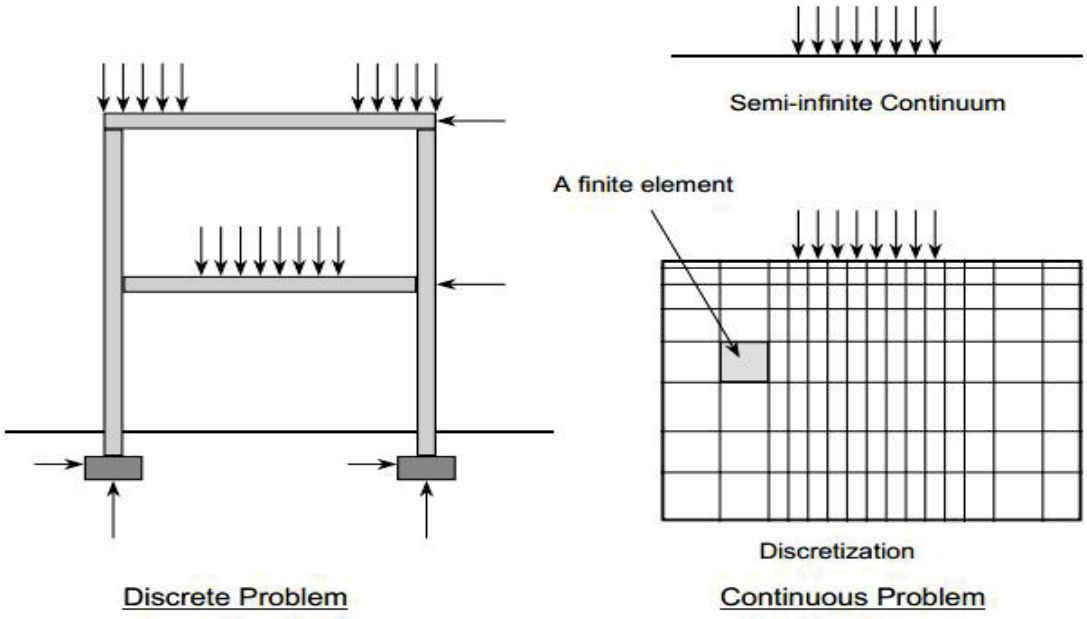

Figure 2.1 Discrete and continuous problem (www.demlateralearthpressure.weebly.com)

Calculation base on finite difference method obtain six principal steps. These steps are:

I. Generate a grid for the domain where we want an approximate solution.
II. Assign material properties
III. Assign boundary/loading conditions,
IV. Use the finite difference equations as a substitute for the ODE/PDE system of equations. The ODE/PDE, thus substituted, becomes a linear or non-linear system of algebraic equations,

V. Solve for the system of algebraic equations using the initial conditions and the boundary conditions. This usually done by time stepping in an explicit formulation,

VI. Implement the solution in computer code to perform the calculations.

5. Finite element method

The idea of representing a given domain as a collection of discrete parts is not unique to the FEM. It was recorded that ancient Greek mathematicians estimated the value of π by noting that the perimeter of a polygon inscribed in a circle approximates the circumference of the circle. They predicted the value of π to accuracies of almost 40 significant digits be representing the circle as a polygon of finitely large number of sides. Searching for approximate solution or comprehension of the whole, by studying the constituent parts of the whole is vital to almost all investigations in science, humanities, and engineering. The FEM is an outgrowth of the familiar procedures such as the frame analysis and the lattice analogy for 2- and 3-dimensional bodies. Its application is not exclusive to engineering. It has been used in other fields such as mathematics & physics. One of the earliest examples of its use was in mathematics by R. Courant who used it for the solution of equilibrium and vibration problems (Courant, 1943). However, Courant did not call his method the FEM. It was R.W. Clough who first coined the term finite element in 1960 when he applied the FEM to plane stress analysis (Clough, 1960).

The finite element method specifications in brief are:

- Evolved from mechanical and structural analysis of beams, columns, frames, etc. and has been generalized to continuous media such as soils.

- General method to solve boundary value problems in an approximate and discretized manner.

- Division of domain geometry into finite element mesh.
- Field variables are defined by elements.

- FEM requires that field variables vary in prescribed fashion using specified functions (interpolation functions) throughout the domain. Pre-assumed interpolation functions are used for the field variables over elements based on values in points (nodes).
- Implicit FEM more common:
  Matrix operations required for solution,
  Stiffness matrix formed. Formulation of stiffness matrix, K, and force vector, r.
- Adjustments of field variables are made until error term is minimized in terms of energy.

6. Constitutive model for soil

Soil is a complicated material that behaves non-linearly and often shows anisotropic and time dependent behavior when subjected to stresses. Generally, soil behaves differently in primary loading, unloading and reloading. It exhibits non-linear behavior well below failure condition with stress dependent stiffness. Soil undergoes plastic deformation and is inconsistent in dilatancy. Soil also experiences small strain stiffness at very low strains and upon stress reversal.

This general behavior was not possibly being accounted for in simple elastic-perfectly plastic Mohr-Coulomb model, although the model does offer advantages which make it a favorable option as soil model.

Brinkgreve (2005) discussed in more detail the five basic aspects of soil behavior. Briefly, the first aspect discussed on the influence of water on the behavior of the soil from the effective stresses and pore pressures. Second aspect is the factor which influences the soil stiffness such as the stress level, stress path (loading and unloading), strain level, soil density, soil permeability, consolidation ratio and the directional-dependent stiffness (stiffness anisotropy) of the soil. The third aspect highlighted the irreversible deformation as a result of loading. Fourth aspect discussed on soil strength with its influencing factor includes loading speed of the tested specimen, age and soil density, undrained behavior, consolidation ratio and directional dependent shear strength (strength anisotropy). Other aspects of soil behavior that should be considered also include factors such as compaction, dilatancy and memory of pre-consolidation stress.

Constitutive modelling of soils is a mathematical form of describing the stress-strain behavior of soils in response to applied loads. It introduces or describes the physical properties of a given material and distinguishes between elastic and plastic deformations. In this chapter two special constitutive soil models that are useful to predict soil liquefaction will be presented.

7. Finn Constitutive model

In this study, FLAC software (Fast Lagrangian Analysis of Continua) which is a Finite Difference Method-based program (FDM) was used. According to FLAC guidance manual, there are several constitutive models that facilitate soil behavior under static and dynamic loadings (Itasca FLAC manual, 2008). Calculation of excess pore water pressure in the soil mass due to dynamic loading is the main factor in the modeling process of liquefaction phenomenon. FLAC has a constitutive model named Finn model which equations represented by Martin et al. (1975) and Byrne (1991) into the standard Mohr-Coulomb plasticity model. Using this model, it is possible to calculate pore water pressure generation by calculating irrecoverable volumetric strains during dynamic analysis. The void ratio in this model is supposed to be constant, also it can be calculated as a function of volumetric strain and other parameters can be defined by void ratio (B.R. Khatibi et al, 2012).

Martin et al. (1975) described initially the effect of cyclic loading on increase of pore water pressure as a result of irrecoverable volume contraction in the soil mass. In these situations, because the matrix of grains and voids is filled by water, the pressure of pore water increases (Itasca FLAC manual, 2008).

They supply the following empirical equation that relates the increment of volume decrease "$\Delta\varepsilon_{vd}$", to the cyclic shear-strain amplitude "γ", where "γ" is presumed to be the "engineering" shear strain (Itasca FLAC manual, 2008):

$$\Delta\varepsilon_{vd} = C_1(\gamma - C_2\,\varepsilon_{vd}) + (C_3\,\varepsilon_{vd}^2)/(\gamma + C_4\,\varepsilon_{vd}) \qquad (2\text{-}1)$$

Where C_1, C_2, C_3 and C_4 are constants.

Note that the equation involves the accumulated irrecoverable volume strain "ε_{vd}", in such a way that the increment in volume strain decreases as volume strain is accumulated. Presumably "$\Delta\varepsilon_{vd}$" should be zero if "γ" is zero; this implies that the constants are related as follows: $C_1 C_2 C_4 = C_3$.

Martin et al. (1975) then go on to compute the change in pore pressure by assuming certain module and boundary conditions ((Itasca FLAC manual, 2008)).

Later, Byrne (1991) presented a simpler equation which correspond irrecoverable volume change and engineering shear strain with two constants. In this model, a soil mass with liquefaction potential was modeled using $(N_1)_{60}$ parameter as a main factor to the Finn model, so all of the soil properties needed for the model were defined for the program by $(N_1)_{60}$.

$$(\Delta\varepsilon_{vd}/\gamma) = C_1 \exp(-C_2(\varepsilon_{vd}/\gamma)) \tag{2-2}$$

Where C_1 and C_2 are constants with different interpretations from those of Eq. (2-1). In many cases, $C_2 = 0.4C_1$, so Eq. (2-2) involves only one independent constant; however, both C_1 and C_2 have been retained for generality (Itasca FLAC manual, 2008).

As mentioned before, to the usual parameters (friction, module, etc.), the model needs the four constants for Eq. (2-1), or two constants for Eq. (2-2). For Eq. (2-1), Martin et al. (1975) describes how these may be determined from a drained cyclic test. For Eq. (2-2), Byrne (1991) notes that the constant, C1, can be derived from relative densities, "D_r", as follows:

$$C1 = 7600(D_r)^{-2.5} \tag{2-3}$$

Further, using an empirical relation between "D_r" and normalized standard penetration test values, "$(N_1)_{60}$",

$$D_r = 15(N_1)_{60}^{1/2} \tag{2-4}$$

Then:

$C_1 = 8.7\ (N_1)_{60}^{-1.25}$ (2-5)

C_2 is then calculated from $C_2 = 0.4C_1$ in this case. Note that, as expected, the volumetric strain is larger for smaller values of the blow count (Byrne, 1991).

8. UBC3D-PLM Constitutive model

UBC2D is used for the UBCSAND model, has defined at first by Puebla et al. and then has used in FLAC software by Beaty and Byrne (Puebla et al., 1997, Beaty & Byrne, 1998).

The UBCSAND model is a simple 2D model developed specially for estimate of liquefaction behavior of sand. Also the model has been verified in various applications related to liquefaction. The original 2D model uses a Mohr-Coulomb yield function and a corresponding non associated plastic potential function. The flow rule is based on the well-known Rowe's stress dilatancy formulation with a modification (Rowe, 1962).

UBCPLM model is based on UBCSAND model which has presented by Anteneh Biru Tsegaye (A. B. Tesegay, 2010). UBCPLM model, primarily based on the elastoplastic functions mentioned accordingly far a generalized 3D formulation has been considered. The new model uses the Mohr - Coulomb yield condition in a generalized stress space (Figure 2.2). The use of non-associated plastic potential based on the same function as the yield function (with mobilized friction angle replaced by mobilized dilatancy angle) has been found to introduce non-coaxially between the stress and the strain in the deviatoric plane.

In 2013, Alexanderos Petalas and Vahid Galavi have introduced UBC3D-PLM code for using in Plaxis (A, Petalas & V, Galavi, 2013). The UBC3D-PLM combination has three aspects:

I. UBC model,
II. 3- Dimension,
III. Past Liquefaction Model.

In next steps, the principle parameters of UBC-PLM will be presented.

8.1. Elastic Response

The elastic strains for this model are a function of changes in either the shear or normal effective stress. The relationship between stresses and strain is controlled by the shear and bulk moduli. Both moduli are isotropic and non-linear, meaning they are a function of the current mean stress:

$$G = K_G^e \cdot P_A \cdot \left(\frac{\sigma'}{PA}\right)^{n_e} \quad (2\text{-}6)$$

$$B = \alpha \cdot K_G^e \quad (2\text{-}7)$$

$$B = K_B^e \cdot P_A \cdot \left(\frac{P'}{PA}\right)^{m_e} \quad (2\text{-}8)$$

Where:

G: Shear modulus;
B: Balk modulus;
K_G^e: Shear modulus respectively (depends on the relative density);
K_B^e: Balk modulus respectively (depends on the relative density);
P_A: Atmospheric pressure;
σ': mean stress in the plane of loading;
m_e, n_e: rate of stress dependency of stiffness.

8.2. Yield Surface

The yield surface for a model controls the boundary between elastic and plastic behavior. For UBCSAND, the yield surface can be described as radial lines which extend outward from the origin at a constant stress ratio. At the onset of loading the current stress ratio is very small so each increment of loading produces an elastic-plastic response. The yield surface is illustrated

schematically in Figure 2.2.

For first time shear loading, the yield surface is controlled by the current stress state, point A in Figure 2.2 As the shear stress increases, the stress ratio η (= τ / σ′) increases and causes the stress point to move to point B. τ and σ′ are the shear and normal effective stresses on the plane of maximum shear stress. The yield surface is dragged to the new location passing through point B and the origin.

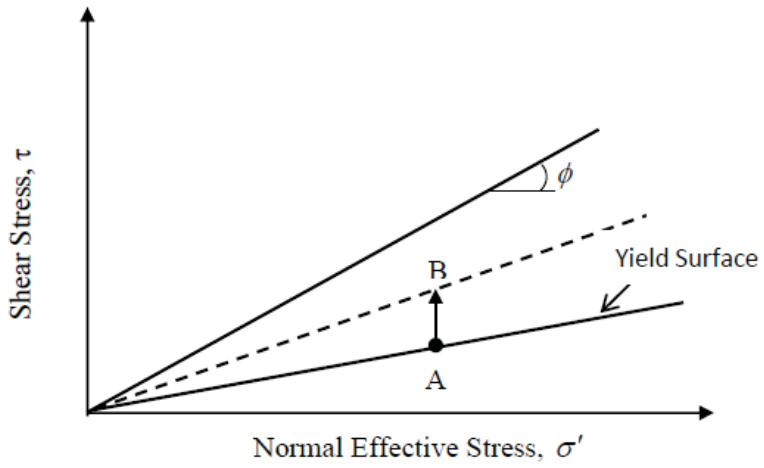

Figure 2.2 Yield surfaces for UBCSAND (Beaty, 2009)

8.3. Plastic response

As the stress ratio of the soil moves outside the yield surface plastic strains will develop. This model utilizes a non-associated flow rule, meaning that the direction of plastic strains is not dependent on the current slope of the yield surface. Plastic shear strains are computed from the current stress ratio through a hyperbolic relationship as shown in Figure 2.3.

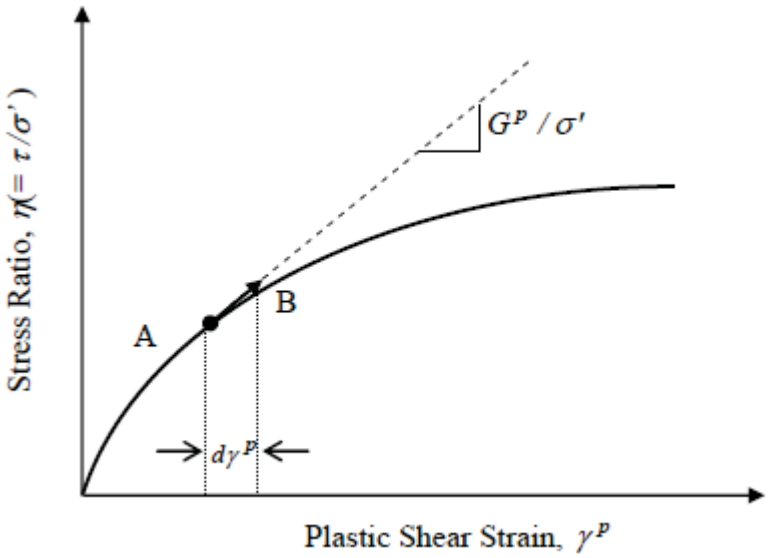

Figure 2.3 Plastic strain increment and plastic modulus (Beaty, 2009)

The plastic shear strain increment, $d\gamma^p$ can be expressed as:

$$d\gamma^p = \frac{1}{GP/\acute{\sigma}} \cdot d\eta \quad (2\text{-}9)$$

Where:

$d\gamma^p$: plastic shear strain increment;

G^p: plastic shear modulus;

$\acute{\sigma}$: shear and normal effective stresses on the plane of maximum shear stress;

$d\eta$: shear stress ratio increment.

G^p is assuming a hyperbolic relationship between shear stress ratio and plastic shear strain , is given by:

$$G^p = G_i^P \cdot \left(1 - \frac{\eta}{\eta f} \cdot R_f\right)^2 \quad (2\text{-}10)$$

Where:

G_i^P = plastic modulus at a low level of stress ratio (η = 0),

η_{peak} = stress ratio at failure and equals sin φ_{peak},

φ_{peak} = peak friction angle,

R_f = failure ratio (generally decreases with increasing relative density).

The magnitude of the plastic volumetric strains is coupled to the shear strain through the angle of dilation. Volumetric strains can either be contractive or dilative and this is determined by the relation of the soil to the critical state line as defined by the constant volume friction angle. Soils at a stress ratio below the constant volume friction angle will undergo contractive behavior while soils above will tend to dilate. Soils at the critical state line will not experience volumetric strains. This is consistent with critical state theory and is illustrated in Figure 2.4.

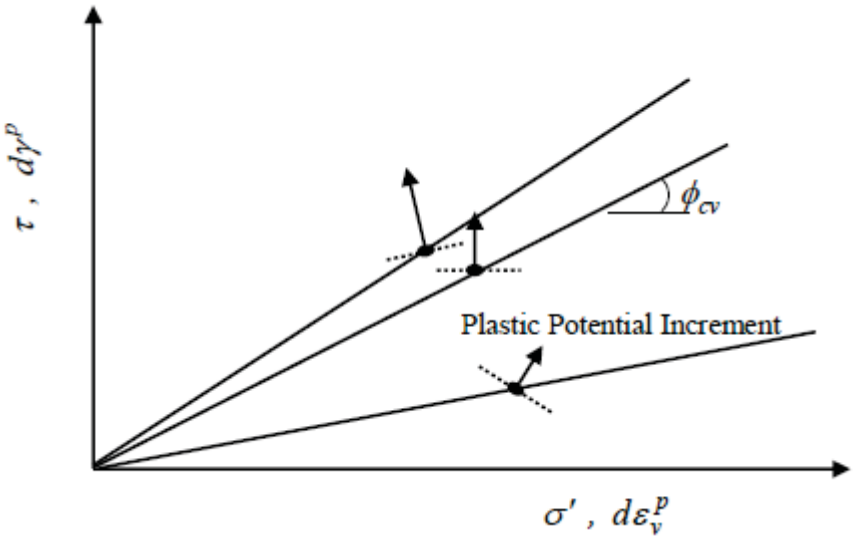

Figure 2.4 Directions of plastic strains associated with location of yield surface (Beaty, 2009).

8.4. Hardening Laws

The yield surface begins as a small radial line extending from the origin, but as the soil is plastically sheared the yield surface "opens". The maximum and minimum stress ratios seen by the soil are tracked separately, so the hardening law is tracked independently for positive and negative stress

ratios. If the soil is unloaded it will behave elastically until the sign of the shear stress reverses. At this point the soil will be "reloading" until it reaches its previous maximum or minimum stress ratio. Reloading does generate plastic strains, but with a shear modulus that is significantly stiffer than for first time or virgin loading.

8.5. UBCSAND model in 3D formulation

The main difference between the UBCSAND model and the UBC3D model is the latter generalized 3-D formulation. The UBC3D model uses the Mohr-Coulomb yield condition in a 3-D principal stress space. Moreover, a modified non-associated plastic potential function based on Drucker-Prager's criterion is used, in order to maintain the assumption of stress-strain coaxially in the deviatoric plane for a stress path beginning from the isotropic line (Tsegaye, 2010). The full set of the Mohr-Coulomb yield functions are introduced (pressure is positive, tension is positive):

$$f_{1a} = \frac{1}{2}(\sigma'_2 - \sigma'_3) + \frac{1}{2}(\sigma'_2 + \sigma'_3)\sin\varphi' - c'\cos\varphi' \quad (2\text{-}11)$$

$$f_{1b} = \frac{1}{2}(\sigma'_3 - \sigma'_2) + \frac{1}{2}(\sigma'_3 + \sigma'_2)\sin\varphi' - c'\cos\varphi' \quad (2\text{-}12)$$

$$f_{2a} = \frac{1}{2}(\sigma'_3 - \sigma'_1) + \frac{1}{2}(\sigma'_3 + \sigma'_1)\sin\varphi' - c'\cos\varphi' \quad (2\text{-}13)$$

$$f_{2b} = \frac{1}{2}(\sigma'_1 - \sigma'_3) + \frac{1}{2}(\sigma'_1 + \sigma'_3)\sin\varphi' - c'\cos\varphi' \quad (2\text{-}14)$$

$$f_{3a} = \frac{1}{2}(\sigma'_1 - \sigma'_2) + \frac{1}{2}(\sigma'_1 + \sigma'_2)\sin\varphi' - c'\cos\varphi' \quad (2\text{-}15)$$

$$f_{3b} = \frac{1}{2}(\sigma'_2 - \sigma'_1) + \frac{1}{2}(\sigma'_2 + \sigma'_1)\sin\varphi' - c'\cos\varphi' \quad (2\text{-}16)$$

8.6. Post-liquefaction rule

The important aspect during the modelling of cyclic liquefaction in sands is the volumetric locking. The evolution of the volumetric strains, after the stress path reaching the yield surface defined by the peak friction angle, becomes constant due to the formulation of the flow rule. Due to this issue the stiffness degradation of the soil due to the post- liquefaction behavior of loose non-cohesive soils or due to the cyclic mobility of dense non-cohesive sands, which is observed in the experimental studies, cannot be modelled. This limitation is solved in the formulation of the UBC3D-PLM with the implementation of an equation which gradually decreases the plastic shear modulus as a function of the generated plastic deviatoric strain during dilation of the soil element. The stiffness degradation is formulated based on the plastic deviatoric strain related with the dilation of the soil element; due to the deconstruction of the soil skeleton which occurs during dilative behavior. This leads to the decreased soil stiffness during contraction which follows after the unloading phase (Pwtalas & Galvi, 2013).

8.7. UBC3D-PLM input parameters

The input parameters of UBC3D-PLM are summarized in table 2.1. UBC3D-PLM model is a descriptive model and the model parameters are determined by curve fitting from cyclic undrained direct simple shear (DSS) test. Nevertheless in many field these tests are not available and data from insitu tests such as Standard Penetration Test (SPT) or Cone Penetration Test (CPT) exist. For this reason for the UBCSAND model, Beaty and Byrne have proposed some correlation for input parameters of model (Beaty & Byrne, 2011). This relation have become from clean sand equivalent SPT blow-count measurements. These correlations are the following:

$$K_G^e = 21.7 * 20.0 * (N_1)_{60}^{0.333} \quad (2\text{-}17)$$

$$K_B^e = K_G^e * 0.7 \quad (2\text{-}18)$$

$$K_G^p = K_G^e * (N_1)_{60}{}^2 * 0.003 + 100.0 \quad (2\text{-}19)$$

$$\varphi_{pi} = \varphi_{cv} + (N_1)_{60}/10.0 \quad (2\text{-}20)$$

φ_{pi} is is the peak friction angle for $(N_1)_{60}$ values lower than 15 while for larger an additional increase is suggested as described by relation:

$$\varphi_p = \varphi_{pi} + \max\left(0.0 , \frac{(N1)60-15}{5}\right) \quad (2\text{-}21)$$

For the failure ratio the following correlation applies:

$$R_f = 1.1 * (N_1)_{60}^{-0.15} \quad (2\text{-}22)$$

As long as the occurring value is smaller than 0.99 otherwise a value of 0.99 is used. Concerning the densification factor (fac_{hard}), the suggested value for UBCSAND is 1.0 (Makra, 2013).

Table 2.1 UBC3D-PLM parameters

Name	Symbol	Method	Default
Constant volume friction angle	φ_{cv}	CD TxC or DSS	-
Peak friction angle	φ_p	CD TxC or DSS	-
Cohesion	c	CD TxC or DSS	0
Elastic Shear Modulus	K_G^e	Curve Fit	-
Plastic Shear Modulus	K_G^p	Curve Fit	-
Elastic Bulk Modulus	K_B^e	Curve Fit	-
Elastic Shear Modulus Index	ne	Curve Fit	0.5
Elastic Bulk Modulus Index	me	Curve Fit	0.5
Plastic Shear Modulus Index	np	Curve Fit	0.5
Failure Ratio	R_f	Curve Fit	0.9
Atmospheric pressure	P_A	Standard Value	100
Tension Cut-off	σ_t	-	0
Densification Factor	fac_{hard}	Curve Fit	1
SPT value	$(N_1)_{60}$	In-Situ Testing	-
Post Liquefaction Factor	Fac_{post}	Curve Fit	0.2-1

From equation (2-18) a direct relation between elastic shear and bulk modulus is derived which corresponds to a Poisson's ratio of 0.02 from the theory of elasticity. This ratio is very low for static calculations and would lead to unrealistic results. However, is has been shown (Hardin 1978 & Negussey, 1984) that Poisson's ratio varies with strain and that for small strains its value can range between 0.0-0.2. For this reason, for dynamic calculations a much lower Poisson's ratio can be used, the same way the small strain shear modulus is used. Still the assumption is on the low side, since the usual assumption for sands is around 0.1 (Byrne et al, 1987 & Makra, 2013).

9. Case study, Wildlife site

The wildlife site is located in the Imperial Valley. This site became of seismic interest after 1981 Westmorland earthquake (M_s = 5.9), which seemed to have caused liquefaction in the area. The site was then instrumented in 1982 by the U.S Geological Service (USGS), with the main objective of recording ground and pore-pressure response data during earthquakes (Holtzer et al., 1989).

Between November 23 and 24, 1987, two earthquakes occurred in the Imperial Valley within a period of 12 hours. The first had its epicenter in Elmore Ranch, 23 km west from the Wildlife Site, with a moment magnitude of Ms = 6.2. At the ground surface, the peak ground acceleration measured was 0.13 g. The second event, which is thought to have caused liquefaction, was the Superstition Hills earthquake, with epicenter 31 km south-west from the Wildlife Site, a moment magnitude of Ms = 6.6, and measured peak ground acceleration of 0.20 g. Figure 2.5 shows the map locating the epicenters of the three earthquakes in the Wildlife Site area.

9.1. Site location

The Wildlife site is located 3.2 km south of Calipatria, California, in the floodplain of the Alamo River, in the Imperial valley Wildlife management area. This is a desert area heavy irrigated for crop cultivation.

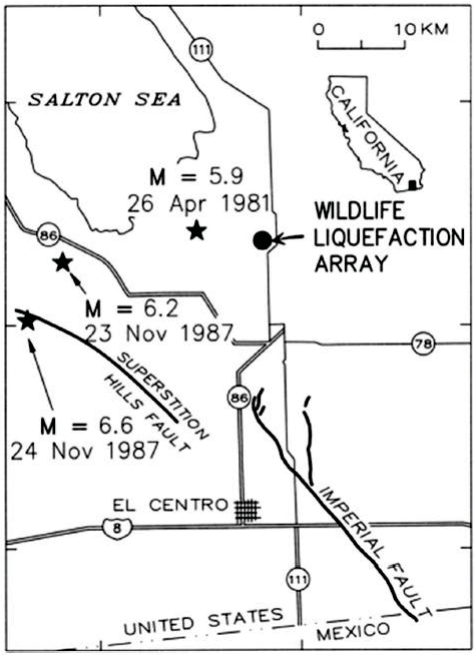

Figure 2.5 Earthquake epicenters in the Wildlife Site area (Holtzer et al., 1989)

According to the description reported by Holzer et al. in 1989, shallower deposits consist of saturated floodplain sediments that fill an old incised channel of the Alamo River. The deposits probably date from catastrophic flooding of the river between 1905 and 1907. The Alamo River runs in a 3.7 m-deep channel located 23 m east from the Wildlife Site and controls the ground water table depth at about 1.2 m. The stream is normally used for drainage and irrigation. The uppermost layer consists of a 2.5 m-thick flat-lying silt bed that overlies a 3.3 m-thick silty sand layer. A 5 m-thick clayey silt layer is found beneath these two layers of floodplain deposits, being the uppermost unit of a dense, extensive, sedimentary deposit. For the silty sand layer, the one believed to have liquefied, fines content (<75 m) range between 16 and 60%, with an average of 33%, and its porosity is about 41%.

Another description, from Gu et al. in 1994, indicates that the sediments susceptible to liquefaction during the Superstition Hills earthquake were identified as the uppermost 2.5 m-thick silt and the 3.3m-thick silty sand. The first is typical floodplain sediment that exhibits low penetration resistance and liquidity index greater than 1, indicating susceptibility to liquefaction. According to Seed et al., and based on a liquidity index greater than 0.9, a liquid limit less than 35 and a sediment

fraction (<0.005 mm) less than 15%, approximately 20% of this sediment is liquefiable (Seed et al., 1983). The second, the 3.3m-thick silty sand, was identified to be the layer that liquefied and formed sand boils, based on the looseness of sediment, the high water table and the similarity to sand boil ejected. The uppermost layer may have not liquefied because it was mainly above the water table. In Figure 2.6 is shown the soil profile at the Wildlife Site according to Bennett et al. in 1984, including grain size percentage, unified soil classification and position of the water table.

A corresponding elastic shear-wave velocity of 125 m/s was found for the Wildlife Site, using the lag time of the E-W record (Davis & Berrill, 2001). The same value of shear-wave velocity is cited in a different investigation by Holzer et al. (1989).In table 2.2 is shown asset of soil properties for the wildlife site was established and presented by Gu et al. (Gu et al., 1994).

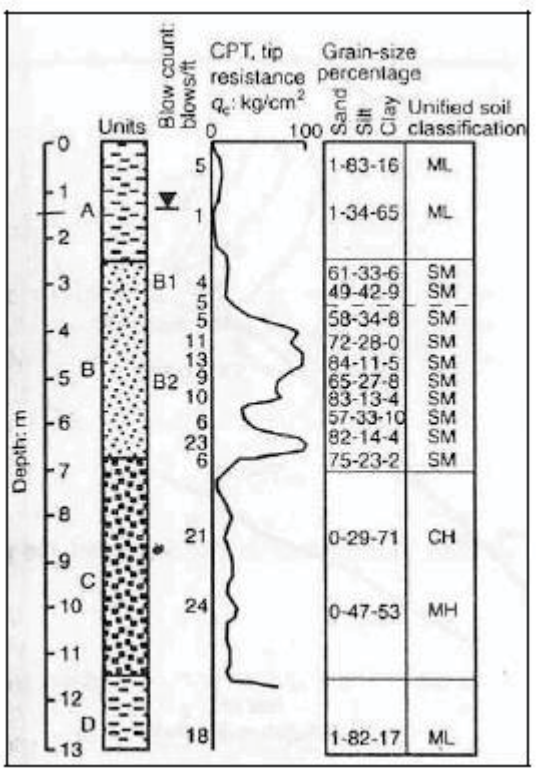

Figure 2.6 Soil profile at the Wildlife site (Bennett et al., 1984)

9.2. Instrumentation of Wildlife

A description of the instrumentation installed at the Wildlife Site is presented by several researchers. Six pore-water pressure transducers, or piezometers, were installed in the site. Five of them are in the liquefiable layer, that is, within the silty sand unit. As can be seen in Figure 2.7, and according to Table 2.3, these piezometers range between 2.9 and 6.6 m in depth. Piezometer P4 failed to function during the 1987 events (Holzer et al, 1989).

Table 2.2 Soil parameters at the Wildlife Site (Gu et al., 1994)

Layer	I	II	III	IV	V
Depth (m)	0.0-1.2	1.2-2.5	2.5-3.5	3.5-6.8	6.8-10
Total Density (kg/m^3)	1600	1940	1970	1970	2000
Bulk Modulus (N/m^2)	$2.61*10^7$	$2.44*10^7$	$4.50*10^7$	$4.50*10^7$	$5.83*10^7$
Shear Modulus (N/m^2)	$1.57*10^7$	$1.47*10^7$	$2.08*10^7$	$2.08*10^7$	$2.70*10^7$
Cohesion (Pa)	$2*10^3$	$2*10^3$	-	-	-
Friction angle	21.3	20.0	22.0	22.0	35.0
Dilation	21.3	20.0	19.0	18.0	5.0
SPT average	6	6.25	7.65	10.65	10
Permeability (m^3.sec/kg)	$5*10^{-11}$	$5*10^{-11}$	$5*10^{-11}$	$2.1*10^{-10}$	$1*10^{-13}$
Porosity	0.4047	0.4431	0.4253	0.4253	0.4075

Table 2.3 Piezometer identification and depths. The Wildlife Site

Identification	**Depth (m)**	**Layer**
P1	5.0	Silty Sand
P2	3.0	Silty Sand
P3	6.6	Silty Sand
P4	3.5	Silty Sand
P5	2.9	Silty Sand
P6	12.0	Silt

The sixth piezometer, identified as P6, is located at 12 m depth within a 1 m-thick silt layer beneath the liquefiable silty sand unit. Two three-component accelerometers, one at the surface and other at

7.5m depth, linked with all the instruments to the same triggering mechanism, were also installed at the site. The down-hole accelerometer was positioned near the upper surface of the stiff clay.

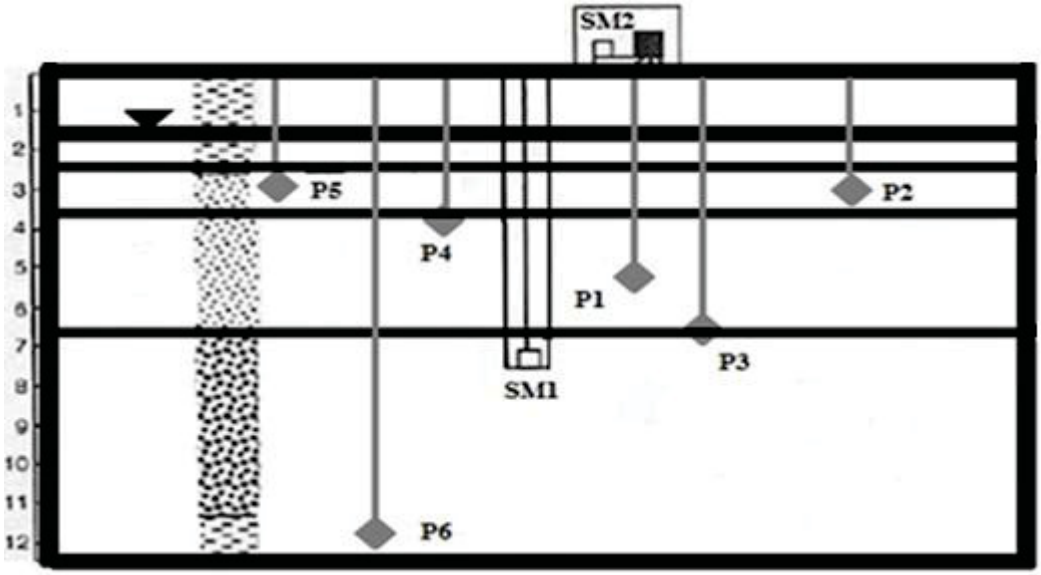

Figure 2.7 instrumentation at the Wildlife Site (Bennett et al., 1984)

Also installed were inclinometer casings to detect permanent lateral subsurface deformation and a series of driven stakes around the instrument array as survey points in order to monitor possible permanent lateral displacements.

9.3. Effects of the Earthquake and Evidence of Liquefaction

Based on recorded pore-pressures and surface evidence, suggested that the silty sand layer liquefied during the 1987-Superstition Hills earthquake (Holzer et al., 1989). Extensive ground cracking, indicative of lateral spreading, accompanied liquefaction at the array. Although most of the cracking seems to be caused by local slumping along the west bank of the Alamo River, ejection of sand from these cracks confirms that they were associated with liquefaction. In Figure 2.8 is presented a photograph showing sand boils at the Wildlife Site (Wills, 1996).

In terms of pore-pressure, questions arose concerning the unexpectedly long times for pore-pressure increase to peak recorded by the transducers in comparison with the duration of the earthquake. A series of recalibrations was made by Hushmand et al., who suggested that the pore-pressure response rise times might be too slow (Hushmand et al., 1992). Finally, Youd and Holzer concluded that interbedding of silt and sand at the site could affect the response of two piezometers separated by a small but significant distance (Youd & Holzer, 1994). In Figure 2.9, pore-pressures for the Superstition Hills earthquake at the Wildlife Site are presented.

Figure 2.8 Sand boils section at the Wildlife Site (Wills, 1996)

10. Liquefaction modelling of Wildlife site with Finn-Byrne Model

In this thesis, the liquefaction of wildlife site has been modeled with Finn-Byrne formulation firstly. This numerical modelling has been performed with FLAC 6.0 software. FLAC (Fast Lagrangian Analysis of Continua) is a two-dimensional explicit finite difference program.

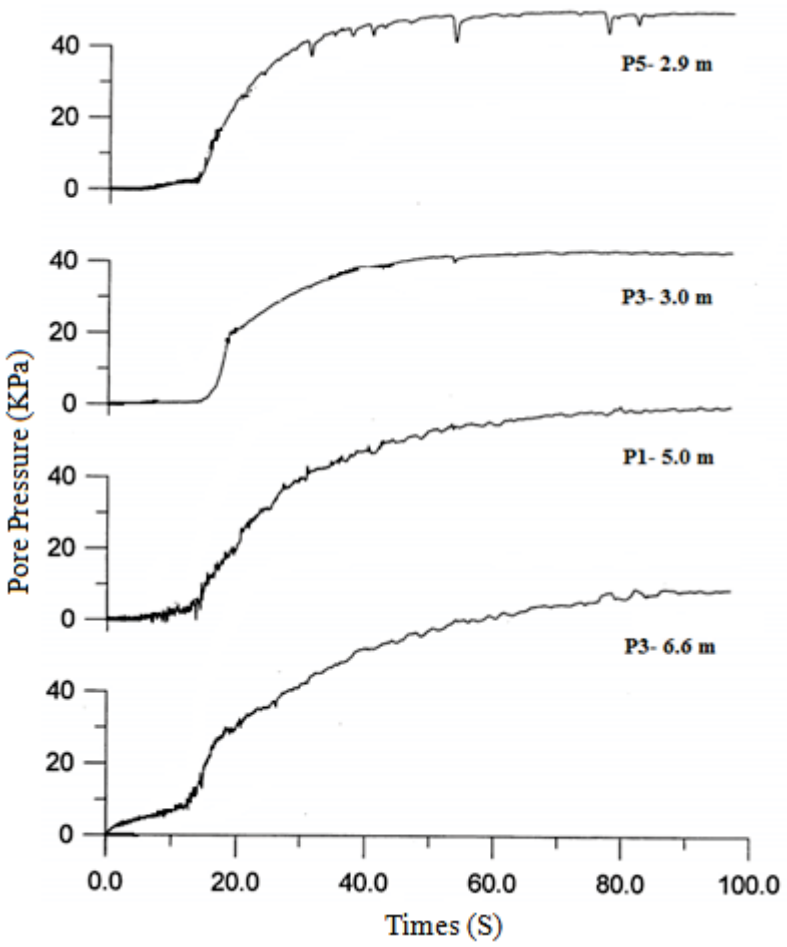

Figure 2.9 Recorded pore-pressures at the Wildlife Site (Davis & Berrill, 2001)

10.1. The overall process of modeling

For modelling of this special liquefaction, Finn constitutive model and equivalent linear method have been used. Also, data of the Superstition Hill earthquake have been analyzed with Seismosignal software. The diagram of modeling has been presented in figure 2.10.

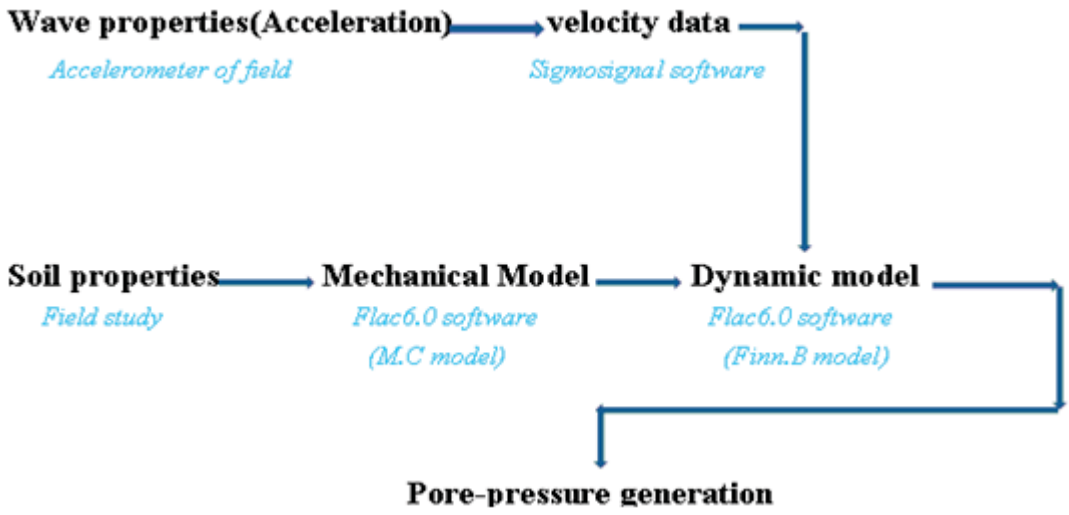

Figure 2.10 the diagram of modeling of Liquefaction at Wildlife Site

10.2. Acceleration Records

The acceleration records from the Superstition Hill earthquake at the Wildlife Site were downloaded directly from the PEER Strong Motion Database. After that, acceleration data have been imported in Sigmosignal Software. After data analyze the data for velocity and displacement with their diagrams were been produced (Figure 2.11).

The diagrams of acceleration data of Superstition Hill earthquake at the Wildlife Site were presented in Figure 2.12 and 2.13.

According to the characteristic of the motion, the ground shaking at the Wildlife Site can be divided to different steps. These three steps are:

0 – 14 s: Ground acceleration of low amplitude, with maximum of 0.13 g at the surface and 0.10 g at the down-hole instruments respectively.

14 s – 21 s: This step corresponds to the strongest shaking, with peak acceleration of 0.20 g at the surface and 0.17 g at the down-hole instruments respectively.

21 s – 50 s: The recorded acceleration did not arise 0.06 g, for both surface and down-hole instruments.

File Edit Format View Help

```
PEER STRONG MOTION DATABASE RECORD. PROCESSING BY PACIFIC ENGINEERING.
SUPERSTITION HILLS 11/24/87 13:16, WILDLIFE LIQUEFACTION ARRAY, 090 (USGS STATION 5210)
ACCELERATION TIME HISTORY IN UNITS OF G. FILTER POINTS: HP=0.1 Hz LP=50.0 Hz
NPTS=  8800, DT= .00500 SEC
  -.4032022E-03  -.7256910E-03  -.1283177E-02  -.1414116E-02  -.1341807E-02
  -.1307360E-02  -.1282433E-02  -.1279967E-02  -.1296292E-02  -.1318094E-02
  -.1326337E-02  -.1305953E-02  -.1254916E-02  -.1191544E-02  -.1146253E-02
  -.1135679E-02  -.1152647E-02  -.1179928E-02  -.1200265E-02  -.1201813E-02
  -.1187730E-02  -.1175615E-02  -.1186775E-02  -.1225765E-02  -.1267265E-02
  -.1272569E-02  -.1227805E-02  -.1155855E-02  -.1096084E-02  -.1089906E-02
  -.1148635E-02  -.1234507E-02  -.1287977E-02  -.1265238E-02  -.1178846E-02
  -.1097606E-02  -.1077787E-02  -.1118194E-02  -.1157379E-02  -.1128207E-02
  -.1055070E-02  -.1005759E-02  -.9855313E-03  -.9777910E-03  -.1008330E-02
  -.1108518E-02  -.1264394E-02  -.1408630E-02  -.1428660E-02  -.1249923E-02
  -.9480985E-03  -.7009726E-03  -.6241127E-03  -.6895437E-03  -.7956740E-03
  -.8673764E-03  -.8762925E-03  -.8515571E-03  -.8760376E-03  -.9776428E-03
  -.1081334E-02  -.1161484E-02  -.1240338E-02  -.1250390E-02  -.1152642E-02
  -.9852146E-03  -.7860396E-03  -.6839057E-03  -.8581300E-03  -.1323464E-02
  -.1850801E-02  -.2109699E-02  -.1892911E-02  -.1298928E-02  -.8111350E-03
  -.9204458E-03  -.1520030E-02  -.1978010E-02  -.1750221E-02  -.6676775E-03
   .9585783E-03   .2144125E-02   .1930557E-02   .6024243E-03  -.6818611E-03
  -.1120278E-02  -.5816217E-03   .3983875E-03   .8916575E-03   .3957701E-03
  -.7502443E-03  -.1737709E-02  -.1721396E-02  -.3864288E-03   .1313253E-02
   .1848089E-02   .8070652E-03  -.8534579E-03  -.2004762E-02  -.2113113E-02
  -.1330551E-02  -.5232201E-03  -.8159289E-03  -.2455592E-02  -.4288448E-02
  -.4702557E-02  -.2895634E-02   .3689847E-03   .2996795E-02   .3076957E-02
   .6199748E-03  -.2476174E-02  -.4161425E-02  -.3468585E-02  -.9926714E-03
   .1275250E-02   .1471244E-02  -.3618064E-03  -.2394483E-02  -.2706839E-02
  -.8019111E-03   .1804759E-02   .2964285E-02   .2090548E-02   .2731989E-03
  -.1086004E-02  -.1082150E-02   .5049098E-03   .2832694E-02   .4243066E-02
   .3827196E-02   .2153061E-02   .1441549E-03  -.1769892E-02  -.3159039E-02
  -.3447076E-02  -.2686037E-02  -.1696949E-02  -.1154312E-02  -.8805413E-03
  -.3987419E-03   .2044224E-03   .3805388E-03  -.3024001E-04  -.3823650E-03
  -.3763009E-04   .9543521E-03   .2149600E-02   .3042501E-02   .3069406E-02
```

Figure 2.11 Acceleration data from the Superstition Hill earthquake at the Wildlife Site

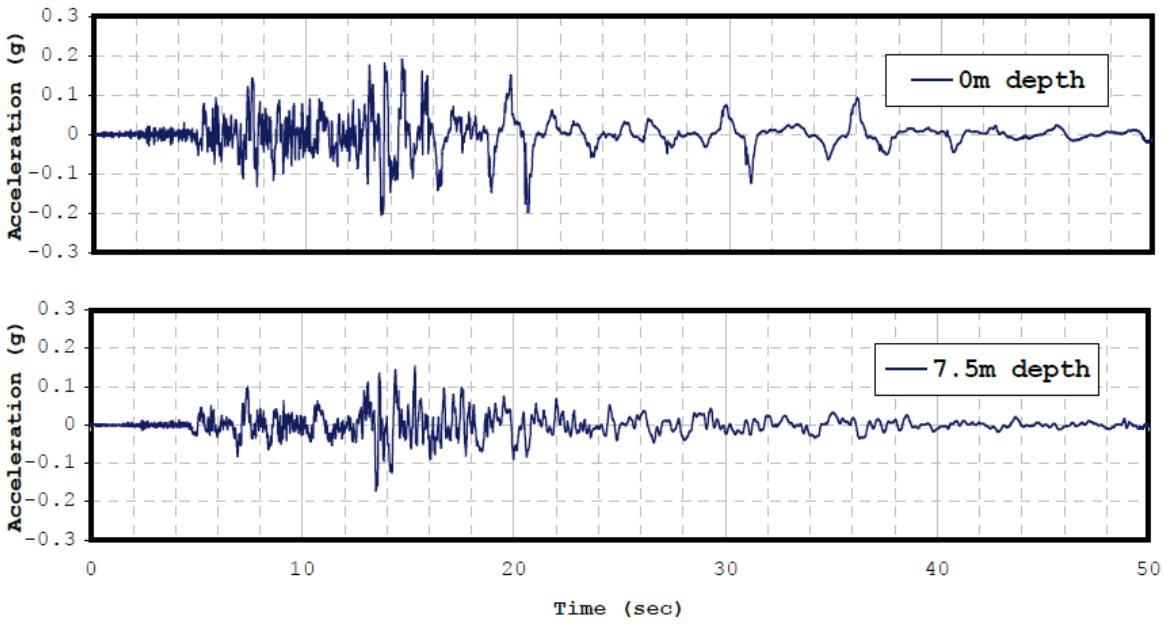

Figure 2.12 Superstition Hills earthquake. N-S acceleration records at the Wildlife Site

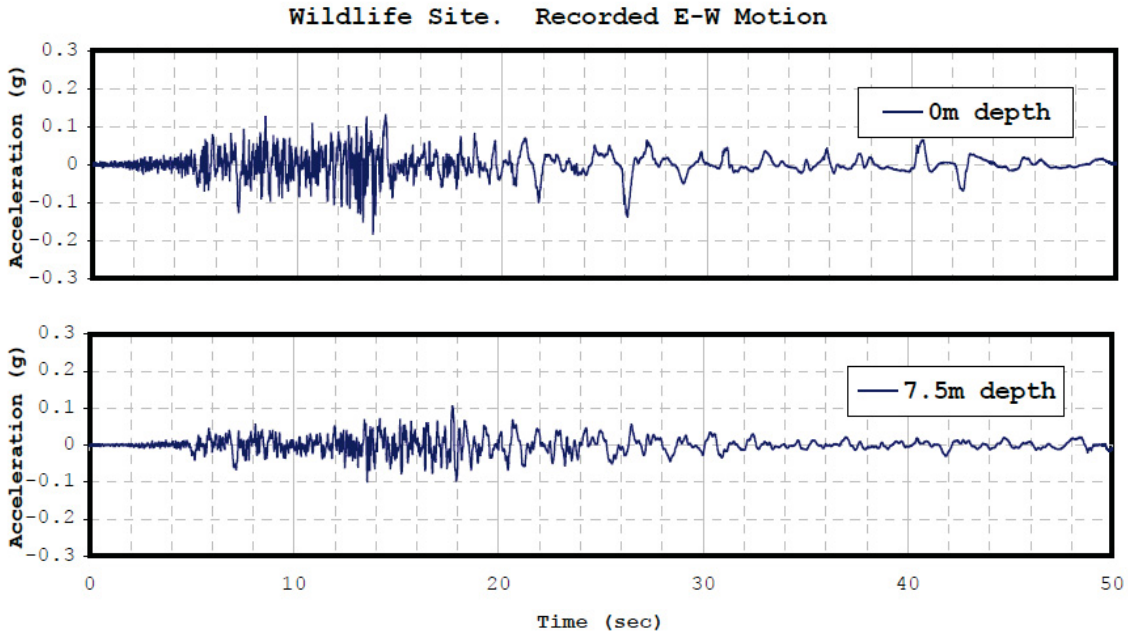

Figure 2.13 Superstition Hills earthquake. E-W acceleration records at the Wildlife Site

10.3. Finn-Byrne Model parameters

As mentioned before, Finn-Byrne model have 2 category data. First, needed for mechanical calculation and second, pore-water pressure generation. The first input parameters are same with Plastic Mohr-Coulomb model. These parameters have been presented in Table 2.4. The result of calculation for second input data have been illustrated in table 2.5.

Table 2.4 Input soil parameters at the Wildlife Site (Gu et al., 1994)

Layer	I	II	III	IV	V
Depth (m)	0.0-1.2	1.2-2.5	2.5-3.5	3.5-6.8	6.8-10
Total Density (kg/m^3)	1600	1940	1970	1970	2000
Bulk Modulus (N/m^2)	$2.61*10^7$	$2.44*10^7$	$4.50*10^7$	$4.50*10^7$	$5.83*10^7$
Shear Modulus (N/m^2)	$1.57*10^7$	$1.47*10^7$	$2.08*10^7$	$2.08*10^7$	$2.70*10^7$
Cohesion (Pa)	$2*10^3$	$2*10^3$	-	-	-
Friction angle (°)	21.3	20.0	22.0	22.0	35.0
Dilation (°)	21.3	20.0	19.0	18.0	5.0
Porosity	0.4047	0.4431	0.4253	0.4253	0.4075

Table 2.5 The result of calculation for Finn-Byrne model

No	Depth (m)	SPT	D_r	C_1	C_2
I	0-1.2	6	36.74	0.93	0.43
II	1.2-2.5	6.25	37.5	0.88	0.45
III	2.5-3.5	7.65	41.48	0.68	0.58
IV	3.5-6.8	10.65	48.95	0.45	0.88
V	<6.8	10	47.43	0.49	0.81

10.4. Results of modelling

After calculation of input parameters, the GII comments for liquefaction modeling on base Finn-Byrne model has been written. Some part of these comments were shown in figure 2.14.

The mechanical modeling of Imperial Valley site and the result of calculation after 100 second earthquake have been presented in figure 2.15 to 2.20.

```
config gwflow ats dynamic extra 5
grid 35,13
model elastic
gen line 0.0,6.2 35.0,6.2
gen line 0.0,9.5 35.0,9.5
gen line 0.0,11.8 35.0,11.8
gen line 0.0,10.5 35.0,10.5
group 'User:I' j 13
model mohr group 'User:I'
prop density=1600.0 bulk=2.61E7 shear=1.57E7 cohesion=2000.0 friction=21.3 dilation=21.3 tension=0.0 group 'User:I'
group 'User:II' j 11 12
model mohr group 'User:II'
prop density=1940.0 bulk=2.44E7 shear=1.47E7 cohesion=2000.0 friction=20.0 dilation=20.0 tension=0.0 group 'User:II'
group 'User:III' j 10
model mohr group 'User:III'
prop density=1970.0 bulk=4.5E7 shear=2.08E7 cohesion=0.0 friction=22.0 dilation=19.0 tension=0.0 group 'User:III'
group 'User:IV' j 7 9
model mohr group 'User:IV'
prop density=1970.0 bulk=4.5E7 shear=2.08E7 cohesion=0.0 friction=22.0 dilation=18.0 tension=0.0 group 'User:IV'
group 'User:V' j 1 6
model mohr group 'User:V'
prop density=2000.0 bulk=5.83E7 shear=2.7E7 cohesion=0.0 friction=35.0 dilation=5.0 tension=0.0 group 'User:V'
initial syy -19200.0 var 0.0,19200.0 region 27 13
initial sxx -19200.0 var 0.0,19200.0 region 27 13
initial szz -19200.0 var 0.0,19200.0 region 27 13
initial sxx -47049.0 var 0.0,47079.0 region 19 12
initial syy -47049.0 var 0.0,47049.0 region 19 12
initial szz -47049.0 var 0.0,47049.0 region 19 12
initial sxx -49231.0 var 0.0,49231.0 region 27 10
initial syy -49231.0 var 0.0,49231.0 region 27 10
```

Figure 2.14 Some part of GII comments in Flac for Liquefaction modeling

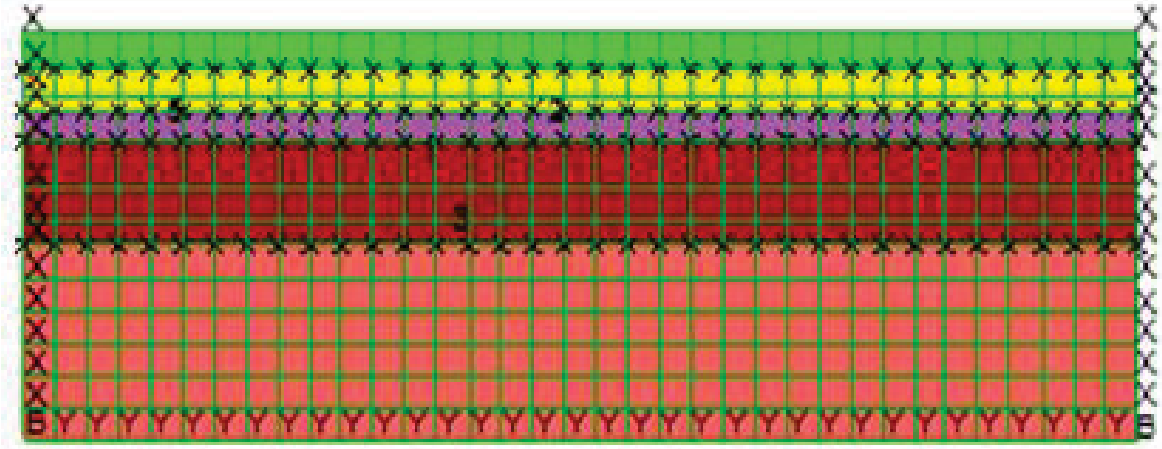

Figure 2.15 Flac model of Soil profile and instrumentation at wildlife

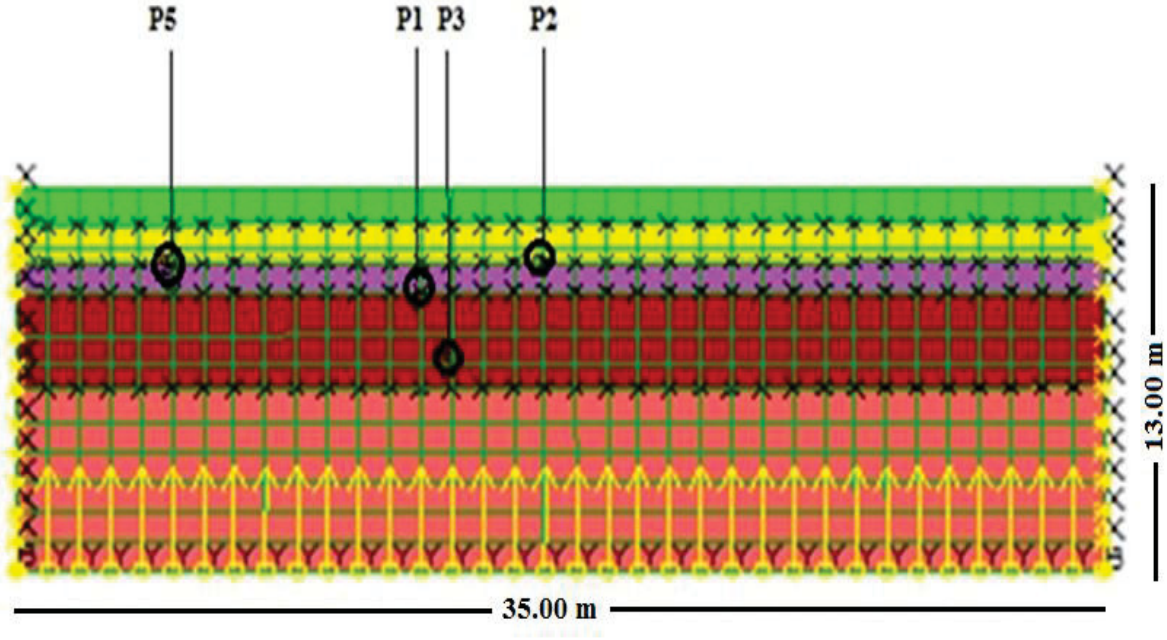

Figure 2.16 Model of Soil profile after superstition hills earthquake

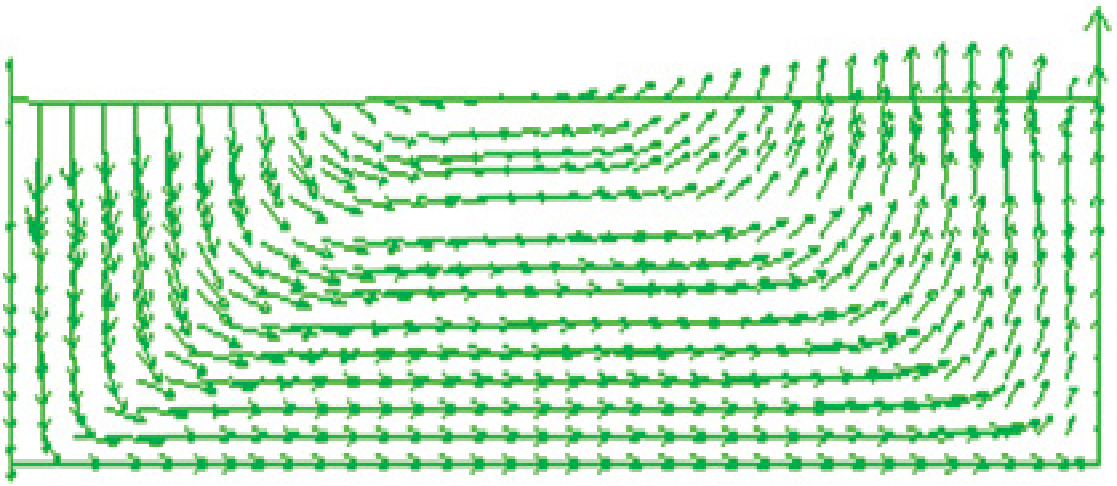

Figure 2.17 Model of displacement vectors after superstition hills earthquake

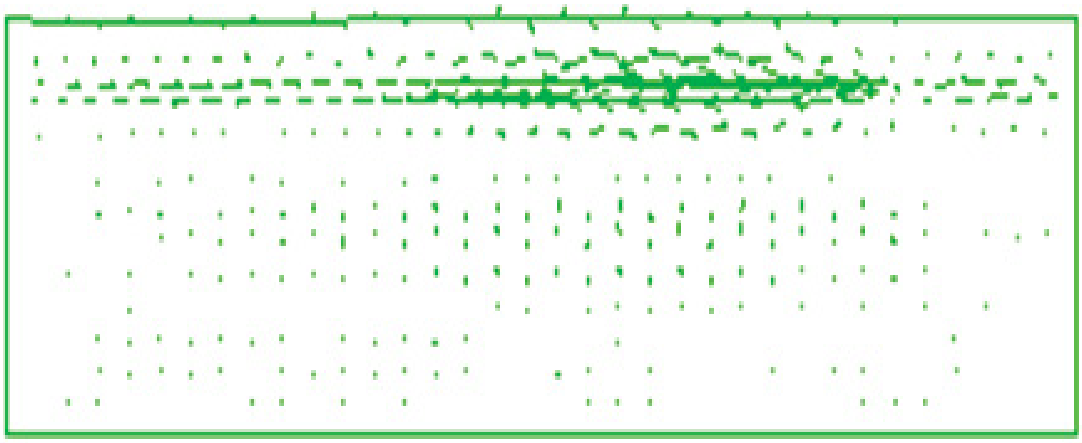

Figure 2.18 Model of velocity vectors after superstition hills earthquake

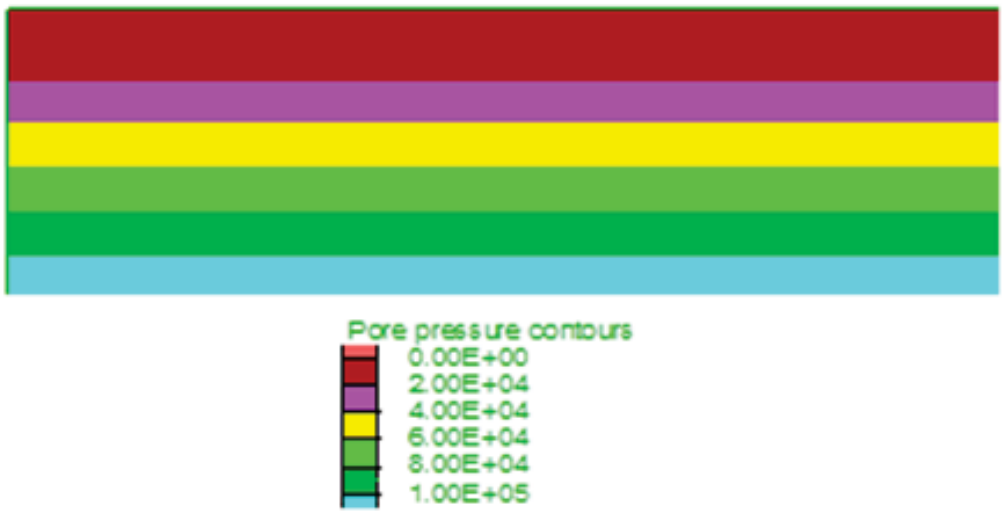

Figure 2.19 Model of pore pressure contours before superstition hills earthquake

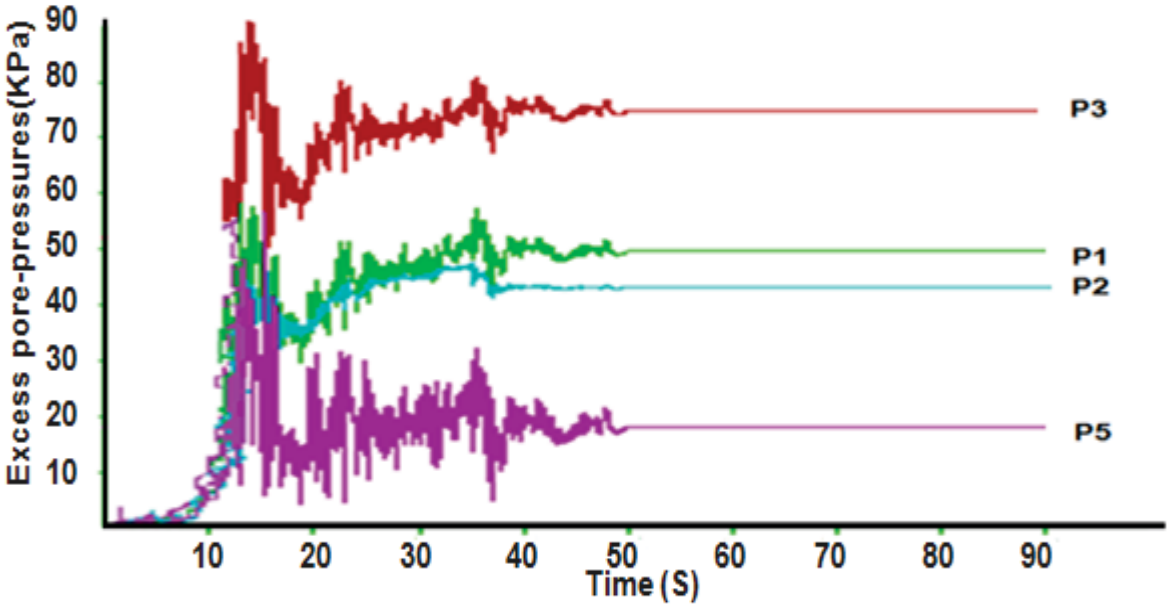

Figure 2.20 Calculated excess pore-pressures at the wildlife site

11. Liquefaction modelling of Wildlife site with UBC3D-PLM Model

In second part of this thesis, the liquefaction of wildlife site has been modeled with UBC3D-Post Liquefaction Model. These calculations have been done with PLAXIS 2012 software. PLAXIS is based on the finite element method and intended for 2-Dimensional and 3-Dimensional geotechnical analysis of deformation and stability of soil structures.

11.1. Planning of modelling

In this research, such as the other numerical modelling, the Geo-mechanical model has been built (Figure 2.21). After the mesh generation and construction Phase, dynamic loading has been used to shaking the model. This input data for shaking, have been extracted from the PEER Strong Motion Database.

Plaxis has three methods for import of dynamic input data. These methods are:

- Mathematical formulation of Wave (Harmonic load multiplier)
- Load multiplier with time series (non- Harmonic load multiplier)
- SMS file (non- Harmonic load multiplier)

In this study by using the Notepad software the load multiplier with time series has been made from the data of PEER Strong Motion Database. Figure 2.21 shows the procedure of numerical modelling briefly.

11.2. UBC3D-PLM parameters for Wildlife site

The UBC3D-PLM model, in addition of Plastic Mohr-Coulomb model has some special parameters. These parameters have been calculated based on valid data and purposed mathematical formula. All parameters of UBC3D-PLM model have presented in table 2.6.

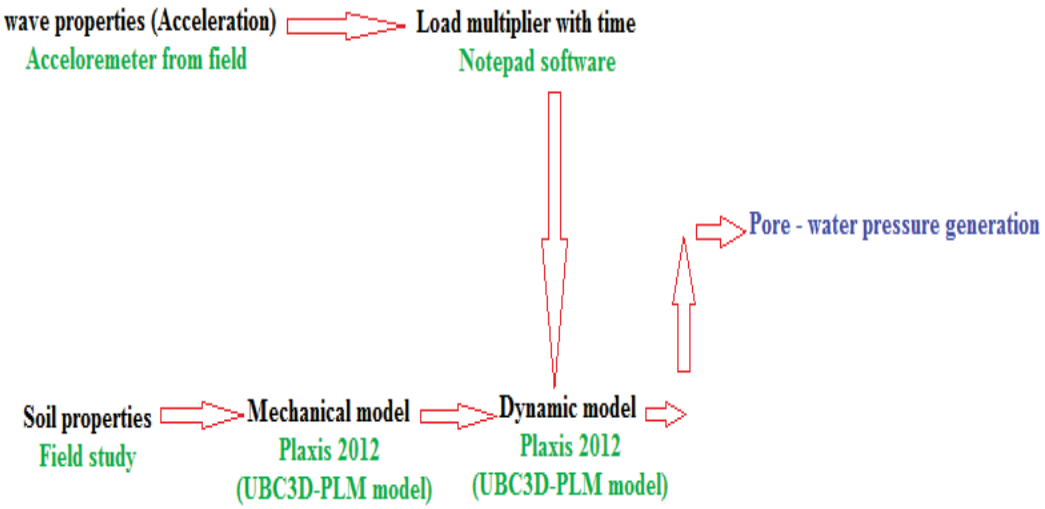

Figure 2.21 the procedure of numerical modeling with PLAXIS

11.3. Results of UBC3D-PLM modeling

The UBC3D-PLM model for Wildlife Site in PLAXIS has been modeled. The model has been calculated for 60 second under dynamic loading. The photos of results have been shown in figure 2.22 to 2.26.

Table 2.6 UBC3D-PLM model parameters of Wildlife Site

Parameters	Symbol	Unit	I	II	III	IV	V
Depth		m	0 – 1.2	1.2 – 2.5	2.5 – 3.5	3.5 – 6.8	< 6.8
Type of soil			Sandy silt	Sandy silt	Sandy silt	Silty sand to fine sand	Clayey silt to silty clay
Young modulus	E_{ref}	kN/m^2	4.71e4	4.41e4	7.28e4	7.28e4	9.45e4
Poisson 's ratio	ν	-	0.25	0.25	0.3	0.3	0.322
Unit weight phreatic level	γ_{unsat}	kN/m^3	16.0	19.4	19.7	19.7	20.0
Unit weight below phreatic level	γ_{sat}	kN/m^3	16.0	21.6	21.8	21.8	22.0
Void ratio	e_{init}	-	0.6799	0.7955	0.7400	0.7400	0.6878
Constant volume friction angle	φ_{cv}	(°)	21.3	20	22	22	35
Peak friction angle	φ_p	(°)	21.9	20.625	22.765	23.065	36
Cohesion	c	kPa	2.00	2.00	0	0	0
Elastic Shear Modulus	K_G^e	-	788.2	798.9	854.6	954.1	934.3
Plastic Shear Modulus	K_G^p	-	185.1	193.6	250	424.7	380.3
Elastic Bulk Modulus	K_B^e	-	551.7	559.3	598.2	667.9	654
Elastic Shear Modulus Index	n_e	-	0.5	0.5	0.5	0.5	0.5
Elastic Bulk Modulus Index	m_e	-	0.5	0.5	0.5	0.5	0.5
Plastic Shear Modulus Index	n_p	-	0.5	0.5	0.5	0.5	0.5
Failure Ratio	R_f	-	0.841	0.836	0.811	0.771	0.779
Atmospheric pressure	P_A	KPa	100	100	100	100	100
Tension Cut-off	σ_t	KPa	0	0	0	0	0
Densification Factor	fac_{hard}	-	0.45	0.45	0.45	0.45	0.45
SPT value	$N1_{60}$	-	6	6.25	7.65	10.65	10
Post Liquefaction Factor	fac_{post}	-	0.2	0.2	0.2	0.2	0.2
Permeability	K	m/s	$5.0*10^{-7}$	$5.0*10^{-7}$	$5.0*10^{-7}$	$2.0*10^{-4}$	$1.0*10^{-4}$
Tangent stiffness for oedometer	E_{oed}^{ref}	KPa	56520	52920	98000	98000	136138
Cohesion	c	kPa	2.00	2.00	$1.0*10^{-4}$	$1.0*10^{-4}$	$1.0*10^{-4}$
Constant volume friction angle	φ_{cv}	(°)	21.3	20	22	22	35
Dilatancy angle	Ψ	(°)	21.3	20.0	19.0	18.0	5.0

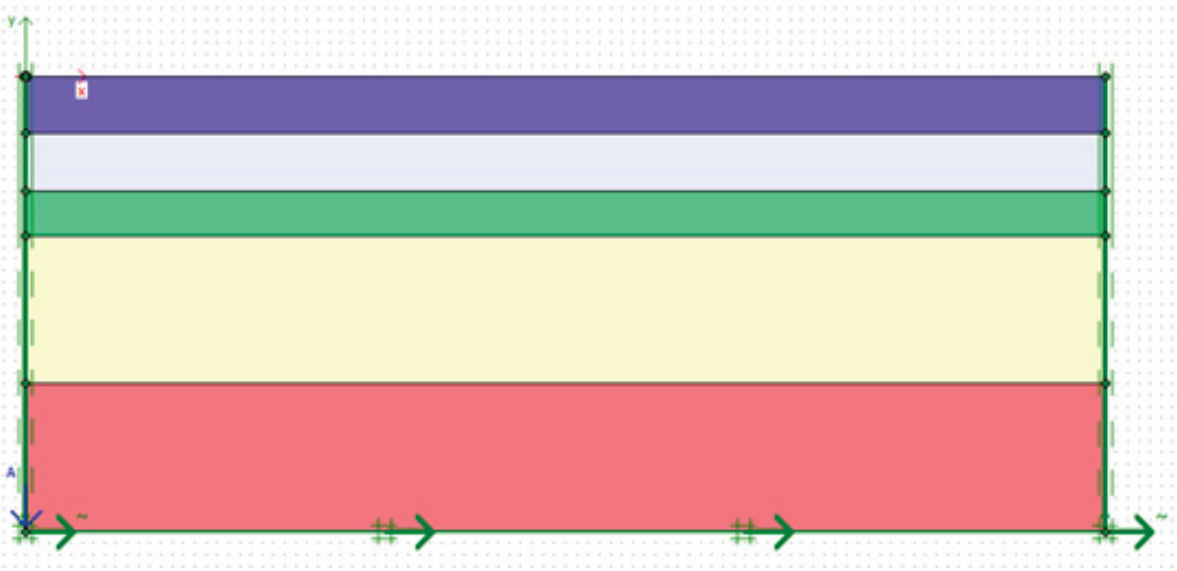

Figure 2.22 Geometry‘s model of wildlife site in Plaxis

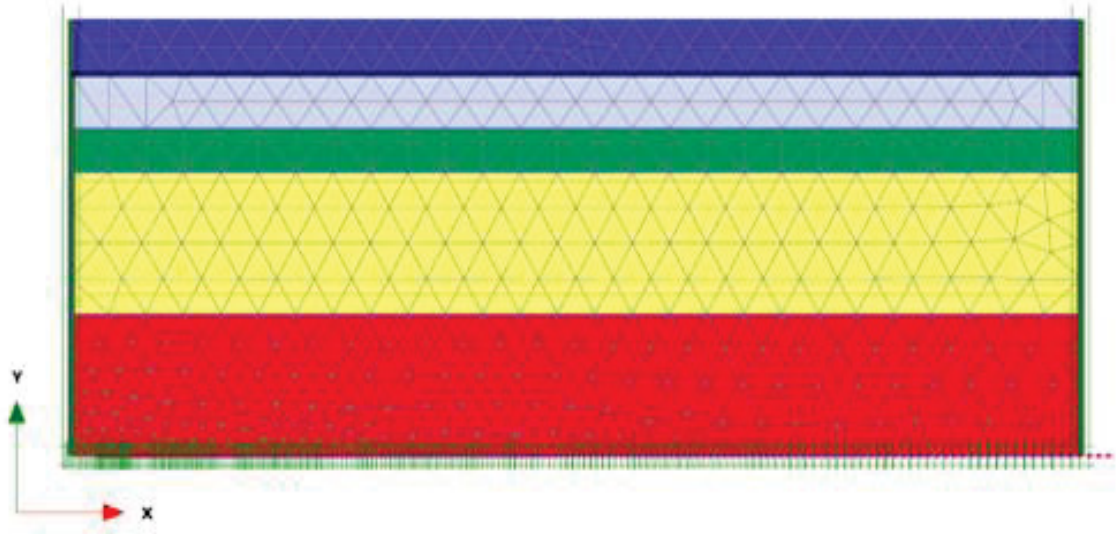

Figure 2.23 Generated mesh of Wildlife site in Plaxis

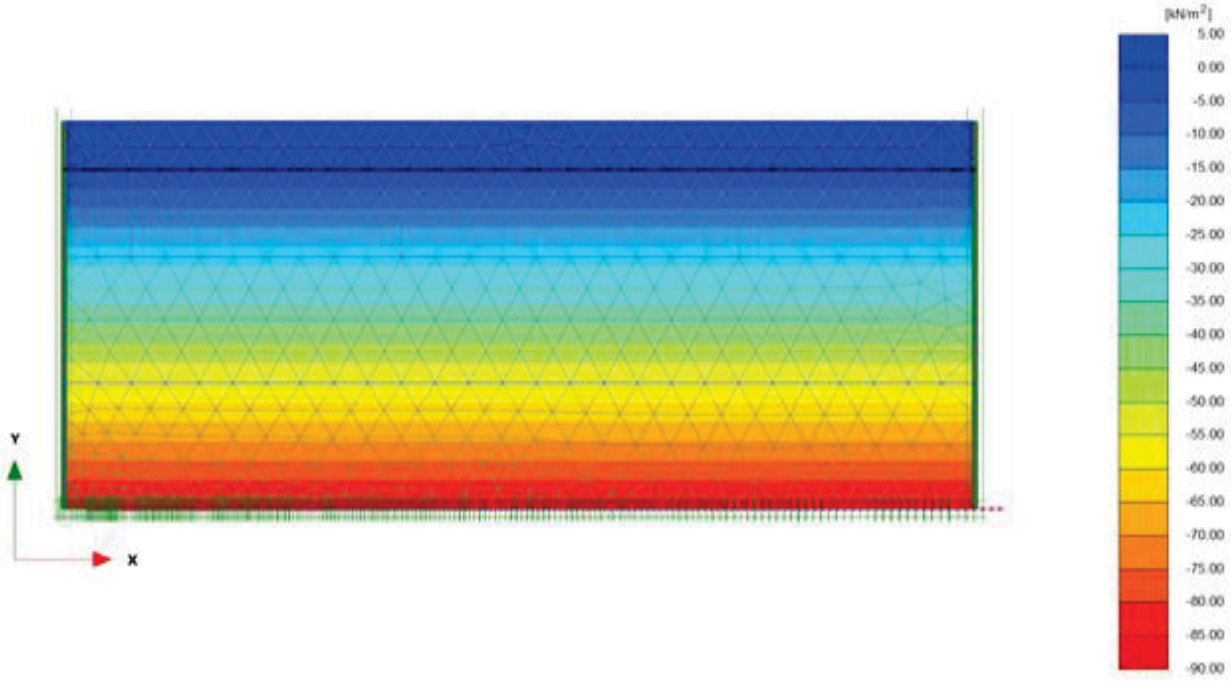

Figure 2.24 pattern of pore-water pressure of Wildlife site in PLAXIS

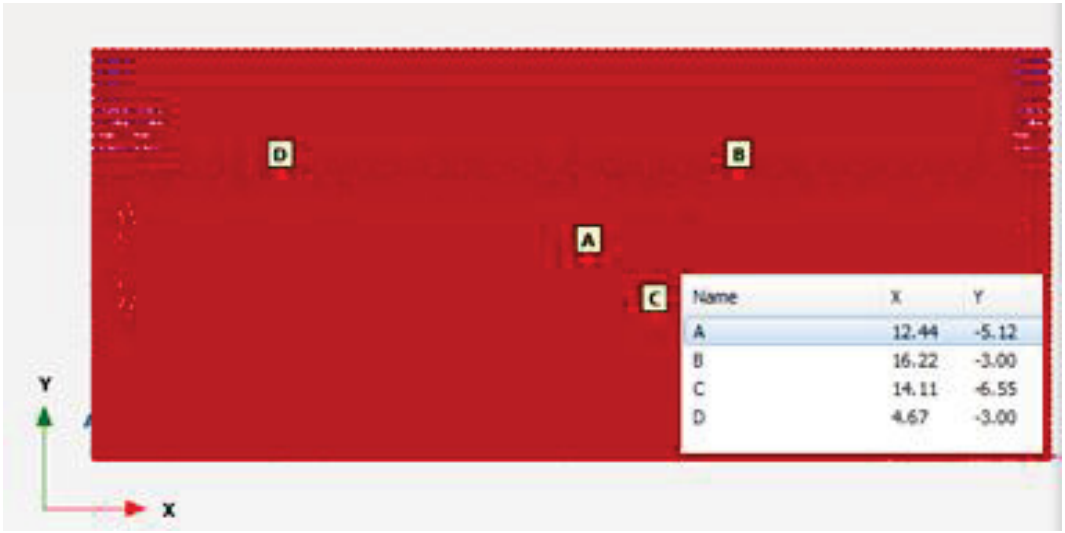

Figure 2.25 Determination of instruments in Wildlife site

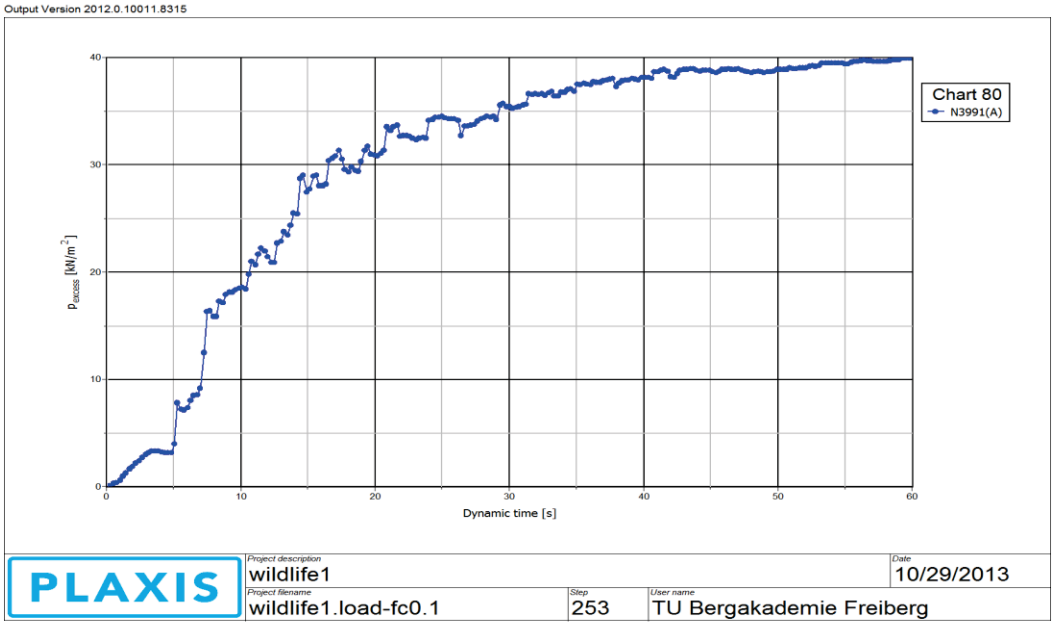

Figure 2.26 Excess pore-water pressure of Piezometer 1 in Wildlife Site

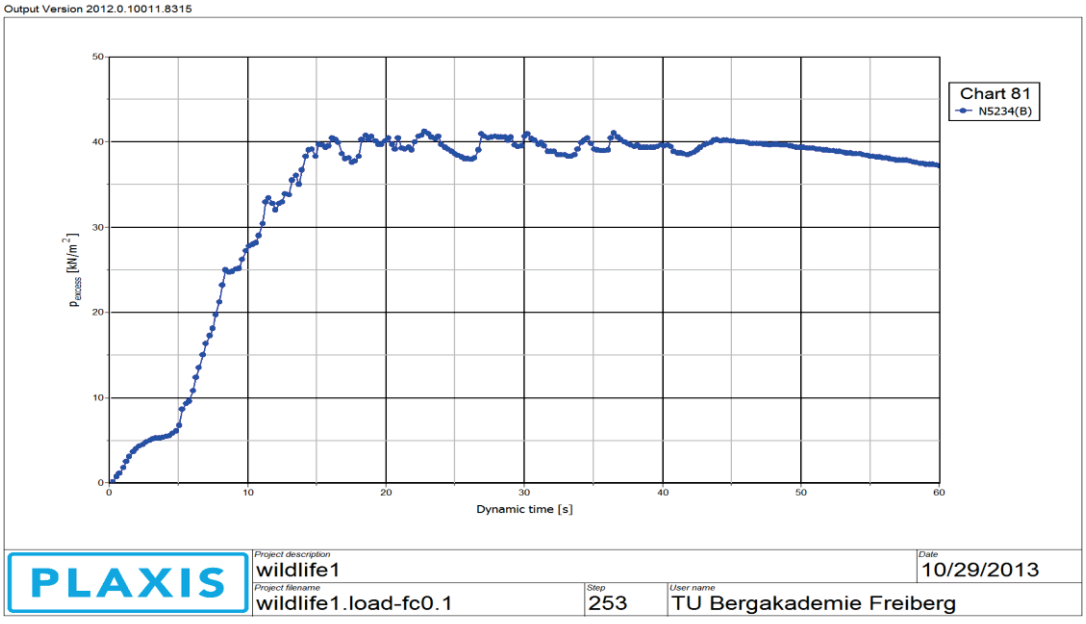

Figure 2.27Excess pore-water pressure of Piezometer 2 in Wildlife Site

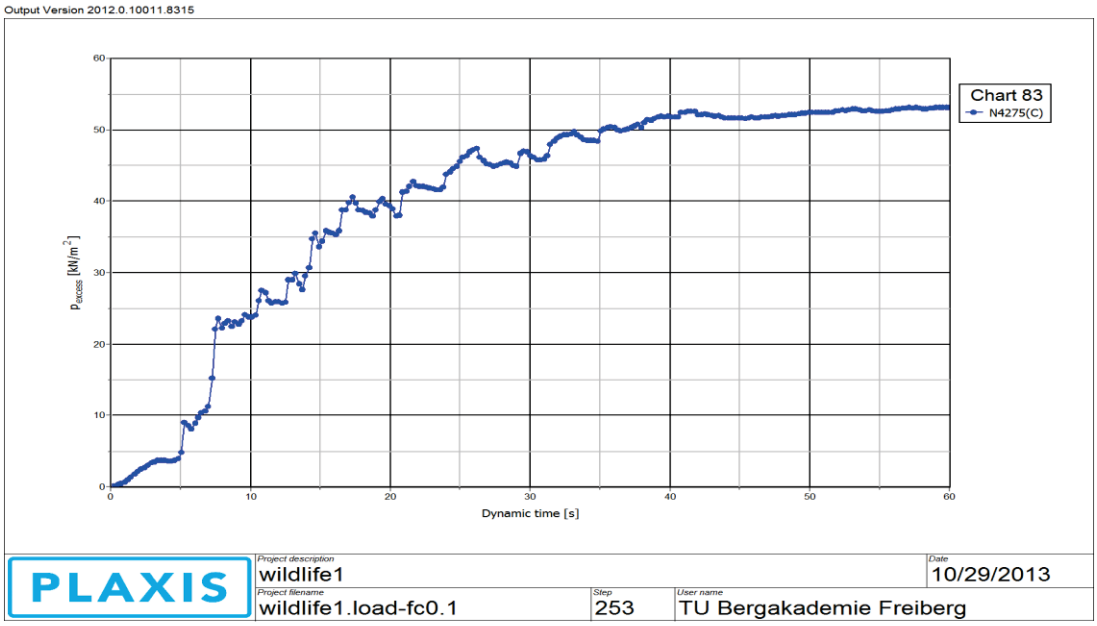

Figure 2.28 Excess pore-water pressure of Piezometer 3 in Wildlife Site

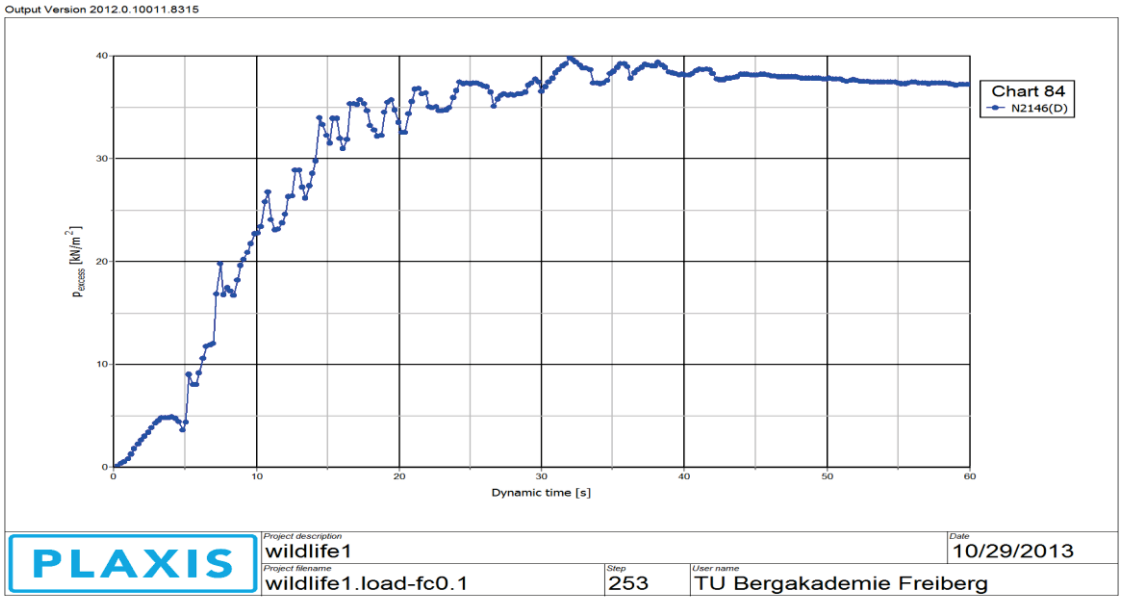

Figure 2.29 Excess pore-water pressure of Piezometer 5 in Wildlife Site

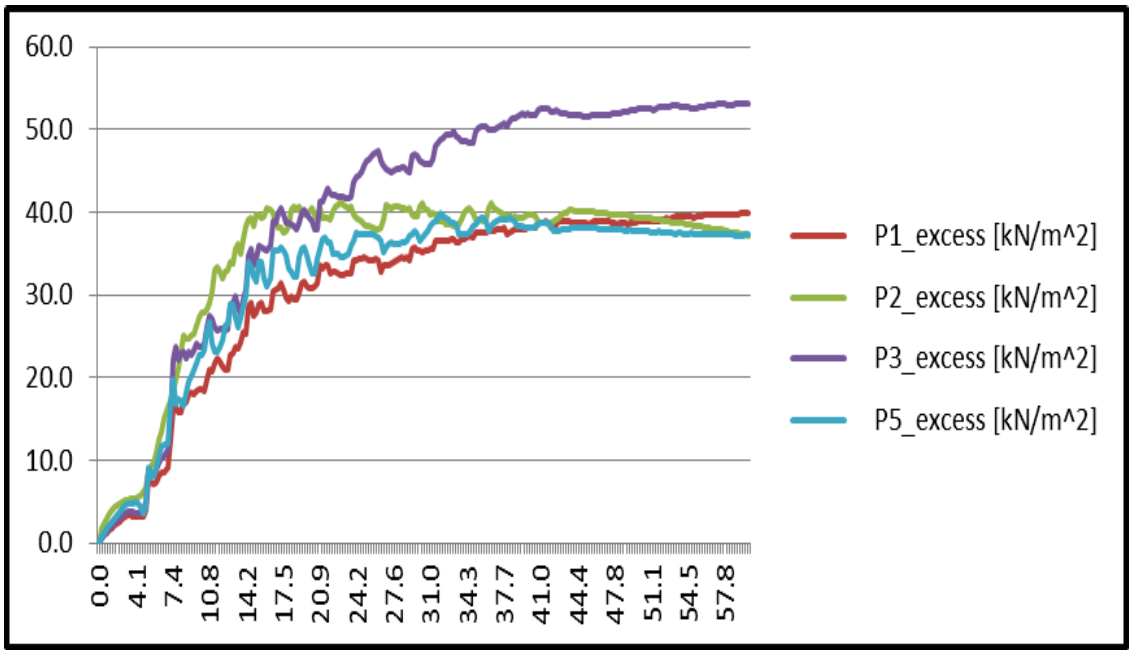

Figure 2.30 Excess pore-water pressures of Piezometers in Wildlife Site

1. Overview

Over the past 30 years, several researches have been presented the studies to develop the correlation between liquefaction, dynamic loading and seismic parameters. Nevertheless this correlation developed using conventional methods are based on limited experimental data and do not provide stable and accurate predictions. The main drawback of these equations is that they do not reflect the complex structure and spatial variability of the soils and liquefaction. Because the soils have fairly complex structures, imprecise physical properties and spatial variability associated with the formation of them. Therefore, their mechanical and dynamic characteristics exhibit the uncertain behavior in contrasts to most of the other engineering materials (Jaksa, 1995). The soft computing approaches such as Fuzzy logic, neural network, Genetic algorithm and hybrid of them which allows developing a model for the complex systems have recently emerged (Goh, 1995, Ural & Saka, 1998, Youd & Gilstrap, 1999, Moss et al., 2003, Shahinet al., 2003, Tutmez & Tercan, 2007, Baykasoglu et al., 2008, Kayadelen et al., 2009, Daftari et al, 2011).

The main purpose of this chapter is to present new approaches based on hybrid of neural network and fuzzy logic for the prediction of the liquefaction phenomena. For this reason, this method was named NFLP (Neural network & Fuzzy logic & Liquefaction & Prediction).

Firstly the fuzzy logic theory and its structure will be presented. In second part the neural network method has been introduced. In third step, NFLP model base on literature data gathering from a lot of research has been made; and in final, the NFLP model has been used for prediction of Wildlife liquefaction. In continue the results of this application will be presented.

2. Fuzzy sets and uncertainties

Uncertainty is the privation of necessary knowledge to make a decision. In geotechnical problems, the results of analyses are greatly influenced by the uncertainties of mechanical characteristics. In contrast, fuzzy set theory enables to present a soft approach for quantifying these ambiguities by efficient participation of engineer's view. As the fuzzy models can cope with the complicated and

ill-defined systems in a flexible and consistent manner, their applications in solving various problems in the field of Geotechnics / Geomechanics have been observed during the past three decades.

3. Classical and Fuzzy sets theory

The fuzzy set was firstly introduced in 1965 by Lotfi Zadeh as a mathematical method to represent linguistic Vagueness (Zadeh, 1965). It can be considered as a generalization of classical set theory. In a classical set, an element belongs to or does not belong to a set. That is, the membership of an element is crisp (0, 1), and an ‘‘A’’ crisp set of real objects are described by a unique membership function such as *XA* in Figure 1a. Contrary, a fuzzy set is a generalization of an ordinary set which assign the degree of membership for each element to range over the unit interval between 0 and 1 (Figure 1b). Values close to 0 indicate a low grade of membership, whereas values close to 1 indicate a high grade of membership. That is, the transition from ‘‘belong to a set’’ to ‘‘not belong to a set’’ is gradual, and this smooth transition is characterized by the membership function that give fuzzy sets flexibility in modeling commonly used linguistic expressions such as ‘‘the cohesion of soil is high’’.

That is so clear; the mathematical operation of Fuzzy sets is completely different with classic one. Nevertheless in this thesis only the application of Fuzzy logic is important. Despite this difference, this chapter does not consist of mathematical operation education.

4. Fuzzy inference system

Fuzzy inference is the process of formulating the mapping from a given input to an output using fuzzy logic. The mapping then provides a basis from which decisions can be made, or patterns discerned. The process of fuzzy inference involves all of the pieces that are described in Membership Functions, Logical Operations, and If-Then Rules.

The Fuzzy inference system has three main parts:

- Fuzzification stage,
- Inference engine,
- Defuzzfication.

The main components of the fuzzy inference system are shown in figure 3.2.

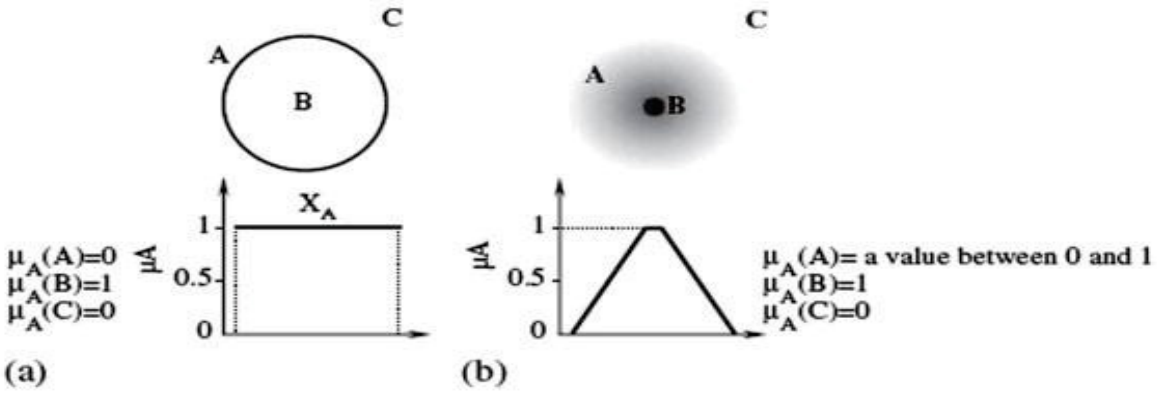

Figure 3.1 (a) Crisp set and (b) fuzzy set (Daftari et al., 2010).

4.1. Fuzzification

In the process of fuzzification, membership functions defined on input variables are applied to their actual values so that the degree of truth for each rule premise can be determined. Fuzzy statements in the antecedent are resolved to a degree of membership between 0 and 1:

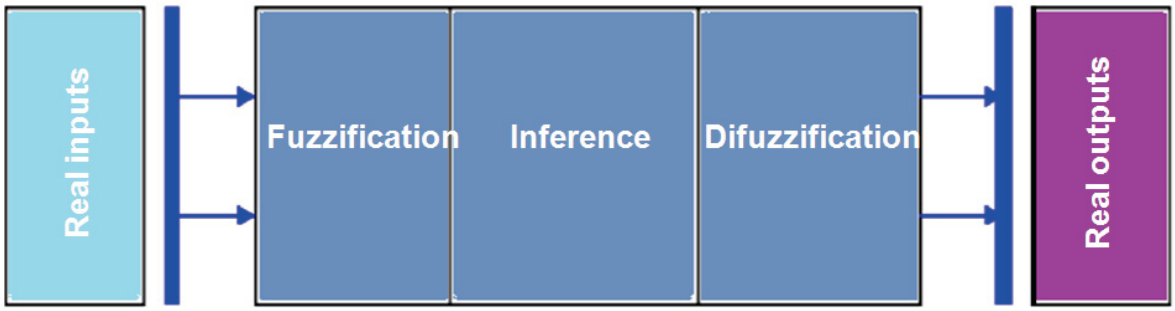

Figure 3.2 Main components of the fuzzy inference system (Daftari et al., 2011)

- If there is only one part to the antecedent, then this is the degree of support for the rule.
- If there are multiple parts to the antecedent, apply fuzzy logic operators and resolve the antecedent to a single number between 0 and 1.

Antecedent may be joined by OR; AND operators.

- For OR -- max
- For AND -- min

4.2. Inference engine base in If – Then rules

The fuzzy inference system (FIS) is a popular computing framework based on the concepts of fuzzy set theory, fuzzy "if–then" rules, and fuzzy reasoning. FISs have been successfully applied in various fields such as automatic control, data classification, decision analyses, expert systems, and computer vision. Because of their multidisciplinary nature, FISs are associated with a number of names such as fuzzy rule-based systems, fuzzy expert systems, fuzzy modeling, fuzzy associative memory, fuzzy logic controllers or simply fuzzy models (Jang et al., 1997).

In the inference stage, the fuzzy propositions are represented by an implication function. The implication function is called fuzzy "if–then" rule. A fuzzy "if–then" rule assumes the form "if x is A then y is B" where A and B are linguistic values defined by fuzzy sets on universes of discourse X and Y, respectively. Often "x is A" is called the antecedent or premise, while "y is B" is called the consequence or conclusion. Thus each fuzzy rule consists of two parts. One part is the premise and other part is conclusion and their writing's form is "IF premise THEN consequent" (Jang et al. 1997).

The basic structure of a FIS consists of three conceptual components:

- Rule base,
- Database,
- Reasoning mechanism.

A rule base, which covers the selection of rules; a database, which expresses the membership functions used in the fuzzy rules; and a reasoning mechanism, which performs the inference procedure upon the rules and given facts to derive a reasonable output or conclusion. Basic FIS can take either fuzzy inputs or crisp inputs, but the outputs which it produces are only fuzzy sets. In cases where a crisp value is needed, defuzzification method should be done (Daftari et al., 2011).

There are several FISs that have been employed in various applications. The most commonly used are: Mamdani model, Takagi–Sugeno–Kang (TSK) model and Tsukamoto model. The differences between these FISs lie in the consequents of their fuzzy rules, thus their aggregation and defuzzification procedures differ accordingly.

4.2.1. Mamdani fuzzy Inference System

The Mamdani is widely used since this model is easier to interpret and analyze when compared with the others. The Mamdani algorithm is perhaps the most appealing fuzzy method to employ in engineering geological problems (Grima, 2000). The general "if-then" rule structure of the Mamdani algorithm is given in the following equation:

R_i : If "$x1$" is "A_i1" and "$x2$" is "A_i2" and...
"xr" is "A_ir" then "y" is "B_i" (for $i = 1,2,..,k$) (3.1)

Where:

k is the number of rules,
x_i is the input variable and ,
y is the output variable.

Although many methods of composition of fuzzy relation (e.g. min–max, max–max, min–min, max–mean, etc.) exist in the literature, max-min and max-product method are the two most commonly used techniques (Ross, 1995). Figure 2 is an illustration of a two-rule Mamadani FIS which derives the overall output z when subjected to two crisp inputs x and y (Janget al., 1997).

4.2.2. Takagi–Sugeno–Kang fuzzy Inference System (TSK)

One of the basic differences between the Mamdani and TSK fuzzy structures is the fact that the consequents are, respectively, fuzzy and crisp sets. Hence, the procedures involved in the computation of the output signals are distinct. While in the case of TSK fuzzy structure the output is computed with a very simple formula (weighted average, weighted sum), Mamdani fuzzy structure require higher computational effort because one is required to compute a whole membership function which is then defuzzyfied. This advantage to the TSK approach makes it highly useful in spite of the more intuitive nature of Mamdani fuzzy reasoning in terms of dealing with uncertainty.

A typical rule-based TSK fuzzy structure with two inputs and one output expressed as:

If a is A_i and b is B_i then y is y_i (3.2)

Where:

$Ai \in \{A1,...,A^{NA}\}$
$Bi \in \{B1,...,B^{NB}\}$

They represent the antecedent MF of the i^{th} rule that corresponds to the input variables a, b respectively. The sets $\{A1,...,A^{NA}\}$ and $Bi \in \{B1 ,...,B^{NB}\}$ are predefined antecedent MFs. The i^{th} rule produces a partial output of form:

$$y_i = f_i (a,b) \quad (3.3)$$

Where:

f_i are predefined functions. In the present work,

$$f_i (a,b) = r_i \; \forall \; a,b \quad (3.4)$$

With r_i = constant.

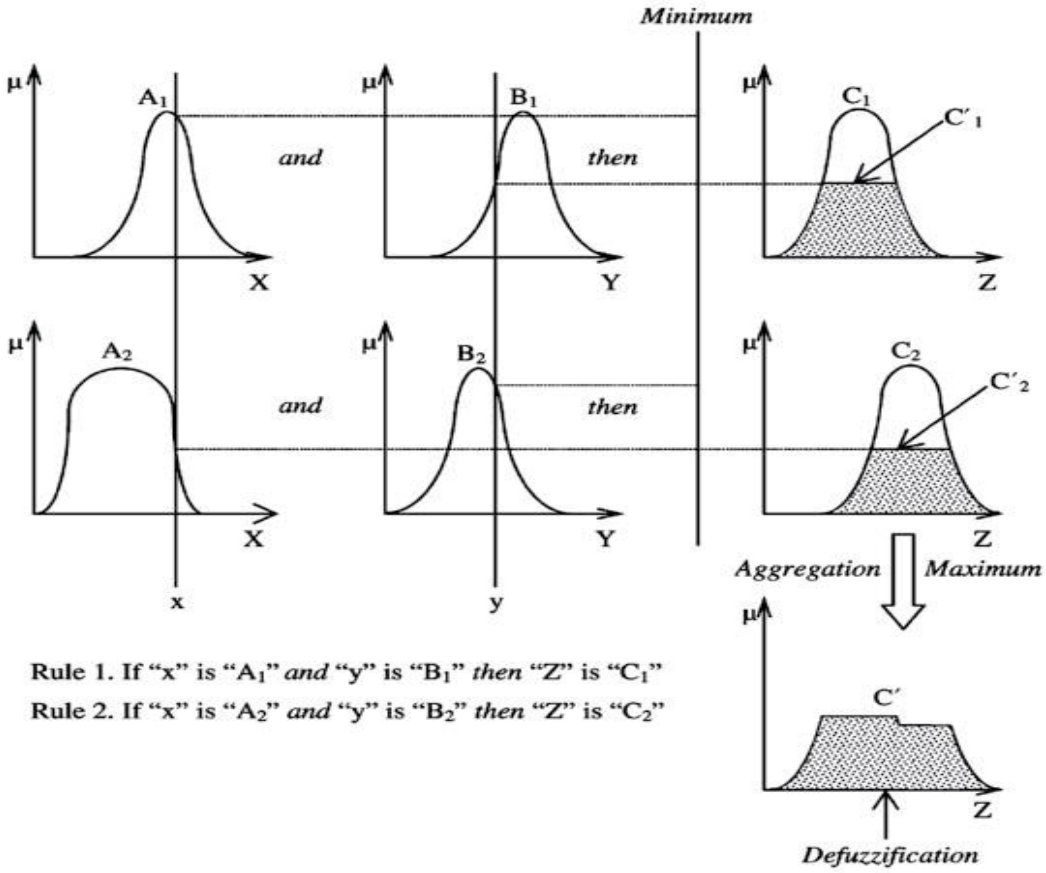

Figure 3.3 The Mamdani FIS (Jang et al., 1997)

Therefore characterizing a crisp consequent MF for the i^{th} rule. The adoption of a particular f_i is required for comparison purposes with respect to Mamadani fuzzy structures. Aggregating the partial outputs of each rule, the output is given by:

$$y = \frac{w1.y1+w2.y2}{w1+w2} \tag{3.5}$$

Where:

w_i = AND($\mu_{Ai}(a)$, $\mu_{Bi}(b)$) is the weight of the i^{th} rule (Schnitman, 2000).

The inference procedure is graphically represented in Figure 3.4.

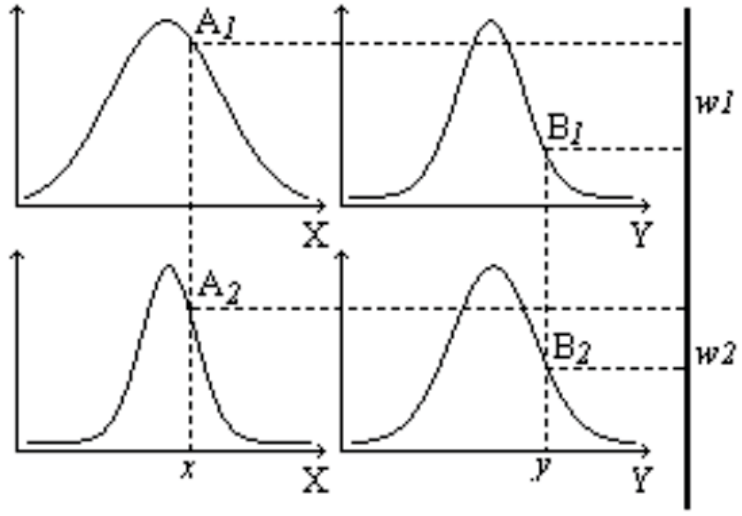

Figure 3.4 TSK rules weight (Schnitman, 2000)

4.2.3. Tsukamoto fuzzy Inference System

In the Tsukamoto fuzzy models, the consequent of each fuzzy if-then rule is represented by a fuzzy set with a monotonical membership function, as shown in Figure 3.5. As a result, the inferred output of each rule is defined as a crisp value induced by the rule's firing strength. The overall output is taken as the weighted average of each rule's output. Figure 3.5 illustrates the reasoning procedure for a two-input two-rule system.

Since each rule infers a crisp output, the Tsukamoto fuzzy model aggregate each rule's output by the method of weighted average and thus avoids the time-consuming process of defuzzification. However, the Tsukamoto fuzzy model is not used often since it is not as transparent as either the Mamdani or Sugeno fuzzy models.

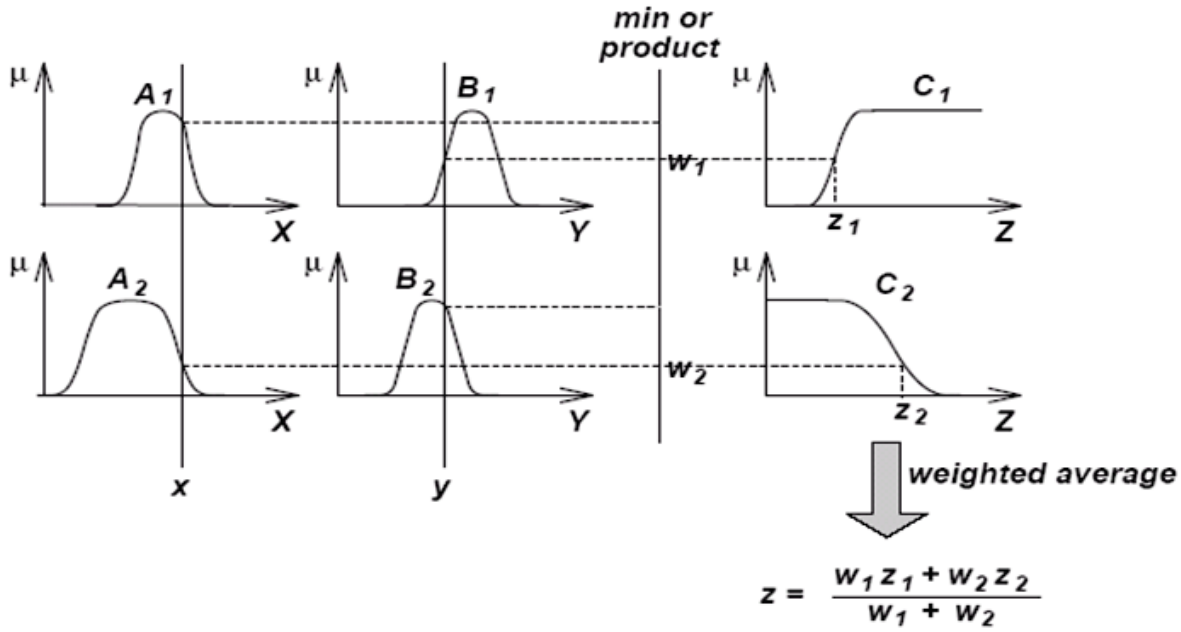

Figure 3.5 The Tsukamoto fuzzy model (www.bindichen.co.uk)

4.3. Defuzzification methods

Defuzzification refers to the way in which a crisp value can be extracted from a fuzzy set as a representative value. The purpose of defuzzification is to convert each conclusion obtained by the inference, expressed in terms of a fuzzy set, to a single real number. Although there are a number of defuzzification methods in the literature such as centroid of area (COA) or center of gravity, mean of maximum, smallest of maximum, etc. The most widely adopted defuzzification method is COA method (Lee, 1990). In continues some famous methods of defuzzification have been present briefly. Figure 3.6 shows the results of using different defuzzification methods (common) for a particular function.

4.3.1. Center of Area (COA)

The centroid defuzzification method selects the output crispy value corresponding to the center of gravity of the output membership function.

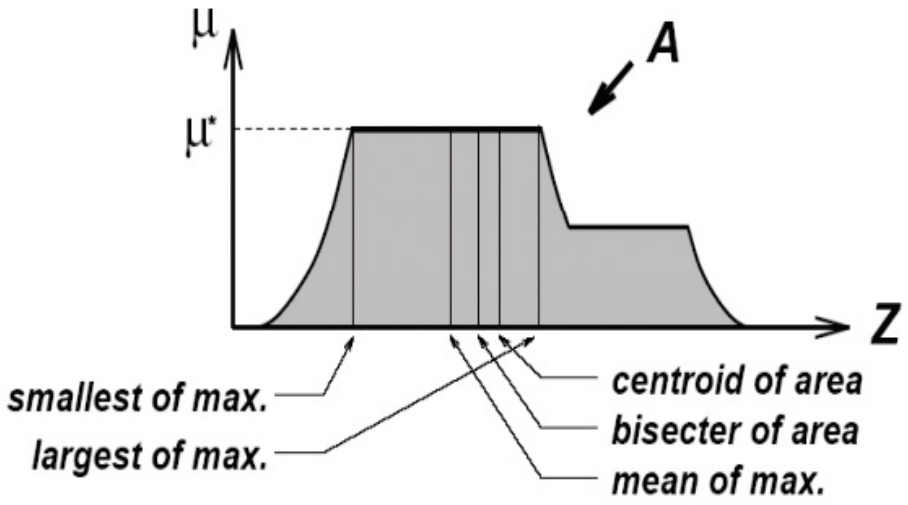

Figure 3.6 Results using different defuzzification methods for a particular function (Naaz et al., 2011)

4.3.2. Center of Sums (COS)

A similar to COA but faster defuzzification method is the center of sums. This method avoids the computation of the union of the fuzzy sets, and considers the contribution of the area of each fuzzy set individually.

4.3.3. Height Method (HM)

In the height method, the centroid of each output membership function for each rule is first evaluated. The final output is then calculated as the average of the individual centroids, weighted by their heights (degree of membership).

4.3.4. Middle of Maxima (MOM)

The MOM strategy generates a control action which represents the mean value of all local control actions whose membership functions reach the maximum.

4.3.5. Center of Largest Area (COLA)

The COLA method is used in the case when universe of discourse is non-convex. It consists of at least two convex fuzzy subsets. Then the method determines the convex fuzzy subset with the largest area and defines the crisp output value, to be the Center of Area of this particular fuzzy subset. It is difficult to represent this defuzzification method formally.

4.3.6. First of Maxima

The FM method uses the union of the fuzzy sets and takes the smallest value of the domain with maximum membership degree.

4.3.7. Height Weighted Second Maxima (HWSM)

In this method, the second maximum of each output membership function for each rule is first evaluated. The final output is calculated as the average of the individual maxima, weighted by their heights (degree of membership).

5. Artificial Neural network model

Artificial neural networks (ANN) try to mirror the brain functions in a computerized way by restoring the learning mechanism as the basis of human behavior. ANN can operate like a black box model, which requires no detailed information about the system or equipment. ANN can learn the relationship between input and output based on the training data.

In the last decades, Artificial neural networks have been used in several applications in Geotechnics, Mining engineering and civil engineering, because of their heuristic problem-solving capabilities. These special applications come from its special ability. It has the ability to simulate the learning capabilities of the human brain by automating the process of knowledge acquisition and data mining. In figure 3.7 one example of Artificial neural networks were illustrated.

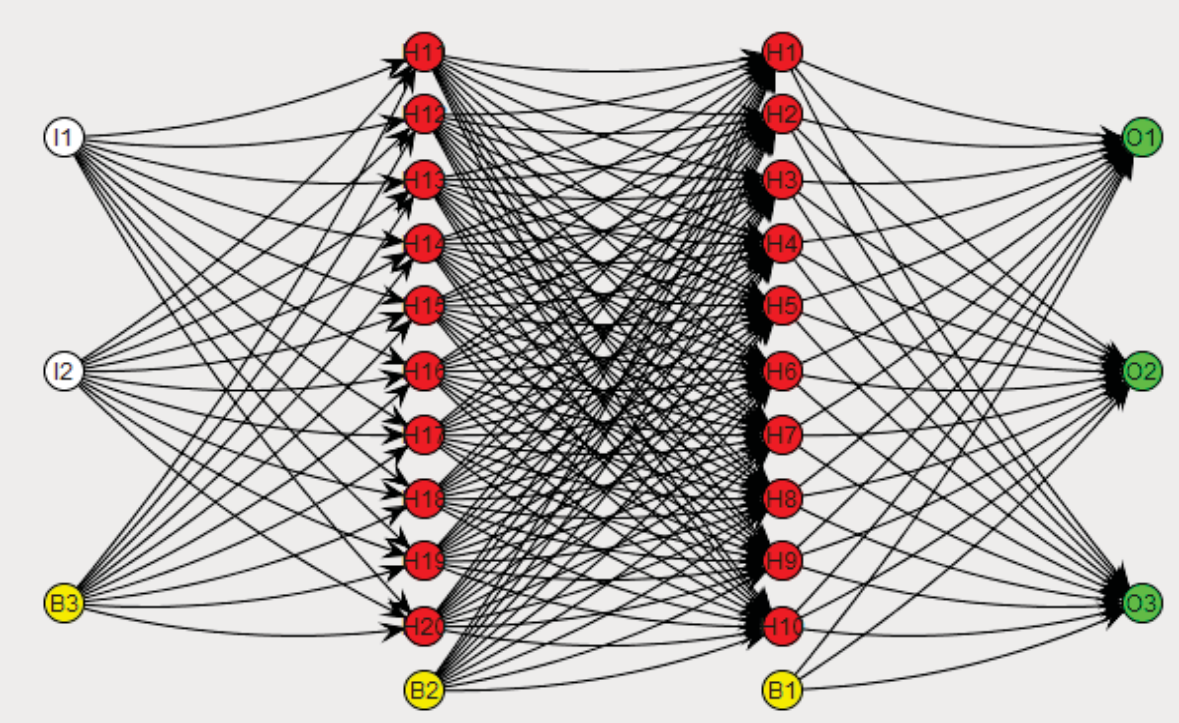

Figure 3.7 examples of Artificial neural networks (www.codeproject.com)

6. Biological Neural Networks and Artificial Neural Networks

Artificial Neural Networks were inspired by models of biological neural networks since much of the motivation came from the desire to produce artificial systems capable of sophisticated, perhaps "intelligent", computations similar to those that the human brain routinely performs, and thereby possibly to enhance our understanding of the human brain (Figure 3.8). Nevertheless the Artificial Neural Networks is simpler than biological neural networks.

The human brain has about 10^{11} neurons and 10^{14} synapses. A neuron consists of a soma (cell body), axons (sends signals), and dendrites (receives signals). A synapse connects an axon to a dendrite. Given a signal, a synapse might increase (excite) or de crease (inhibit) electrical potential. A neuron fires when its electrical potential reaches a threshold. Learning might occur by changes to synapses (Figure 3.9).

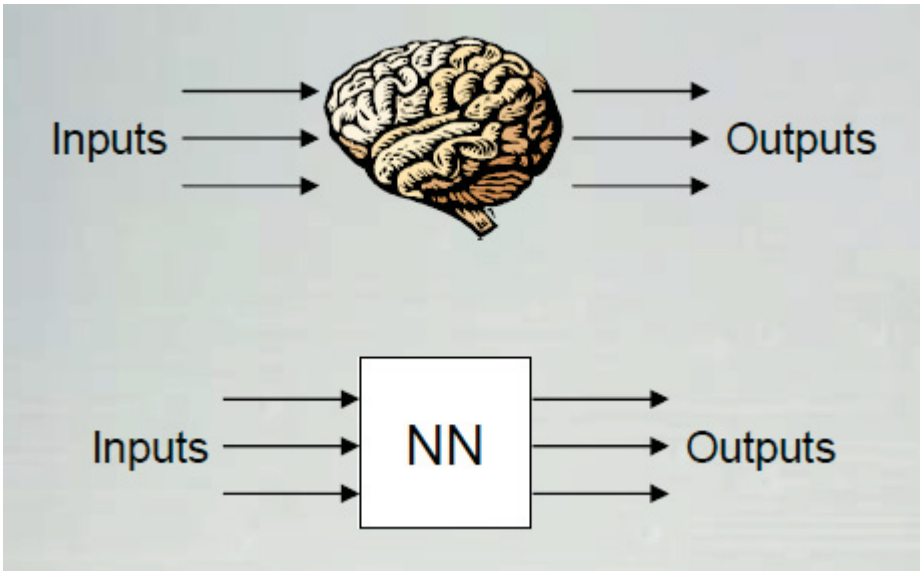

Figure 3.8 ANN inspirations from BNN (www.neuralnetworksanddeeplearning.com)

An (artificial) neural network consists of units, connections, and weights. Inputs and outputs are numeric (Figure 3.10). In table 3.1 main different between biological neural networks and artificial neural networks was presented.

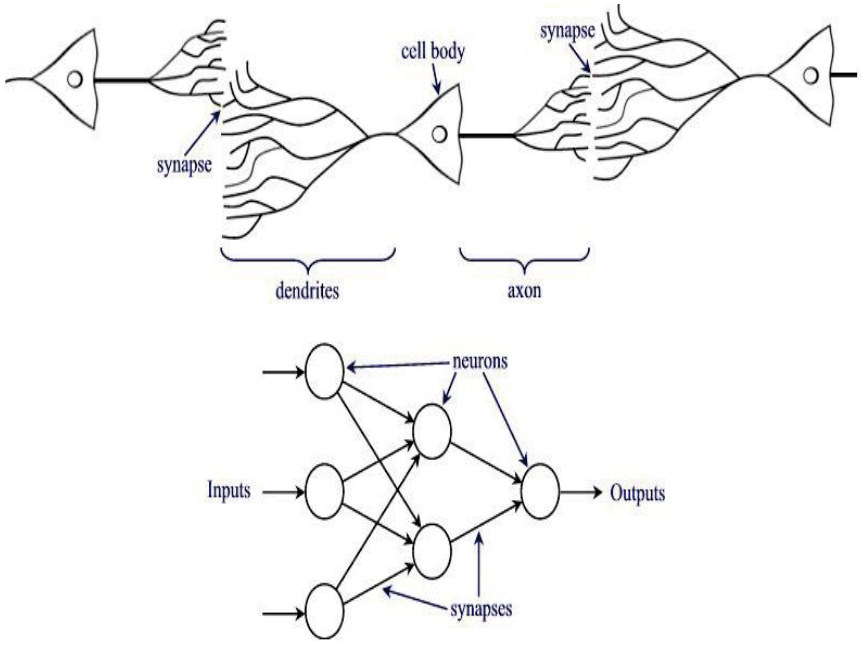

Figure 3.9 Schematic of BNN (www.neuralnetworksanddeeplearning.com)

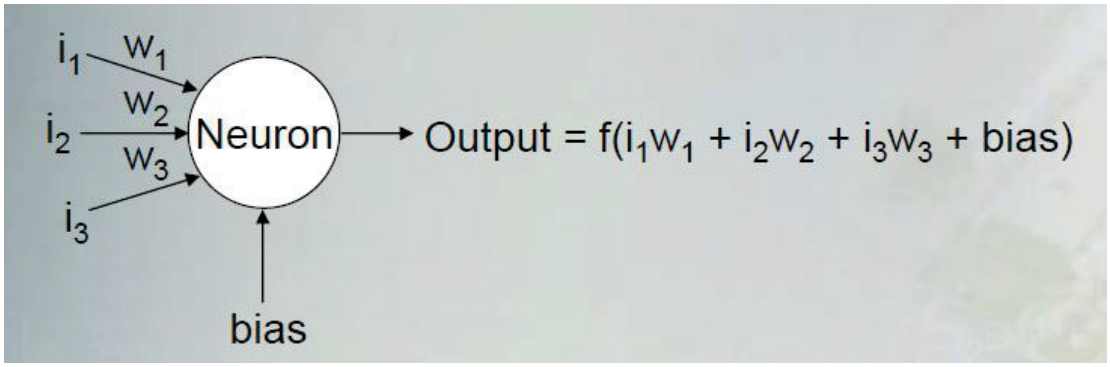

Figure 3.10 Schematic of ANN (www.neuralnetworksanddeeplearning.com)

7. Artificial neural network structure

The basic structure of neural networks has been explained with several researchers. A typical back-propagation artificial neural network is shown in figure 3.11.

Table 3.1 Main different between BNN and ANN

biological neural networks	Artificial Neural Networks
Soma	Unit
Axon & Dendrite	Connection
Synapse	Weight
Potential	Weighted Sum
Threshold	Bias Weighted
Signal	Activation

The various n (i) taken together form an S-element vector n. Finally, the neuron layer outputs form a column vector a. The layers of a multilayer network play different roles. The layer that produces the network output is called an output layer. The layer that gets the inputs is called input layer. All other layers are called hidden layers. It is common for the number of inputs to a layer be different from the number of neurons.

A network can have several layers. The outputs of each intermediate layer are the inputs to the following layer. Each layer has a weight matrix W, a bias vector b, and an output vector a. Each

element of the input vector p is connected to each neuron input through the weight matrix W. The i^{th} neuron has a summer that gathers its weighted inputs and bias to form its own scalar output n(i). The network shown in figure 3.11 has R inputs (R neurons in the input layer), S1 neurons in the hidden layer, and S2 neurons in the output layer. The number of hidden layers can be varied based on the application. A constant input value of 1 is fed to the biases for each neuron (Rahman & Wang, 2002, Rumelhart & McClelland, 1986, Lippmann, 1987, Flood & Kartam, 1994).

Designation of artificial neural network has two main stages:

- Learning rolls,
- Training stage.

These to phase have been explanted in continue.

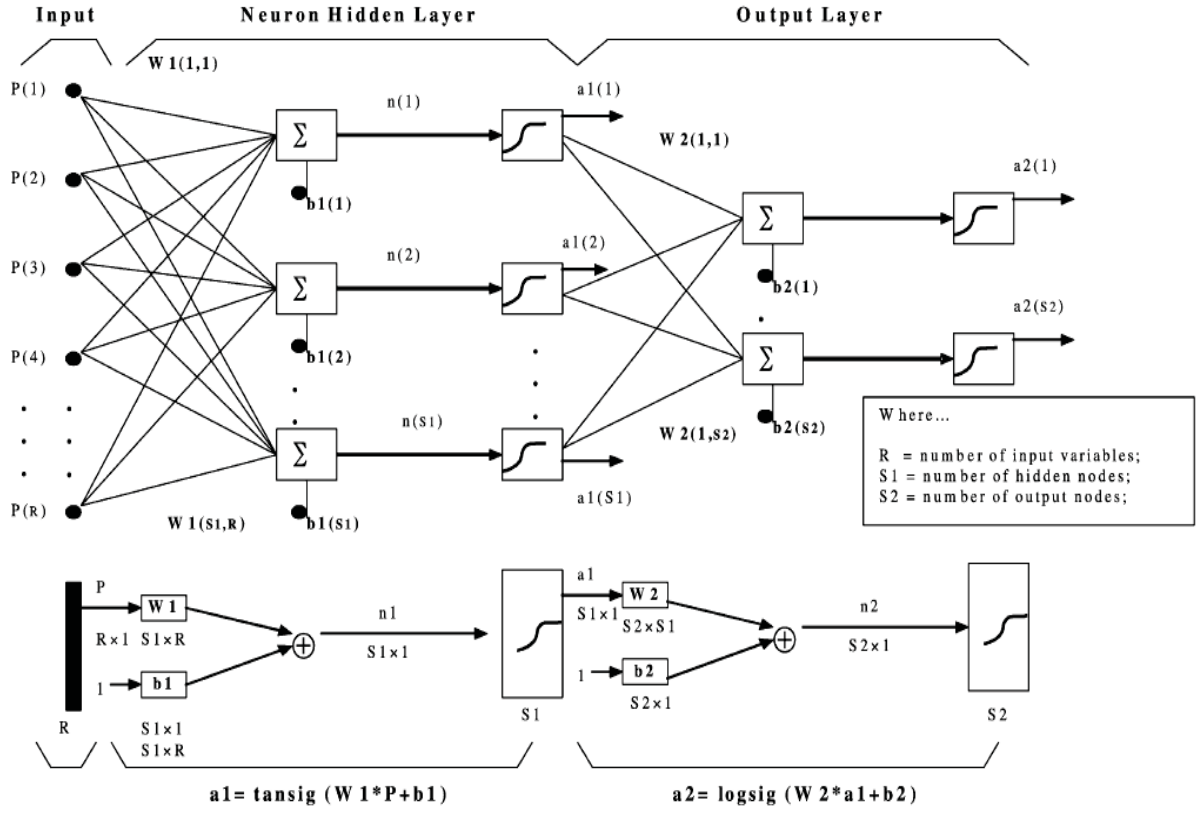

Figure 3.11 The architecture of artificial neural network (www.neuralnetworksanddeeplearning.com)

8. Learning rule

The most interesting characteristic of neural networks is their capability to familiarize with problems by means of training and, after sufficient training, to be able to solve unknown problems of the same class.

Neural network could learn from many things but, of course, there will always be the question of how to implement it. In principle, a neural network changes when its components are changing, as we have learned above. Theoretically, a neural network could learn by:

- Developing new connections,
- Deleting existing connections,
- Changing connecting weights,
- Changing the threshold values of neurons,
- Varying one or more of the three neuron functions (remember: activation function, propagation function and output function),
- Developing new neurons, or
- Deleting existing neurons (and so, of course, existing connections).

The learning methods in neural networks are classified in to three basic types:

- Supervised learning,
- Unsupervised learning,
- Reinforced learning.

These three types of learning roles based on two differences:

- Presence or absence of teacher,
- The information provided for the system to learn.

Base on the rules learning methods have four categories:

- Hebbian,
- Gradient descent,
- Competitive,
- Stochastic.

Figure 3.12 shows the classification of learning algorithms. Table 3.2 presents the main characters of three main categories of learning methods.

9. Training Stage

The preparation neural network consists of two stages: train and test. Firstly, neural networks learn the relationship between input-output from an educational group, then are tested against an educational group which is not given the network during the training to measure the generalization capability of the network, the power of trained network and understanding of input-output relationship. Education will be repeated by adjustment of parameters until logical and right outputs are produced by appropriate inputs.

Selecting data for training the neural networks is one of the most important steps for developing the neural network. Neural networks are powerful in interpolation against of extrapolation. So, the selection of training data is important because it should cover all aspects of the problem. The other point in the input of information to network is ignorance of law or a specific sort because random delivery of information leads to better training power and thus, neural network do better function. If input data is sorted, it will be possible that neural network will not learn the data and just will store them. This state is not desirable and the network loses its learning power.

10. Combination of Fuzzy logic and artificial neural network

Adaptive Neuro Fuzzy Interface System or ANFIS is a multi-layer feed forward network. This model consists of nodes and directional links, which combines the learning capabilities of a neural network and reasoning capabilities of fuzzy logic (Jang, 1993). The structure of ANFIS is depicted in figure 3.13.

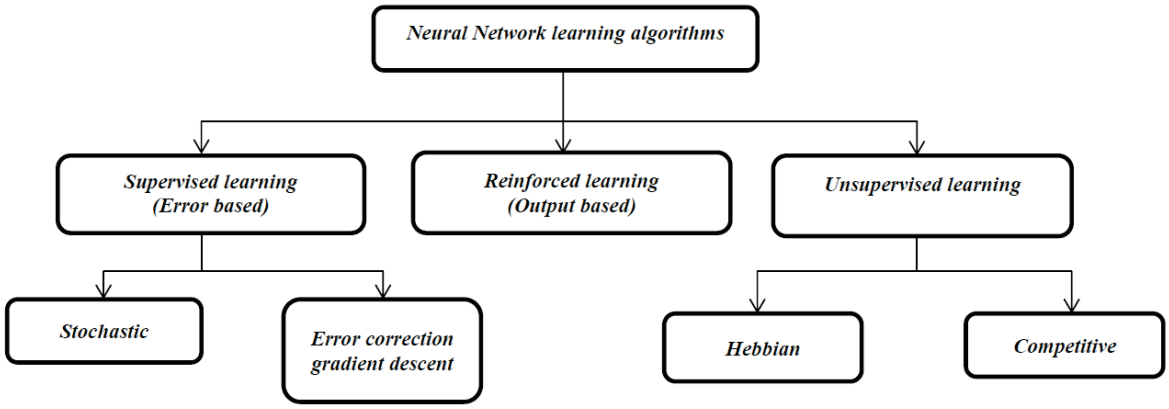

Figure 3.12 the classification of learning algorithms

Table 3.2 main characters of main categories of learning methods.

Supervised learning	- A teacher is present during learning process and presents expected output. - Every input pattern is used to train the network. - Learning process is based on comparison, between network's computed output and the correct expected output, generation error. - The error generation used to change network parameters that result improved performance.
Unsupervised learning	- No teacher is present. - The expected or desired output not presented to the network. - The system learns of its own by discovering and adapting to the structural features in the input patterns.
Reinforced learning	- A teacher is present but does not present the expected or desired output but only indicated output is correct or incorrect. - The information provided helps the network in its learning process. - A reward is given for correct answer computed and penalty for wrong answer.

This hybrid structure of the network (ANFIS) can extend the prediction capabilities beyond ANN and fuzzy logic techniques when they are used alone. ANFIS architecture consists of fiver layers. The first layer in the network is called fuzzy layer. The adjustable nodes in this layer are represented by square nodes and marked by A_1, A_2, B_1 and B_2 with x and y outputs.

The second layer is called product layer and every node in this layer is a fixed node marked by a circle node and labeled by M. The outputs w_1 and w_2 are the weight functions of the next layer.

The third layer is a normalized layer and every node in this layer is a fixed node, marked by a circle node and labeled by N. The nodes normalize the firing strength by calculating the ratio of firing strength for this node to the sum of all the firing strengths.

The fourth layer is the de-fuzzy layer having adaptive nodes and marked by square nodes.

The fifth layer computes the overall system output as the summation of all incoming signals (Mohanraj et al., 2012).

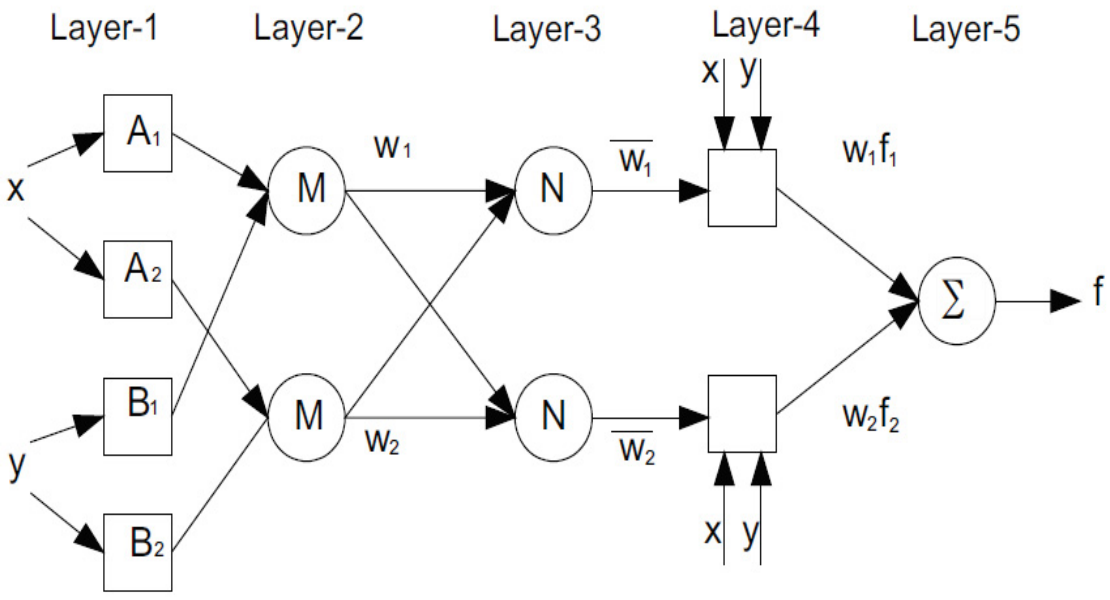

Figure 3.13 Structures of ANFIS(Jang, 1993, Mohanraj et al., 2012)

11. Application of ANFIS to Prediction of Liquefaction

The main purpose of this chapter is to present new approaches based on ANFIS for the prediction of the liquefaction happening of soils (Neural & Fuzzy & Liquefaction & Prediction: NFLP). The data set for training were obtained from the literatures. The Occurrence of liquefaction is used as output. Eight parameters were selected as input parameters. These parameters are:

- Earthquake magnitude (M),
- N-Value ($N1_{60}$),
- Effective overburden pressure (σ'),
- Soil fines content (FC),
- Peak ground acceleration (a_{max}),
- Depth of water (D_w),
- Depth of soil layer (D_s),
- Cyclic stress ratio (CSR).

The procedure of parameters selection will be presented in next part.

12. Selection of principal parameters and case history data for NLFP

As already stated, this part of study intends to estimate the probability of liquefaction in soils. This consideration, is taking account physical and dynamical properties of soil. Researchers have presented several analytic and empirical prediction methods to reach this goal. They have used a lot of parameters to make better relation between input parameters and their goal. Some of these more useful parameters are:

- CPT resistance test (q_c)
- N- value ($N1_{60}$)
- Soil fines content (FC)
- Depth of water (D_w)

- Soil mean grain size (D_{50})

- Depth of soil (D_s)
- Earthquake magnitude (M)
- Peak ground acceleration (a_{max})
- Shear wave velocity (v_s)
- Effective overburden pressure (σ')
- Nearest horizontal distance to seismic source (R)

- Free face ratio (w)
- Thickness of saturated cohesionless soil (T_{15})
- Depth of lowest SPT value (Z_N)
- Depth to lowest SPT $(N1)_{60}$ (Z_{N160})
- $(N1)_{60}$ value corresponding to J_s ($N1_{60s}$)
- Average fines content in T_{15} (F_{15})
- Ground slope (S)
- Thickness of Saturated (T_{20})
- Average fines content in T_{20} (F_{20})
- Cyclic stress ratio (CSR)
- Angle of shear resistance (φ')
- Total vertical stress (σ_{vo})
- Threshold acceleration (a_t)
- Cyclic stress ratio (τ_{av} / σ_{vo})
- Peak horizontal acceleration ratio (a_{max} / g)
- Critical depth of liquefaction (D_{cr})

Table 3.3 consists of the models, which used these parameters. Eight useful parameters were chosen based on table 3.3. These parameters have been used as input parameters for NFLP model. As mentioned before these parameters are:

- Earthquake magnitude (M),

- N-Value ($N1_{60}$),
- Effective overburden pressure (σ′),
- Soil fines content (FC),
- Peak ground acceleration (a_{max}),
- Depth of water (D_w),
- Depth of soil layer (D_s),
- Cyclic stress ratio (CSR).

Moment magnitudes are used for all earthquakes in the updated liquefaction database (Tables 3.4).

Table 3.3 Common models for liquefaction prediction I

	q_c	SPT	FC	D_w	D_{50}	D_s	M	a_{max}	V_s	σ′	R	W	T_{15}	Z_N
Seed et al.		*	*				*	*		*				
Japan railway		*	*		*		*	*		*				
Tokimatsu		*	*				*	*		*				
China simplified		*	*	*		*	*							
Shibata & Teparaks	*				*		*	*		*				
Tokimatsu & Achida		*	*				*	*	*	*				
New Japan railway		*	*		*			*		*				
Zhang I		*		*		*	*							
Zhang II	*				*		*			*				
Wang & Rahman							*	*			*	*	*	*
Kayadelen		*	*							*				
Hanna et al.		*	*	*		*	*	*	*	*				
Rahman & Wang		*		*	*		*			*				

Table 3.3 Common models for liquefaction prediction II

	Z_{N160}	$N1_{60s}$	F_{15}	S	T_{20}	F_{20}	CSR	φ'	σ_{vo}	a_t	τ_{av} / σ_{vo}	a_{max} / g	D_{cr}
Seed et al.													
Japan railway													
Tokimatsu													
China simplified													
Shibata & Teparaks													
Tokimatsu & Achida													
New Japan railway													
Zhang I													
Zhang II													
Wang & Rahman	*	*	*	*	*	*							
Kayadelen							*	*					
Hanna et al.							*	*	*	*			
Rahman & Wang							*		*		*	*	*

The liquefaction databases compiled by Seed et al. (1984) and Cetin et al. (2004) often referenced the earthquake magnitudes that had been refer to in the original case history reference. These original references, nevertheless, often used other scales for the earthquake magnitude. For the

updated database, in this study moment magnitudes obtained from the Next Generation Attenuation (NGA) project flat file (Chiou et al. 2008) and the USGS Centennial Earthquake Catalog (Engdahl & Villasenor, 2002, Idriss & Bounlager, 2010).

Data sets used to develop NFLP models in this thesis were obtained from 24 earthquakes. The data for Superstition Hills earthquakes were applied for test and validation. Finally, the NFLP model was designed with 25 earthquakes data and 2070 parameters. These data were presented in table 3.5. (Liq? 1= happened, 0= not happened). Table 3.6 shows the name of earthquakes and site of measurement.

Table 3.4 Earthquake magnitudes in the liquefaction (Idriss & Boulanger, 2010)

Erthquake	**Seed et al. (1984)**	**Cetin et al. (2004)**	**Idriss & Boulanger (2004)**	**Idriss & Boulanger (2010) and this study**
1944 Tohnankai	8.0	8.0	8.0	8.1
1948 Fukui	7.3	7.3	7.3	7.3
1964 Niigata	7.5	7.5	7.5	7.6
1968 Tokachi-Oki	7.9	7.9 & 7.8	7.9	8.3
1971 San Fernando	6.6	6.6	6.6	6.6
1975 Haicheng	7.3	7.3	7.3	7.0
1976 Guatemala	7.5	7.5	7.5	7.5
1976 Tangshan	7.6	8	8.0	7.6
1977 Argentina	7.4	7.4	7.4	7.5
1978 Miyagiken-Oki – Feb. 20	6.7	6.7	6.7	6.5
1978 Miyagiken-Oki – June 12	7.4	7.4	7.4	7.7
1979 Imperial Valley	6.6	6.5	6.5	6.5
1981 Westmoreland	5.6	5.9	5.9	5.9
1982 Urakawa-Oki	-	-	-	6.9
1983 Nihonkai-Chubu – June 21	-	7.1	7.1	6.8
1983 Nihonkai-Chubu – May 26	-	7.7	7.7	7.7
1987 Superstition Hills	-	6.7 & 6.6	6.5	6.5
1989 Loma Prieta	-	7.0	6.9	6.9
1990 Luzon	-	7.6	7.6	7.7
1993 Kushiro-Oki	-	8.0	8.0	7.6
1994 Northridge	-	6.7	6.7	6.7
1995 Hyogoken-Nambu (Kobe)	-	6.9	6.9	6.9

Table 3.5 Data sets of Earthquake (Idriss & Boulanger, 2010)

	M	a_{max}(g)	Ds(m)	Dw(m)	σ(KPa)	$N1_{60}$	FC (%)	CSR	Liq?
1									
A	8.1	0.2	5.2	2.1	68	8.2	10	0.182	1
B	8.1	0.2	4.3	2.4	61	3.4	30	0.144	1
C	8.1	0.2	3.7	2.1	39	1.7	27	0.225	1
2									
A	7	0.4	4	1.2	48	11.8	0	0.39	1
B	7	0.35	7,5	3.7	104	21.1	4	0.283	1
3									
A	7.6	0.09	3.3	1	41	4.7	5	0.089	1
B	7.6	0.16	7	0.9	72	9.9	2	0.179	1
C	7.6	0.16	5.3	0.9	43	12.7	8	0.199	1
D	7.6	0.162	3.8	2	53	6.8	5	0.136	1
E	7.6	0.18	7	1.8	81	22.7	2	0.179	0
F	7.6	0.18	10.1	1.8	109	23.5	2	0.184	0
G	7.6	0.16	10.1	0.9	100	11	2	0.178	1
H	7.6	0.16	10.1	0.9	100	17.5	2	0.178	0
I	7.6	0.16	4.6	0.6	47	9.4	0	0.183	1
J	7.6	0.18	6.1	2.4	79	14.1	0	0.162	0
K	7.6	0.16	4.3	0	39	7	10	0.21	1
L	7.6	0.18	6.1	1.2	67	35.5	0	0.191	0
4									
A	7.5	0.242	2.895	2	45	12.1	36	0.185	0
5									
A	8.3	0.213	5.7	0	38	16.5	3	0.335	
B	8.3	0.23	6.1	2.1	76	35.3	5	0.221	0
C	8.3	0.23	4	0.9	45	23	5	0.246	0
D	8.3	0.23	4	0.6	42	9.1	5	0.265	1
E	8.3	0.2	4	0.9	45	7.6	20	0.213	1
6									

	M	a_{max}(g)	Ds(m)	Dw(m)	σ(KPa)	$N1_{60}$	FC (%)	CSR	Liq?
A	6.61	0.45	6.1	4.6	96	3.9	55	0.312	1
B	6.61	0.45	6.1	4.6	96	8.1	50	0.312	1
7									
A	7	0.2	8.2	1.5	89	7.6	67	0.203	1
B	7	0.2	8.2	1.5	92	8.9	50	0.199	0
C	7	0.3	7.8	1.5	85	13.3	48	0.304	1
D	7	0.3	8.2	1.5	92	11	5	0.298	1
8									
A	7.5	0.135	10.4	1.5	86	5	3	0.126	1
B	7.5	0.135	4.6	2.4	34	9.7	3	0.138	***
C	7.5	0.135	10.7	3.4	71	14.3	3	0.149	0
9									
A	7.6	0.13	4.5	1.1	54	11.7	12	0.13	1
B	7.6	0.2	4.4	1.5	53	11.5	12	0.194	1
C	7.6	0.22	3.5	1.1	38	24.4	5	0.226	0
D	7.6	0.22	3.5	1.1	32	8.5	3	0.241	1
E	7.6	0.35	5.3	0.9	59	20.1	20	0.378	1
F	7.6	0.5	5.3	3.1	75	31.6	10	0.405	0
G	7.6	0.2	6.1	0.9	67	10.5	20	0.218	1
10									
A	7.5	0.2	8.2	4.6	106	6.3	20	0.16	1
B	7.5	0.2	11.1	6.7	156	7.6	5	0.169	1
C	7.5	0.2	3.7	1.2	39	14.3	4	0.204	0
D	7.5	0.2	3.1	2.1	44	13.6	3	0.154	0
E	7.5	0.2	5.2	1.8	56	5.8	50	0.198	1
11									
A	6.5	0.1	6.4	0.9	67	12.8	0	0.105	0
B	6.5	0.14	5.2	2.4	71	11.1	20	0.116	0
C	6.5	0.12	3.5	1.4	45	5.5	10	0.109	0

	M	a_{max}(g)	Ds(m)	Dw(m)	σ(KPa)	$N1_{60}$	FC (%)	CSR	Liq?
D	6.5	0.14	3.4	3.1	59	12.3	5	0.092	0
E	6.5	0.14	6.1	2.4	79	14.1	3	0.12	0
F	6.5	0.12	2.8	0.5	30	6.9	5	0.128	1
G	6.5	0.12	3.4	1.3	42	9.6	4	0.112	0
H	6.5	0.14	6.4	4.3	85	9.4	5	0.102	0
I	6.5	0.14	4	2.4	60	7.5	10	0.108	0
J	6.5	0.12	4.3	1.8	56	5.4	10	0.105	0
K	6.5	0.12	2.5	1.2	34	16.2	7	0.112	0
L	6.5	0.12	4.3	0.3	42	11.8	12	0.142	0
M	6.5	0.12	5.5	1.8	63	2.5	60	0.113	0
N	6.5	0.12	4.3	0.9	47	15.1	0	0.125	0
12									
A	7.7	0.2	6.4	0.9	67	12.8	0	0.223	1
B	7.7	0.24	5.2	2.4	71	11.1	20	0.207	1
C	7.7	0.2	3.5	1.4	45	5.5	10	0.186	1
D	7.7	0.2	4.5	1.4	57	2.9	10	0.188	0
E	7.7	0.28	3.4	3.1	59	12.3	5	0.187	1
F	7.7	0.28	4.8	3.1	73	17.6	0	0.216	0
G	7.7	0.24	4.6	2.4	65	12.7	26	0.2	0
H	7.7	0.24	6.1	2.4	79	14.1	3	0.217	1
I	7.7	0.32	3.4	0.9	39	26.2	4	0.329	0
J	7.7	0.32	2.8	0.5	30	6.9	5	0.346	1
K	7.7	0.32	3.4	1.3	42	9.6	4	0.306	1
L	7.7	0.24	6.4	4.3	85	9.4	5	0.185	1
M	7.7	0.24	4	2.4	60	7.5	10	0.19	1
N	7.7	0.24	4.3	1.8	56	5.4	10	0.216	1
O	7.7	0.24	2.5	1.2	34	16.2	7	0.212	1
P	7.7	0.24	4.3	0.3	42	11.8	12	0.293	1
Q	7.7	0.24	7.3	1.2	78	20.1	17	0.26	0
R	7.7	0.24	5.5	1.8	63	2.5	60	0.236	1
S	7.7	0.24	4.3	0.9	47	15.1	0	0.258	1
T	7.7	0.24	5.5	2.1	70	24.6	0	0.22	0

	M	a_{max}(g)	Ds(m)	Dw(m)	σ(KPa)	$N1_{60}$	FC (%)	CSR	Liq?
13									
A	6.53	0.78	2.9	1.8	42	37.8	12	0.62	0
B	6.53	0.78	3.7	1.8	50	2.9	18	0.661	1
C	6.53	0.78	4	1.8	56	16.2	25	0.69	0
D	6.53	0.13	4.3	2.7	62	6.2	92	0.099	0
E	6.53	0.51	2.1	1.5	32	4.6	31	0.385	1
F	6.53	0.2	3.4	2.1	50	2.9	64	0.154	1
G	6.53	0.2	2.3	2.1	38	15.2	30	0.132	0
H	6.53	0.24	1.8	0.3	20	4.6	80	0.266	1
J	6.53	0.17	4.6	1.2	54	10.3	30	0.178	0
J	6.53	0.17	4,6	1.2	54	10.3	30	0.178	0
14									
A	6	0.095	6.1	0.9	57	7.1	13	0.104	0
B	6	0.095	14.3	0.9	123	3.9	27	0.089	0
15									
A	5.9	0.32	4.3	2.7	62	6.2	92	0.24	1
B	5.9	0.09	2.1	1.5	32	4.6	31	0.068	0
C	5.9	0.2	3.4	2.1	50	2.9	64	0.152	1
D	5.9	0.2	2.3	2.1	38	15.2	30	0.131	0
E	5.9	0.21	1.8	0.3	20	4.6	80	0.231	0
F	5.9	0.21	4.3	0.3	45	15.2	18	0.237	0
G	5.9	0.26	4.6	1.2	54	10.3	30	0.267	1
16									
A	6.9	0.168	2.4	1.6	35	17	5	0.129	0
17									
A	6.8	0.15	4.3	1	37	5.1	5	0.172	0
B	6.8	0.15	9.2	1	77	18.1	0	0.172	0
C	6.8	0.111	4.3	0.35	42	13.3	0	0.132	1
18									

	M	a_{max}(g)	Ds(m)	Dw(m)	σ(KPa)	$N1_{60}$	FC (%)	CSR	Liq?
A	7.7	0.116	5.7	0	38	16.5	3	0.178	1
B	7.7	0.2	4.3	1	37	5.1	5	0.234	1
C	7.7	0.227	7.5	0.4	53	12.4	1	0.32	1
D	7.7	0.25	3.5	1.7	38	16.2	1	0.232	1
E	7.7	0.283	4.3	4	42	13.3	0	0.397	1
F	7.7	0.205	2.865	1.75	41	18.7	3	0.166	0
G	7.7	0.205	2.895	1.75	41	13.8	3	0.167	0
H	7.7	0.116	0.338	1.14	41	13.1	5	0.113	0
I	7.7	0.205	6.9125	1.5	79	8.7	3	0.211	1
J	7.7	0.205	9.7986	1.47	107	6.9	4	0.214	1
K	7.7	0.052	4.295	1.6	54	4.2	66	0.049	0
L	7.7	0.205	6.47	1.46	74	9.9	8	0.21	1
M	7.7	0.205	7.1314	1.45	81	13.5	3	0.213	1
N	7.7	0.205	3.7825	1.5	48	9.3	7	0.191	1
O	7.7	0.205	6.0356	1.58	71	10.2	2	0.205	1
P	7.7	0.205	5.7443	1.51	68	11.5	2	0.206	1
Q	7.7	0.205	3.905	1.2	47	18.9	3	0.203	0
R	7.7	0.205	3.42	1.2	42	23.5	2	0.198	0
S	7.7	0.205	2.5833	1.2	34	23	1	0.184	0
T	7.7	0.205	5.1767	1.2	60	34.6	3	0.213	0
U	7.7	0.205	2.2167	1.2	31	37.3	1	0.175	0
V	7.7	0.205	4.48	1.2	53	20.3	2	0.208	0
W	7.7	0.205	5.21	0.72	56	5.4	2	0.229	1
X	7.7	0.205	5.41	1.37	63	7.4	2	0.209	1
Y	7.7	0.205	5.48	1.35	64	5.6	2	0.21	1
Z	7.7	0.205	3.91	1.46	49	8.1	2	0.194	1
AA	7.7	0.205	4.5425	1.45	55	23.5	2	0.2	0
BB	7.7	0.205	6.67	1.6	77	22.5	4	0.208	0
CC	7.7	0.205	3.5667	1.45	46	25.9	0	0.19	0
19									
A	6.9	0.268	2.895	2	45	12.1	36	0.203	0
20									

	M	a_{max}(g)	Ds(m)	Dw(m)	σ(KPa)	$N1_{60}$	FC (%)	CSR	Liq?
A	6.22	0.09	3.4	2.1	50	2.9	64	0.069	0
B	6.22	0.133	4.6	1.2	54	10.3	30	0.138	0
C	6.54	0.156	2.9	1.8	42	37.8	12	0.124	0
D	6.54	0.15	3.7	1.8	50	2.9	18	0.127	0
E	6.54	0.13	4	1.8	56	16.2	25	0.115	0
F	6.54	0.174	4.3	2.7	62	6.2	92	0.132	0
G	6.54	0.16	2.1	1.5	32	4.6	31	0.121	0
H	6.54	0.2	3.4	2.1	50	2.9	64	0.154	0
I	6.54	0.18	2.3	2.1	38	15.2	30	0.119	0
J	6.54	0.19	1.8	0.3	20	4.6	80	0.21	0
K	6.54	0.19	4.3	0.3	45	15.2	18	0.218	0
L	6.54	0.206	4.6	1.2	54	10.3	30	0.216	1
21									
A	6.93	0.24	6.5	3	91	43.3	7	0.198	0
B	6.93	0.37	6	4.5	92	10.2	8	0.259	1
C	6.93	0.28	2.5	1.4	35	21.4	5	0.232	0
D	6.93	0.14	4.6	3.5	64	5.7	30	0.102	0
E	6.93	0.28	4.6	2.4	65	13.1	3	0.23	1
F	6.93	0.28	3.5	2.5	55	14.9	3	0.207	1
G	6.93	0.28	5.3	1.5	64	17.6	3	0.27	1
H	6.93	0.28	2	2	35	22.6	1	0.179	0
I	6.93	0.28	3.4	1.8	47	14.9	1	0.235	0
J	6.93	0.28	3.4	1.9	48	21.2	5	0.231	0
K	6.93	0.28	3.4	2	48	14.7	4	0.226	0
L	6.93	0.39	6.2	4.9	101	9.9	32	0.252	1
M	6.93	0.39	7	4.7	108	20.9	13	0.28	1
N	6.93	0.39	6	4.4	95	9.8	25	0.274	1
O	6.93	0.39	8.4	3	105	20.2	20	0.338	0
P	6.93	0.28	6.3	3	89	15.4	3	0.229	1
Q	6.93	0.28	6.3	3	89	17	3	0.229	***
R	6.93	0.18	5.9	3.5	73	5.1	50	0.142	1
S	6.93	0.28	3	1.8	43	15.3	2	0.226	1
T	6.93	0.28	6.1	1.8	73	34.4	5	0.266	0

	M	a_{max}(g)	Ds(m)	Dw(m)	σ(KPa)	$N1_{60}$	FC (%)	CSR	Liq?
U	6.93	0.27	6.3	3	86	8.6	8	0.222	1
V	6.93	0.28	3.4	1.8	46	10.3	1	0.234	1
W	6.93	0.28	4.9	2.6	67	18.4	1	0.229	1
X	6.93	0.16	6.5	1.5	67	6.4	20	0.165	1
Y	6.93	0.28	1.8	1	25	9.1	35	0.233	1
22									
A	7.7	0.25	5	2.3	68	24.9	19	0.218	0
B	7.7	0.25	7.2	2.3	90	13	19	0.236	1
23									
A	7.6	0.4	5.2	2	68	16.4	2	0.366	1
B	7.6	0.4	10.8	1.6	118	30.9	0	0.408	0
C	7.6	0.47	3.8	2	47	25.9	5	0.41	1
24									
A	6.69	0.84	8.5	7.2	143	13.1	50	0.428	1
B	6.69	0.51	9.3	3.9	101	27.2	25	0.431	0
C	6.69	0.43	7.1	2	88	8.5	64	0.32	1
D	6.69	0.51	6.7	4.3	105	11.6	33	0.39	1
25									
A	6.9	0.4	5.8	2.4	80	52	3	0.345	0
B	6.9	0.4	8	2.9	103	39.5	15	0.345	0
C	6.9	0.4	5.8	2.5	77	49.8	3	0.344	0
D	6.9	0.4	4.3	2.1	54	36.6	1	0.35	0
E	6.9	0.35	8.9	3	116	6.1	1	0.298	1
F	6.9	0.4	5.9	2.3	72	17.8	21	0.36	0
G	6.9	0.4	3.3	3.2	60	10.9	0	0.314	1
H	6.9	0.5	5	3	65	24.1	0	0.402	1
I	6.9	0.5	4.3	2.8	64	12.2	2	0.383	1
J	6.9	0.6	7.5	4.5	107	27.4	9	0.45	0
K	6.9	0.5	6.8	1.5	62	8.5	5	0.546	1
L	6.9	0.5	5.3	3.2	72	24.7	14	0.393	0

	M	a_{max}(g)	Ds(m)	Dw(m)	σ(KPa)	$N1_{60}$	FC (%)	CSR	Liq?
M	6.9	0.5	6.5	2.3	74	12.7	15	0.464	1
N	6.9	0.5	4.8	3.1	69	20.3	19	0.382	0
O	6.9	0.5	5.7	3.7	82	19.2	5	0.375	1
P	6.9	0.6	4.5	2.5	60	25	5	0.495	0
Q	6.9	0.5	4.5	0.8	43	21.1	5	0.574	1
R	6.9	0.7	10.5	7.7	171	42.6	0	0.448	0
S	6.9	0.6	7.5	6.1	124	21.3	10	0.391	0
T	6.9	0.55	6	2	75	63.7	0	0.505	0
U	6.9	0.6	3.5	1.7	44	33.5	0	0.531	0
V	6.9	0.6	6	2.4	79	38.6	6	0.524	0
W	6.9	0.6	5	3	72	24	10	0.468	0
X	6.9	0.5	3.5	2.4	51	24.6	0	0.383	1
Y	6.9	0.7	3.5	2.2	50	35.8	3	0.555	0
Z	6.9	0.6	3.5	0.9	37	37	0	0.633	0
AA	6.9	0.6	2.5	1.1	29	40.8	10	0.568	0
BB	6.9	0.4	3.5	1.8	44	21.1	8	0.348	1
CC	6.9	0.4	3.8	2	49	17.9	0	0.337	1
DD	6.9	0.6	8.5	1.5	78	40.1	10	0.649	0
EE	6.9	0.6	4	1.2	46	49.7	0	0.599	0
FF	6.9	0.5	3.5	1.4	41	29.1	6	0.472	0
GG	6.9	0.5	8	2	83	27.9	50	0.496	0
HH	6.9	0.4	7	1.8	73	24.2	9	0.403	1
II	6.9	0.5	4.5	2.1	55	18.9	6	0.445	1
JJ	6.9	0.6	3.5	0.9	36	31.6	3	0.639	0
KK	6.9	0.35	5	4	79	19.3	0	0.241	1
LL	6.9	0.5	8	3	94	19.1	5	0.441	1
MM	6.9	0.6	4.5	2.6	66	61	0	0.476	0
NN	6.9	0.6	3.5	2.8	59	39.7	0	0.421	0
OO	6.9	0.4	4.1	2	50	15	0	0.352	1
PP	6.9	0.4	5	1.2	46	12.1	10	0.445	1
QQ	6.9	0.35	4.7	2.2	55	15.2	20	0.311	1
RR	6.9	0.4	4	1.6	43	8.3	5	0.388	1
SS	6.9	0.4	5.2	3.5	80	21.1	18	0.295	0
TT	6.9	0.4	8.8	3.5	115	12.5	2	0.331	1

	M	a_{max}(g)	Ds(m)	Dw(m)	σ(KPa)	$N1_{60}$	FC (%)	CSR	Liq?
UU	6.9	0.34	7.8	2.4	96	6.8	20	0.307	1
VV	6.9	0.4	8.5	5	125	22.7	20	0.293	0
WW	6.9	0.4	10	5	140	19.5	20	0.301	0
XX	6.9	0.4	9.5	5	135	34.6	20	0.299	0
YY	6.9	0.34	10	3	123	10.8	20	0.295	1
ZZ	6.9	0.4	7.5	4	107	16.8	25	0.31	1
AAA	6.9	0.34	11.5	4	146	12.3	20	0.275	1
BBB	6.9	0.25	4.7	0	46	14	20	0.308	1

Table 3.6 Name of Earthquake and there sites (Idriss & Boulanger, 2010)

Index	Earthquake / Site	Index	Earthquake / Site	Index	Earthquake / Site
1	1994, Dec 7Tohnankai earthquake	K	Showa Br 2	C	Ying Kou Glass Fibre Plant
A	Komei	L	Showa Br 4	D	Ying Kou Paper Plant
B	Ienaga				
C	Meiko	4	1968, April 1, Hososhima earthquake	8	1976, Feb 4, Guatemala earthquake
		A	Hososhima	A	Amatitlan B-1
2	1948, June 28, Fkui earthquake			B	Amatitlan B-2
A	Shonenji Temple	5	1968, May 16, Takachi-Oki earthquake	C	Amatitlan B-3&4
B	Takaya 45	A	Amori Station		
		B	Hachinohe -2		
3	1964, June 16, Nigata earthquake	C	Hachinohe -4	9	1976, July 27, Tangshan earthquake
A	Arayamotomachi	D	Hachinohe -6	A	Coastal Region
B	Cc17-1	E	Nanaehamal -2 -3	B	Le Ting L8-14
C	Cc17-2			C	Luan Nan -L1
D	Kawagishi-cho	6	1971, Feb 9, Haicheng earthquake	D	Luan Nan -L2
E	Old Town-1	A	Juvenile Hall	E	Qing Jia Ying
F	Old Town -2	B	Van Norman	F	Tangshan City
G	Rail Road -1			G	Yao Yuan Village
H	Rail Road -2	7	1975, Feb 4, Haicheng earthquake		
I	River Site	A	Panjin Chemical Fertilizer Plant	10	1977, Nov 23, Argentina earthquake
J	Road Site	B	Shung Tai Zi River Sluice Gate	A	San Juan B-1

Index	Earthquake / Site	Index	Earthquake / Site	Index	Earthquake / Site
B	San Juan B-3	12	1978, June 12, Miyagiken- Oki earthquake	S	Yuriagekami -2
C	San Juan B-4	A	Arahama	T	Yuriagekami -3
D	San Juan B-5	B	Hiyori		
E	San Juan B-6	C	Ishinomaki -2	13	1979, Oct 15, Imperial Valley earthquake
		D	Ishinomaki -4	A	Hober Road A1
11	1978, Feb 20, Miyagiken – Oki earthquake	E	Kitawabuchi -2	B	Hober Road A2
A	Arahama	F	Kitawabuchi -4	C	Hober Road A3
B	Hiyori	G	Nakajimi- 2	D	Kombloom B
C	Ishinomaki	H	Nakajimi- 18	E	McKim Ranch A
D	Kitawabuchi	I	Nakamura Dyke N-1	F	Radio Tower B1
E	Nakajimi- 18	J	Nakamura Dyke N-4	G	Radio Tower B2
F	Nakamura Dyke N-4	K	Nakamura Dyke N-5	H	River Park A
G	Nakamura Dyke N-5	L	Oiiri -1	J	Wildlife B
H	Oiiri -1	M	Shomi -6		
I	Shomi -6	N	Yuriage Br-1		
J	Yuriage Br-1	O	Yuriage Br-2	14	1980, Sep 24, Mid-Chiba earthquake
K	Yuriage Br-2			A	Owi-1
L	Yuriage Br-3	P	Yuriage Br-3	B	Owi-2
M	Yuriagekami -1	Q	Yuriage Br-5		
N	Yuriagekami -2	R	Yuriagekami -1	15	1981, April 26, WestMarland earthquake

Table 3.6 Name of Earthquake and there sites (Idriss & Boulanger, 2010)

Index	Earthquake / Site	Index	Earthquake / Site	Index	Earthquake / Site
A	Kombloom B	C	Gaiko Wharf B-2	W	Ohama No. 2 (2)
B	McKim Ranch A	D	Noshiro Section N-	X	Ohama No. 3 (1)
C	Radio Tower B1	e	Takeda Elementary Sch	Y	Ohama No. 3 (3)
D	Radio Tower B2	f	Akita Station (1)	Z	Ohama No. 3 (4)
E	River Park A	g	Akita Station (2)	AA	Ohama No. Rvt (1)
F	River Park C	H	Aomori Port	BB	Ohama No. Rvt (2)
G	Wildlife B	I	Gaiko 1	CC	Ohama No. Rvt (3)
		J	Gaiko 2		
16	1982, Mar 21, Ukrakawa – Oki earthquake	K	Hakodate	19	1984, Aug 7, Hososhima earthquake
A	Tokachi	L	Nakajima No.1 (5)	A	Hososhima
		M	Nakajima No.2 (1)		
17	1983, June 21, Nihonkai _ Chubu earthquake	N	Nakajima No.2 (2)	20	1987, Nov 24, Superstition Hill earthquake
A	Arayamotomachi	O	Nakajima No.3 (3)	A	Radio Tower B1
B	Arayamotomachi Coarse Sand	P	Nakajima No.3 (4)	B	Wildlife B
C	Takeda Elementry Sch	Q	Ohama No. 1(1)	C	Heber Road A1
		R	Ohama No. 1 (2)	D	Heber Road A2
		S	Ohama No. 1 (3)	E	Heber Road A3
18	1983, May 26, Nihonkai – Chubu earthquake	T	Ohama No. 1 (4)	F	Kombloom B
A	Aomori Station	U	Ohama No. 1 (5)	G	McKim Ranch A
B	Arayamotomachi	V	Ohama No. 1 (58-22)	H	Radio Tower B1

Index	Earthquake / Site	Index	Earthquake / Site	Index	Earthquake / Site
I	Radio Tower B2	O	Miller Farm CNF 10	24	1994, Jan 17, Northridge
J	River Park A	P	POO7-2	A	Balboa Blv. Unit C
K	River park C	Q	POO7-3	B	Malden Street Unit D
L	Wildlife B	R	POR- 2&3&4	C	Potero Canyon C1
		S	Sandholdt UC-B10	D	Wynne Ave. Unit C1
21	1989, 18 Oct, Loma Prieta earthquake	T	Sandholdt UC-B10		
A	Alameda Bay Farm Dike	U	SFOBB- 1&2	25	1995, Jan 16, Hyogoken-Nambu earthquake
B	Farris farm	V	State Beach UC-21	A	1
C	General Fish	W	State Beach UC-B2	B	2
D	Hall Avenue	X	Treasure Island	C	3
E	Marine Laboratory B1	Y	WoodMarine UC-B4	D	4
F	Marine Laboratory B2			E	5
G	Marine Laboratory UCB-6-12 & F1-F6	22	1990, July 16, Luzon earthquake	F	6
		A	Cereenan St. B-12	G	7
H	MBARI No. 3: EB-1	B	Perez Blv, B-11	H	8
I	MBARI No. 3: EB-5			I	9
J	MBARI No. 4	23	1993, Jan 15, Kushiro – Oki earthquake	J	10
K	MBARI Technology	A	Kushiro Port Quay Wall Site A	K	11
L	Miller Farm CMF 3	B	Kushiro Port Quay Wall Site D	L	12
M	Miller Farm CMF 5	C	Kushiro Port Seismo St.		

Table 3.6 Name of Earthquake and there sites (Idriss & Boulanger, 2010)

Index	Earthquake / Site	Index	Earthquake / Site	Index	Earthquake / Site
N	14	HH	34	BBB	54
O	15	II	35		
P	16	JJ	36		
Q	17	KK	37		
R	18	LL	38		
S	19	MM	39		
T	20	NN	40		
U	21	OO	41		
V	22	PP	42		
W	23	QQ	43		
X	24	RR	44		
Y	25	SS	45		
Z	26	TT	46		
AA	27	UU	47		
BB	28	VV	48		
CC	29	WW	49		
DD	30	XX	50		
EE	31	YY	51		
FF	32	ZZ	52		
GG	33	AAA	53		

13. Design of NFLP based on data sets

In this part, the system of Neuro-Fuzzy Liquefaction Prediction will be presented. The MATLAB or Matrix Laboratory software was used to design NFLP structure. As mentioned before, every ANFIS system has three parts such as Fuzzy system. Input and output parameters, inference system engine. The figure 3.14 shows the Fuzzy Inference System (FIS) of NFLP.

The input parameters which were selected for NFLP are 8 parameters:

- In 1: Earthquake magnitude (M),
- In 2: N-Value ($N1_{60}$),
- In 3: Effective overburden pressure (σ'),
- In 4: Soil fines content (FC),

- In 5: Peak ground acceleration (a_{max}),
- In 6: Depth of water (D_w),
- In 7: Depth of soil layer (D_s),
- In 8: Cyclic stress ratio (CSR).

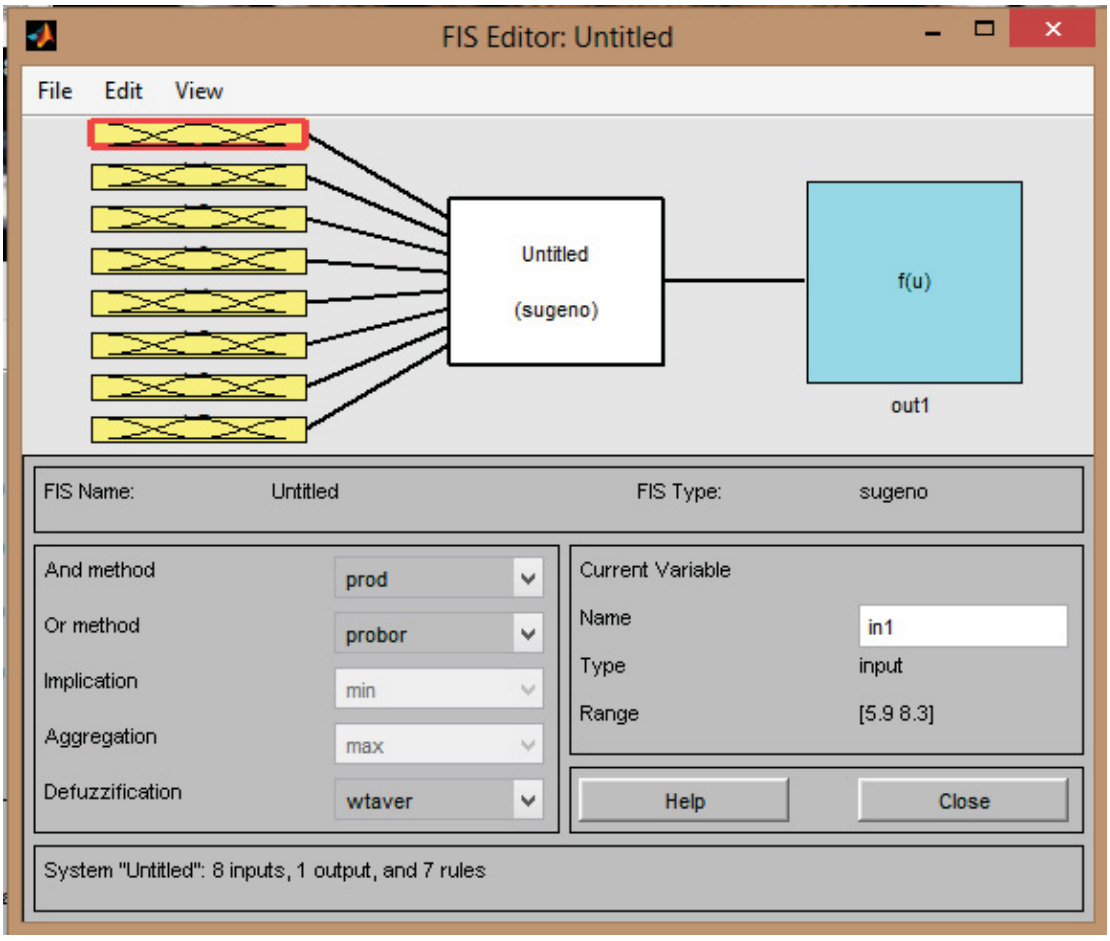

Figure 3.14 Fuzzy Inference System of NFLP

The method for member function classify was selected as Sub-Clustering/Gaussian. Every parameter has 7 clusters. This classification was made based on Frequency of available data. Figures 3.15 to 3.22 present these membership functions. Figure 3.23 and 3.24 show the importing of input data in area of MATLAB software.

The outputs of NFLP consist of 7 clusters to predict liquefaction happening in wide rang. These clusters define the probability of soil liquefaction. These classifications are:

0.0 – 0.09: Impossible
0.10 – 0.24: Very weak
0.25 – 0.39: Weak
0.40 – 0.59: Moderate
0.60 – 0.74: Strength
0.75 – 0.89: Very strength
0.90 – 1.0: Imperative

Figure 3.25 presents membership function of these 7 clusters. The inference engine by training of inputs and outputs data was made. This part of modelling, using neural network training method. The algorithm of training is based on minimizing of error. The final error of training has reached to 0.264. Figures 3.26 and 3.27 present the middle and final step of this training.

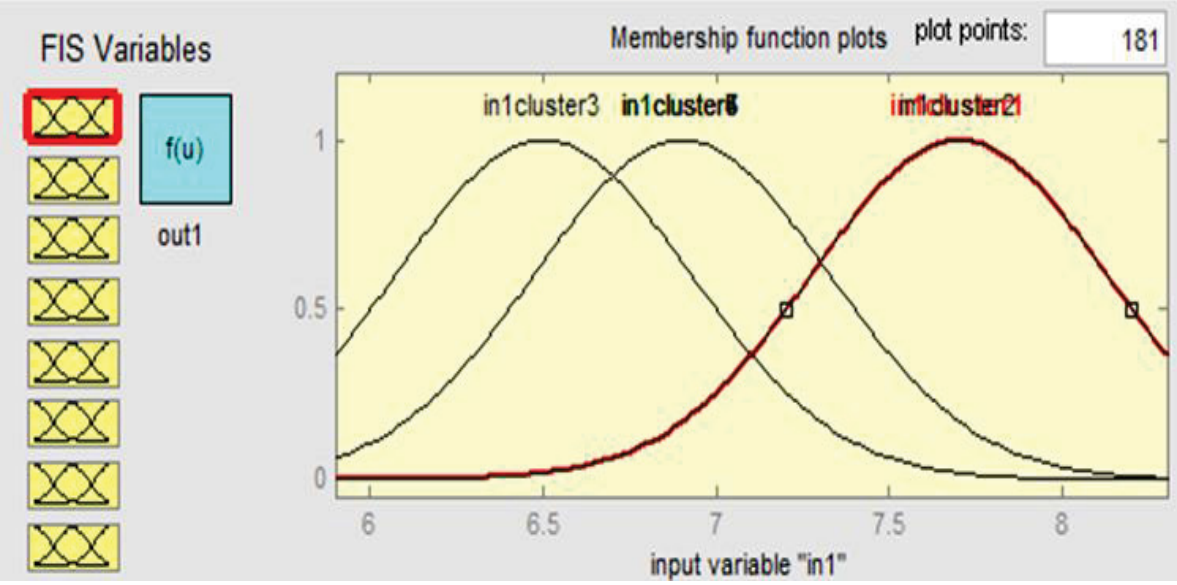

Figure 3.15 Membership function of Input 1: Earthquake magnitude.

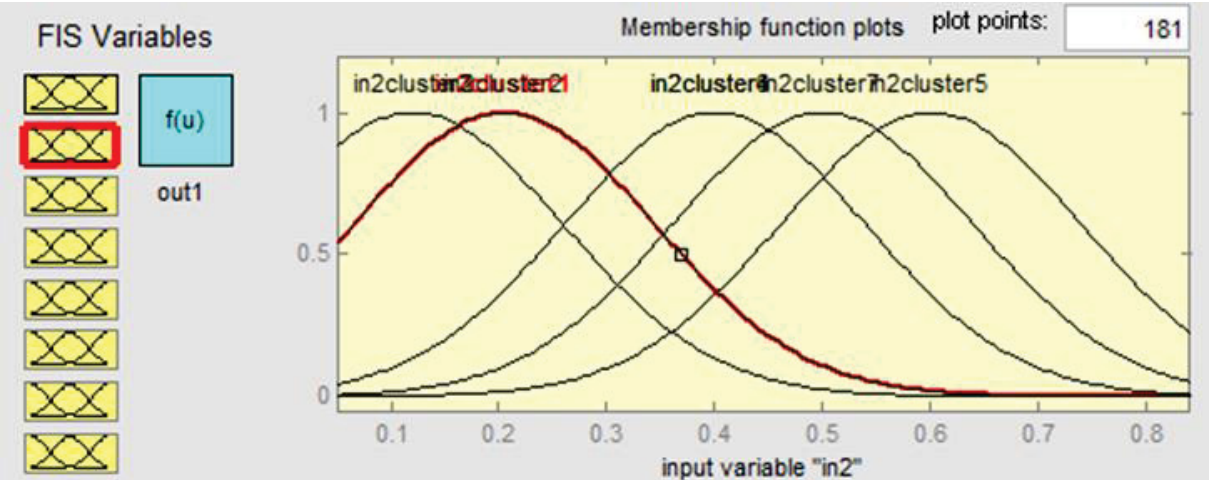

Figure 3.16 Membership function of Input 2: N-Value.

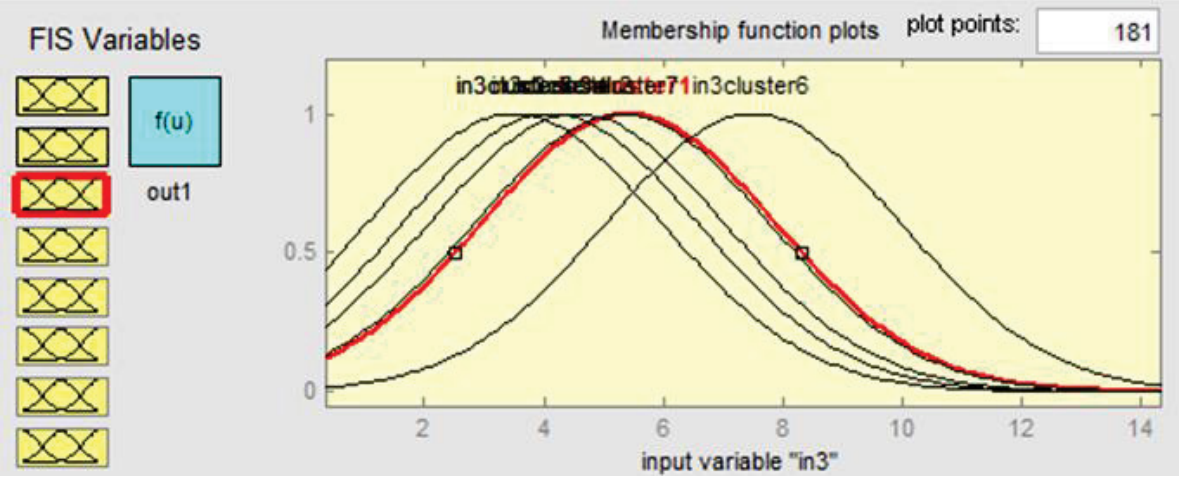

Figure 3.17 Membership function of Input 3: Effective overburden pressure.

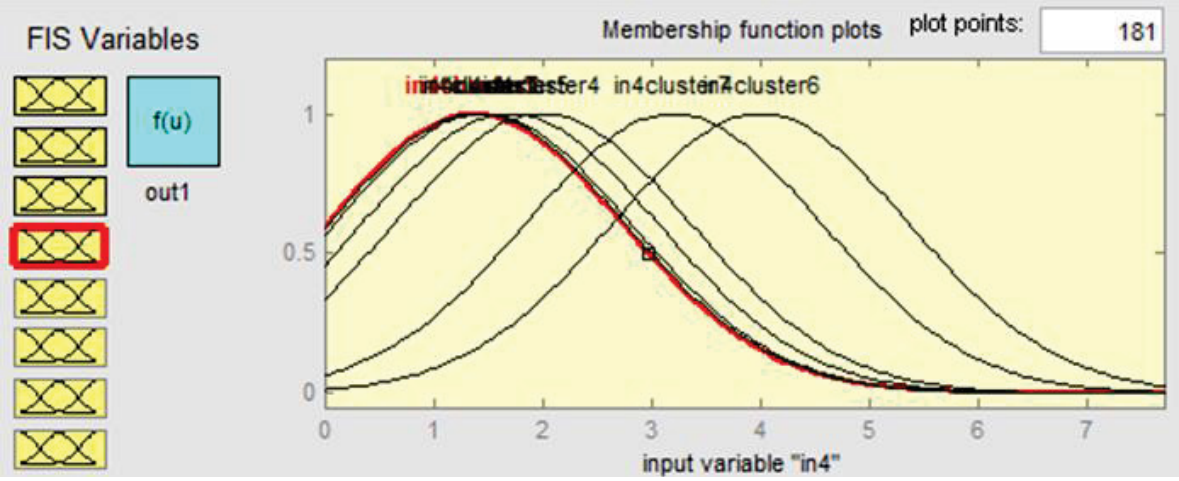

Figure 3.18 Membership function of Input 4: Soil fines content.

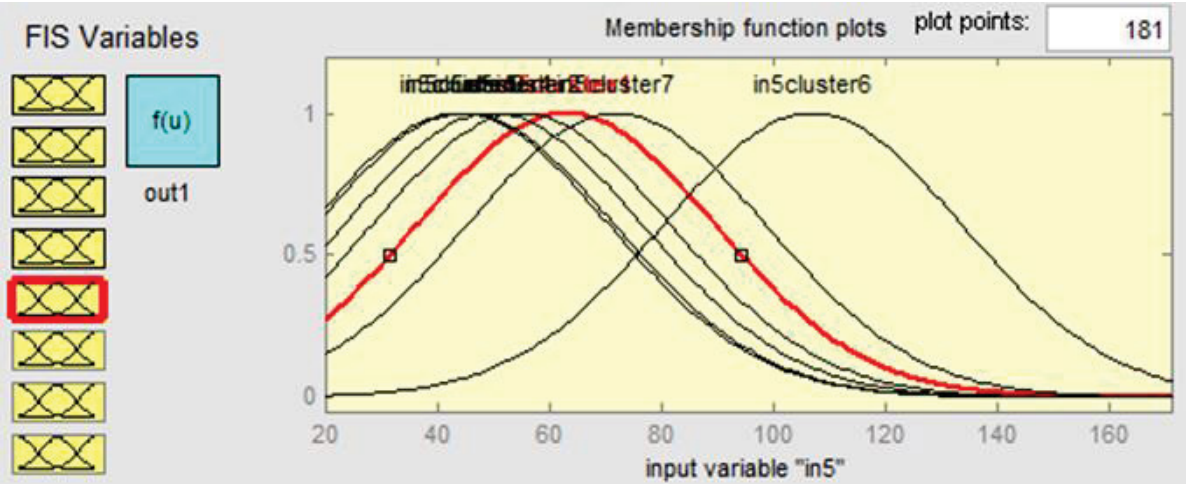

Figure 3.19 Membership function of Input 5: Peak ground acceleration.

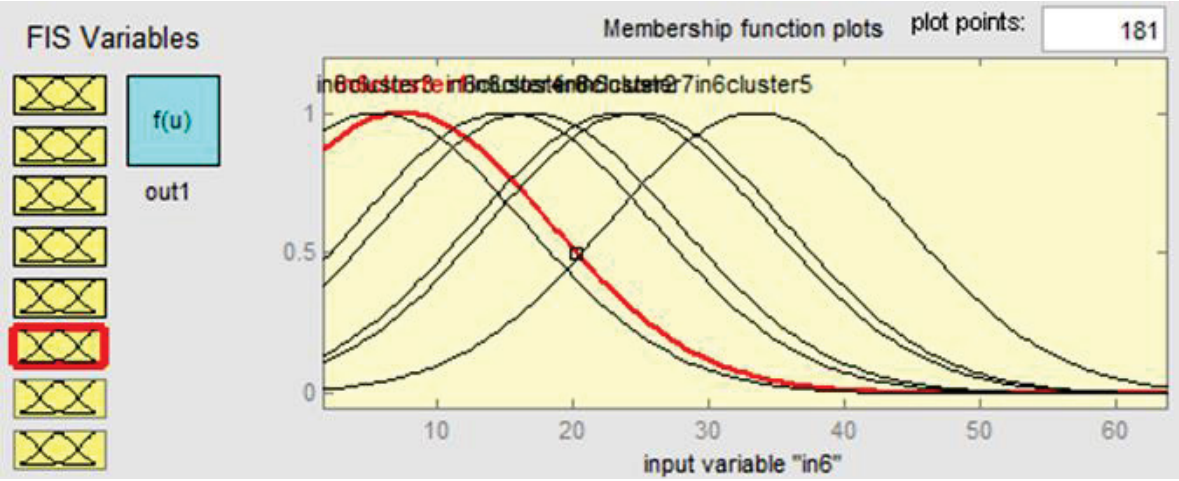

Figure 3.20 Membership function of Input 6: Depth of water.

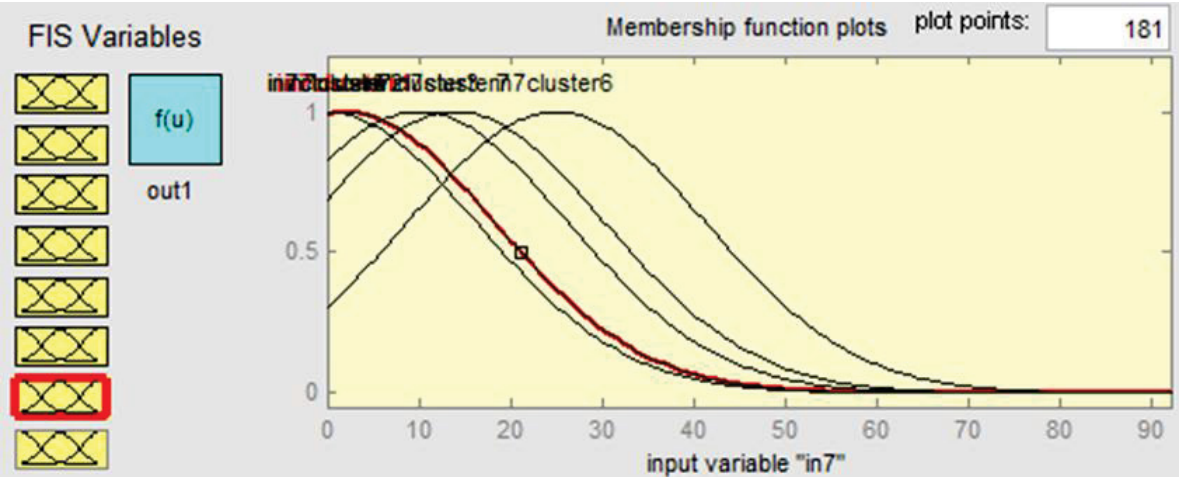

Figure 3.21 Membership function of Input 7: Depth of soil layer.

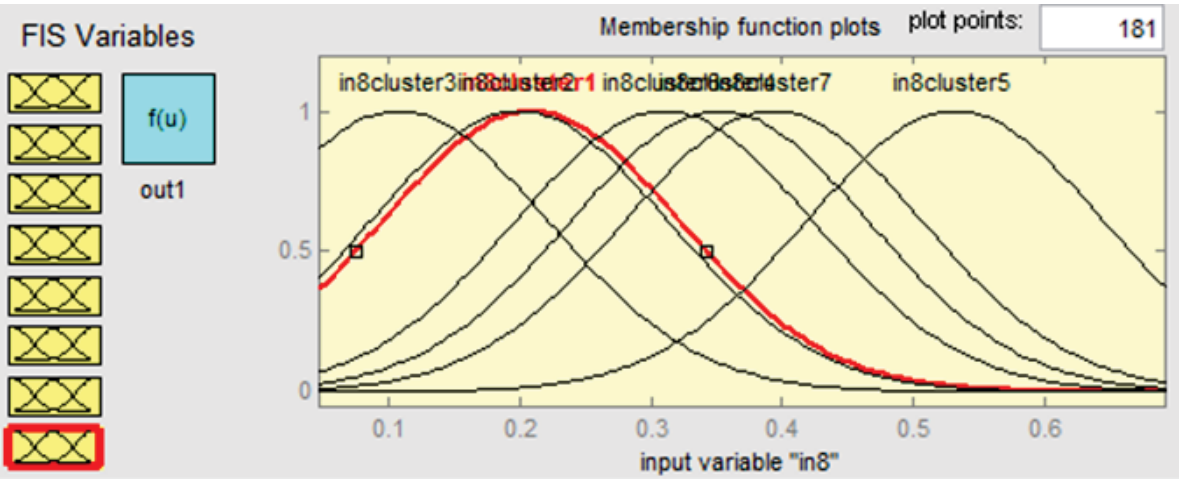

Figure 3.22 Membership function of Input 8: Cyclic stress ratio.

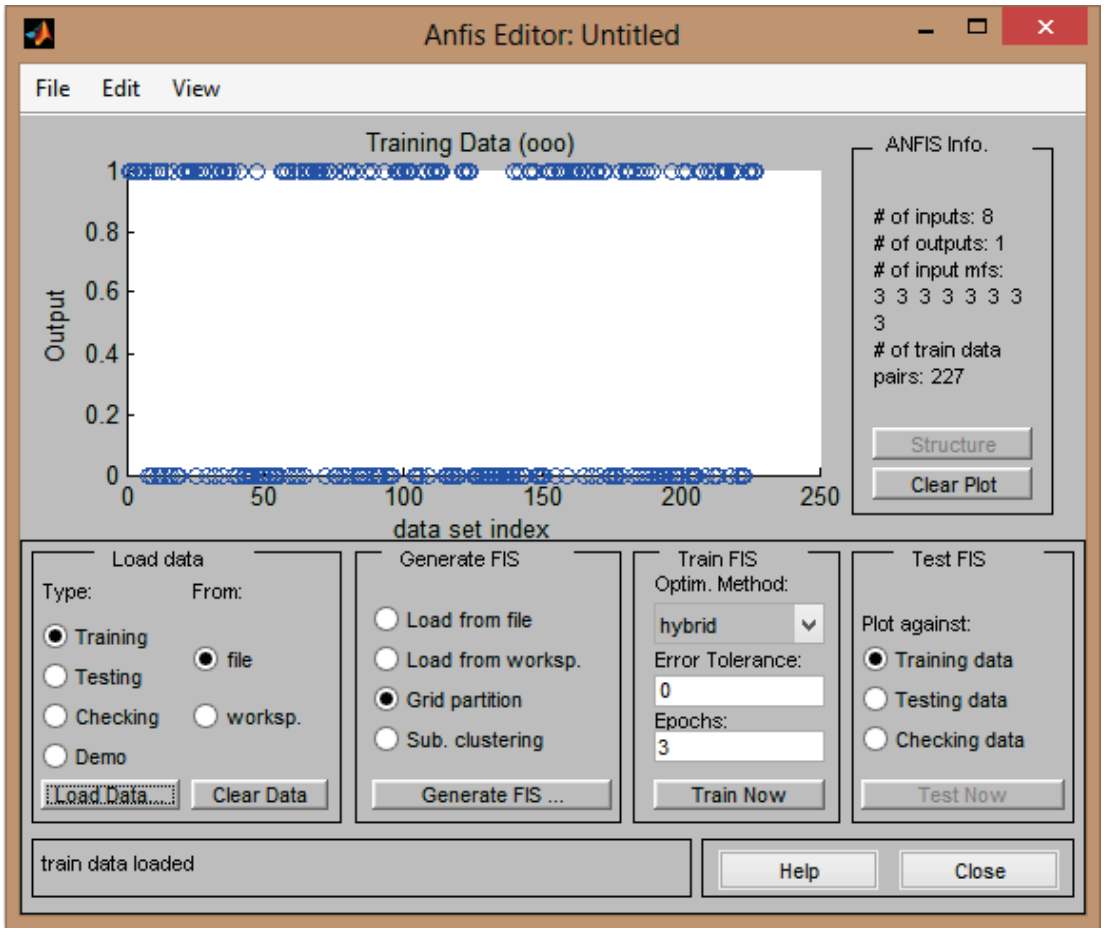

Figure 3.23 Training data of NFPL in Matlab area

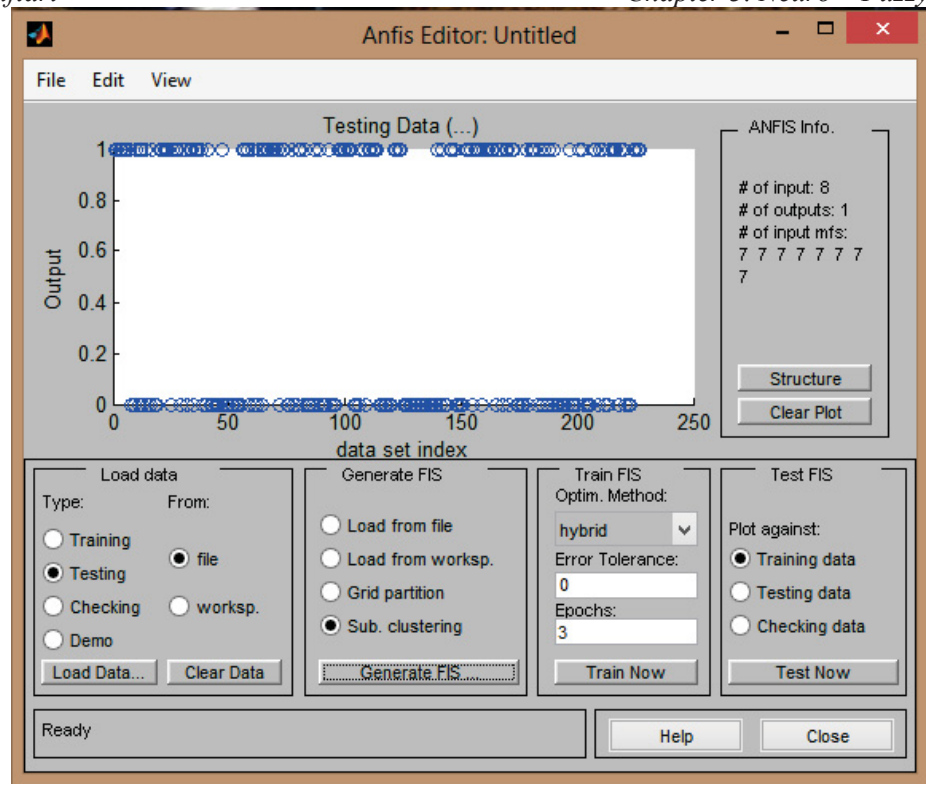

Figure 3.24 Test data of NFPL in Matlab area (5 piezometers of Wildlife site)

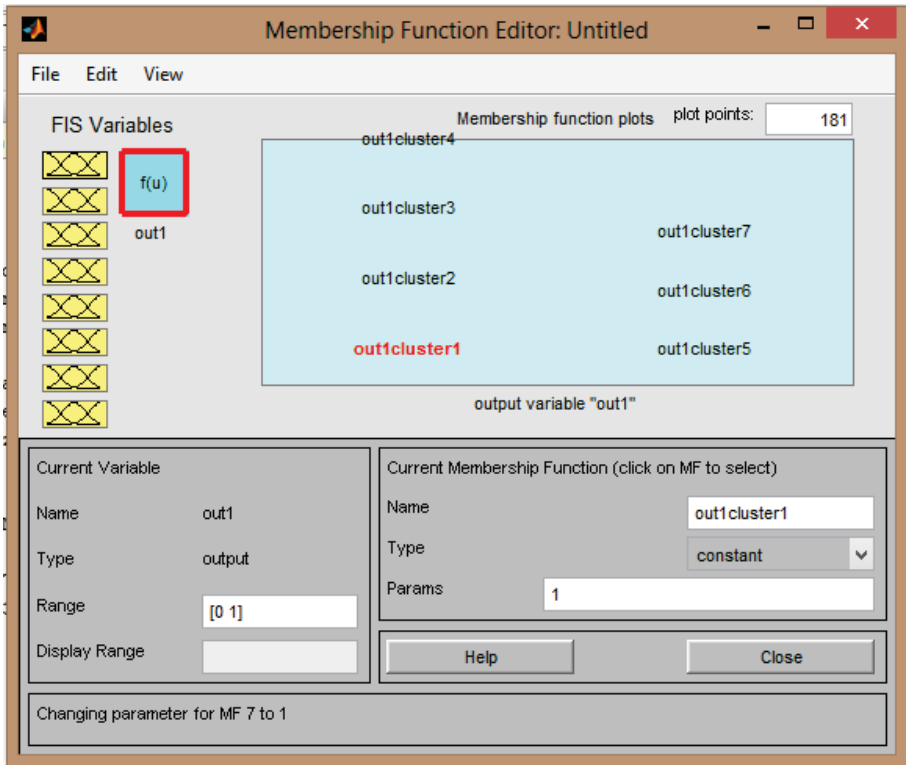

Figure 3.25 Membership function of output.

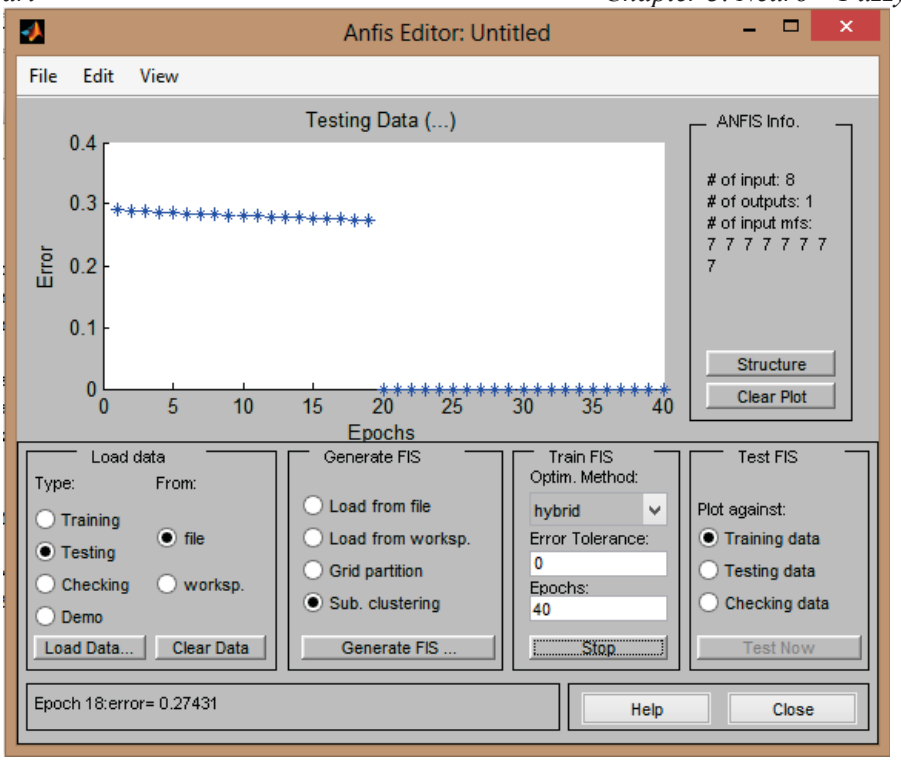

Figure 3.26 NFLP training system after 20 epochs.

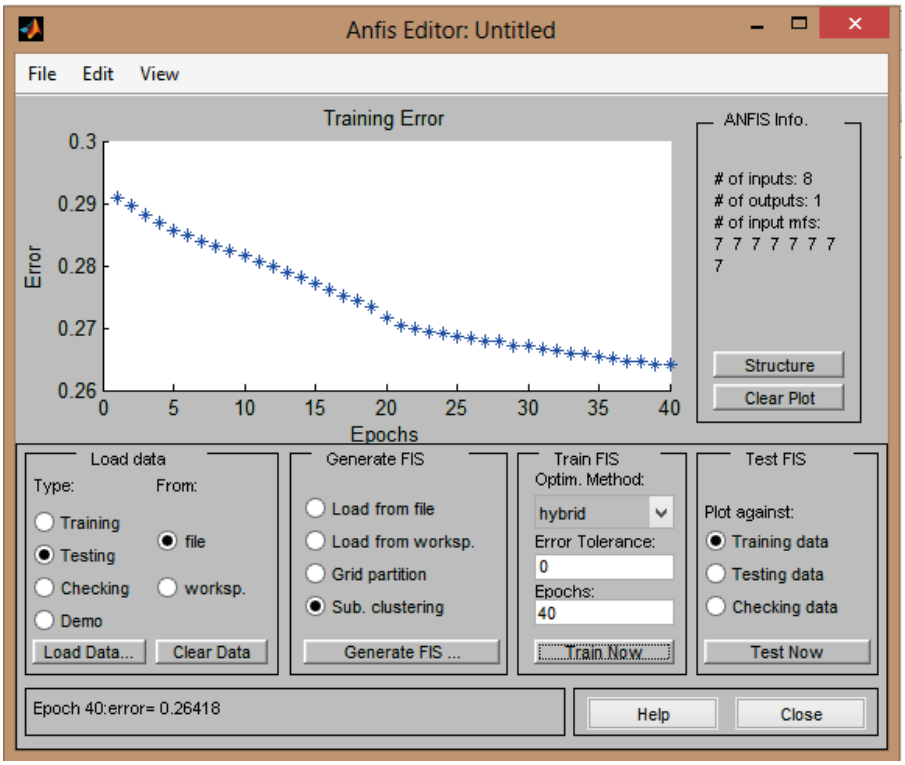

Figure 3.27 NFLP training system at end of steps.

The structure of NFLP after 40 epochs has stabilized. After this time, the quantity of error will be constant. This structure was illustrated in figure 3.28. The ANFIS‘s rule of NFLP was presented in figure 3.29. This rules network has 7 rules. Minimization of rules number is one of the sub-clustering advantages than Grid partition method. Figure 3.30 to 3.37 have presented the surface of calculation. These surfaces have built with 2 input parameters and output.

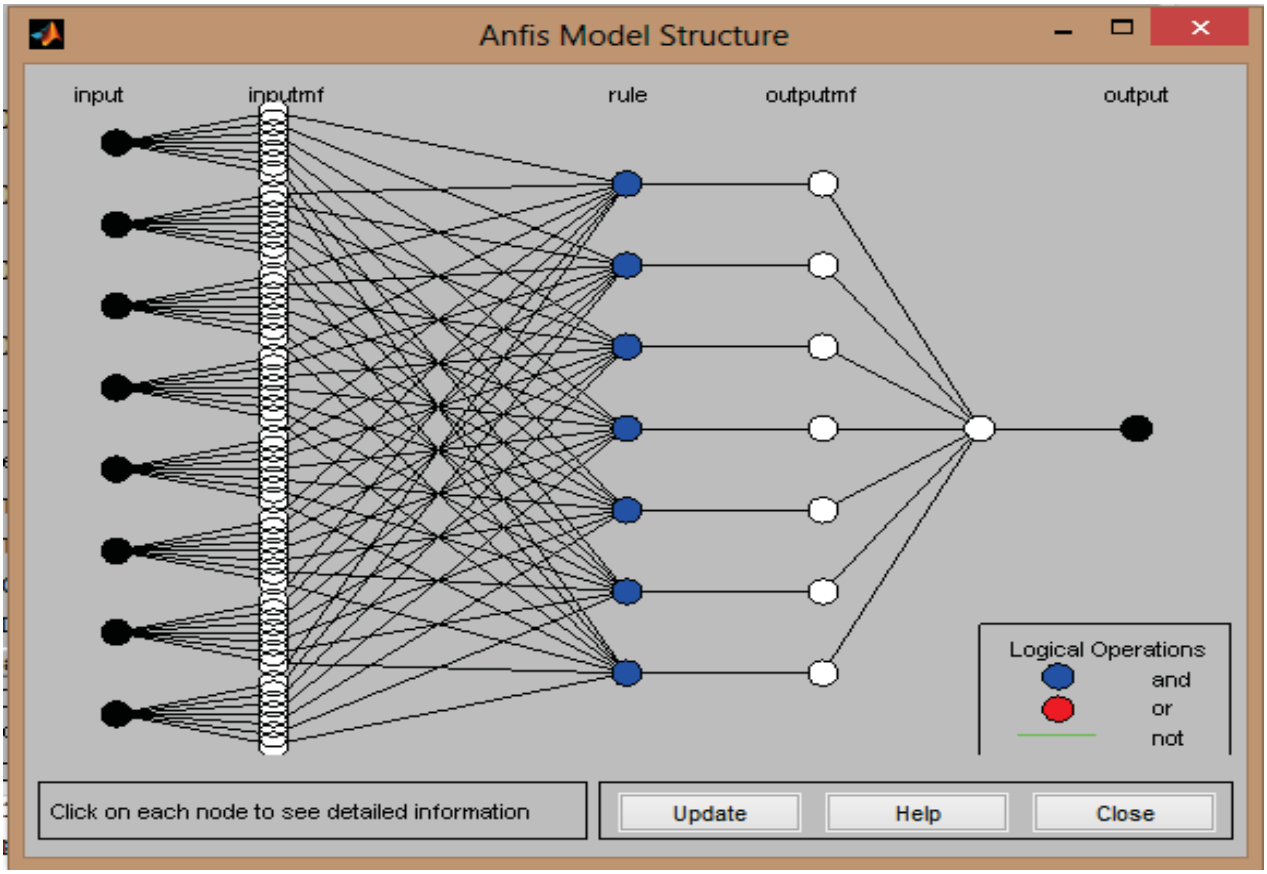

Figure 3.28 The structure of NFLP System

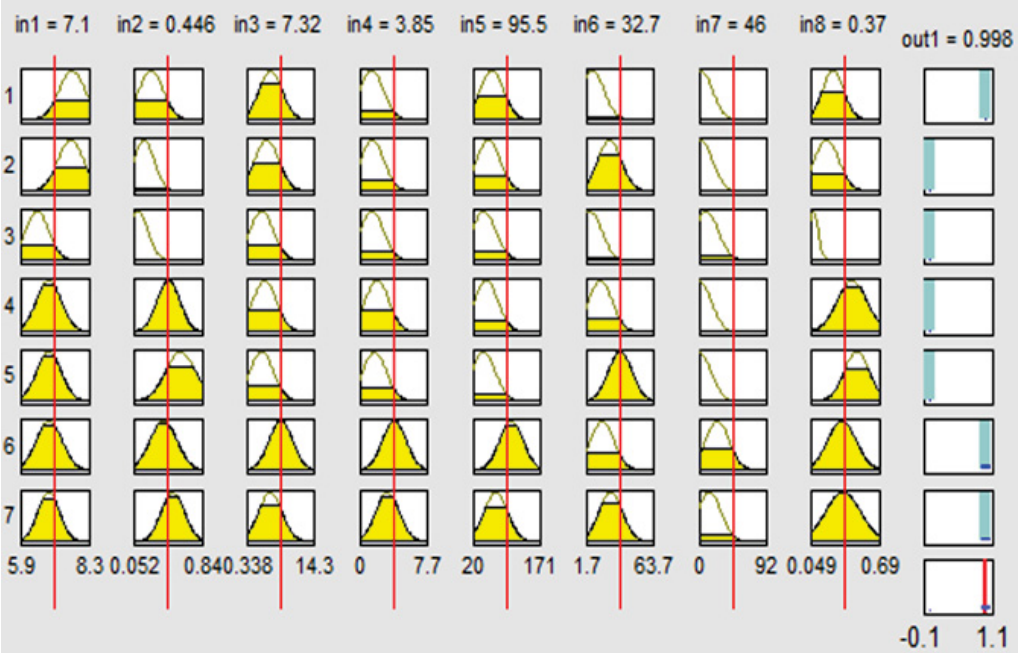

Figure 3.29 The rules network of NFLP

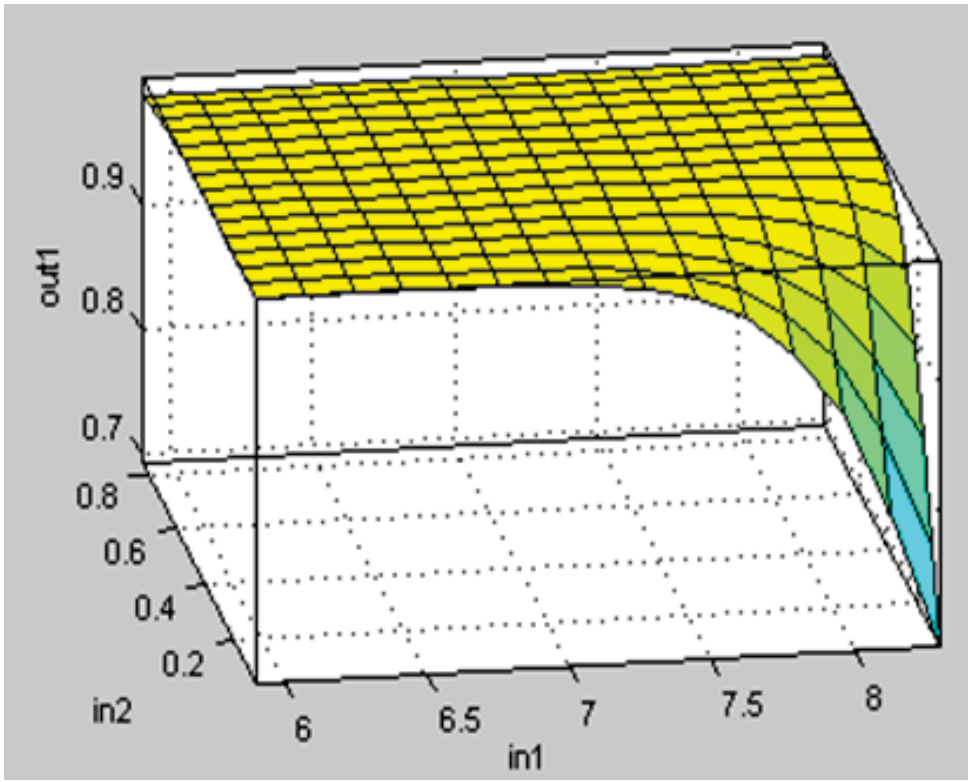

Figure 3.30 Surface between Earthquake magnitudes and N1-Value.

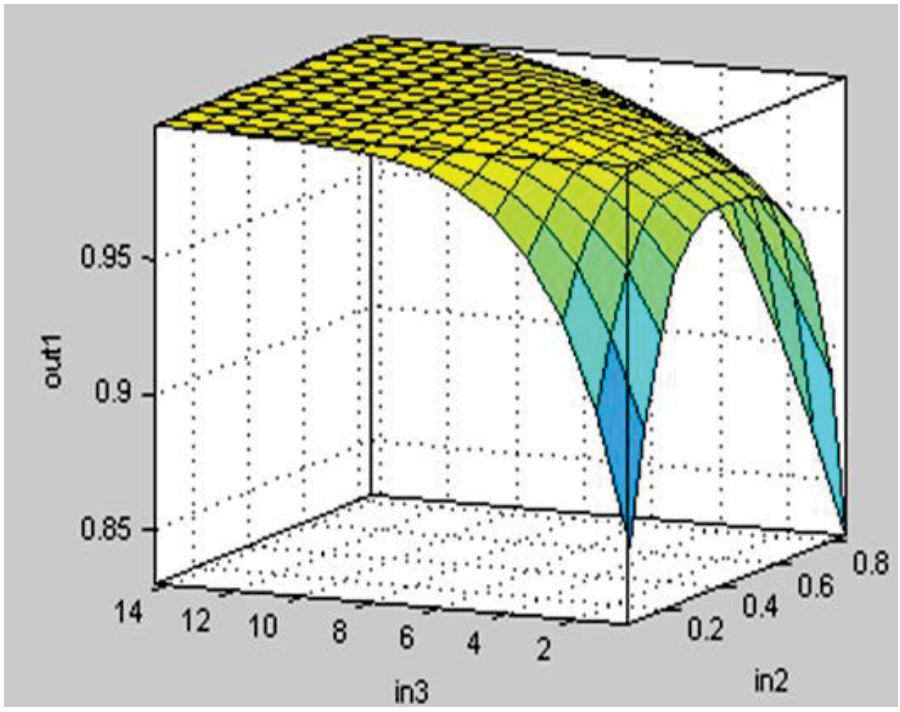

Figure 3.31 Surface between N1-Value and Effective overburden pressure

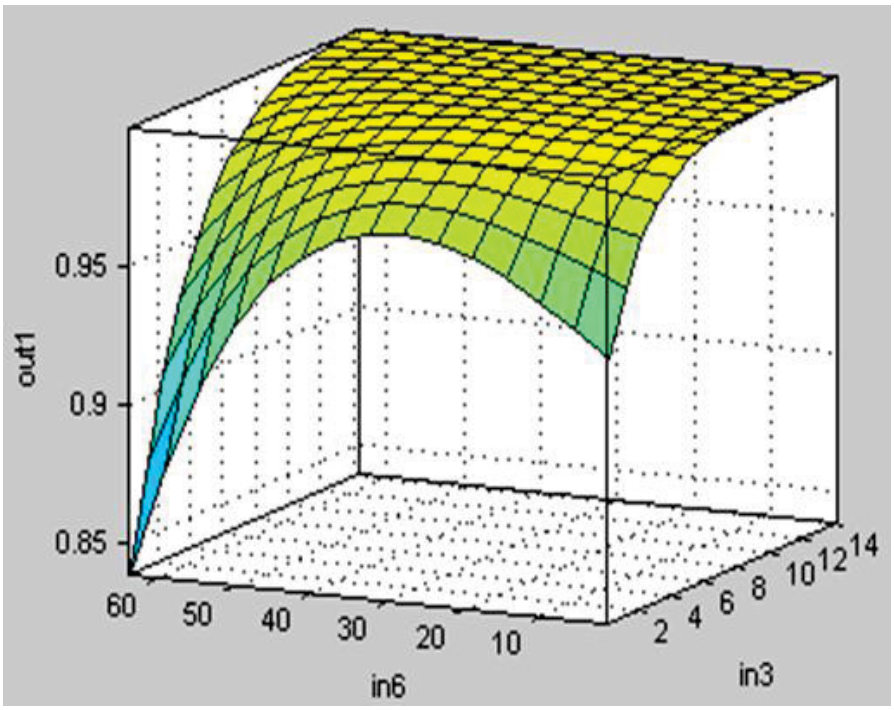

Figure 3.32 Surface between Effective overburden pressures Depth of water

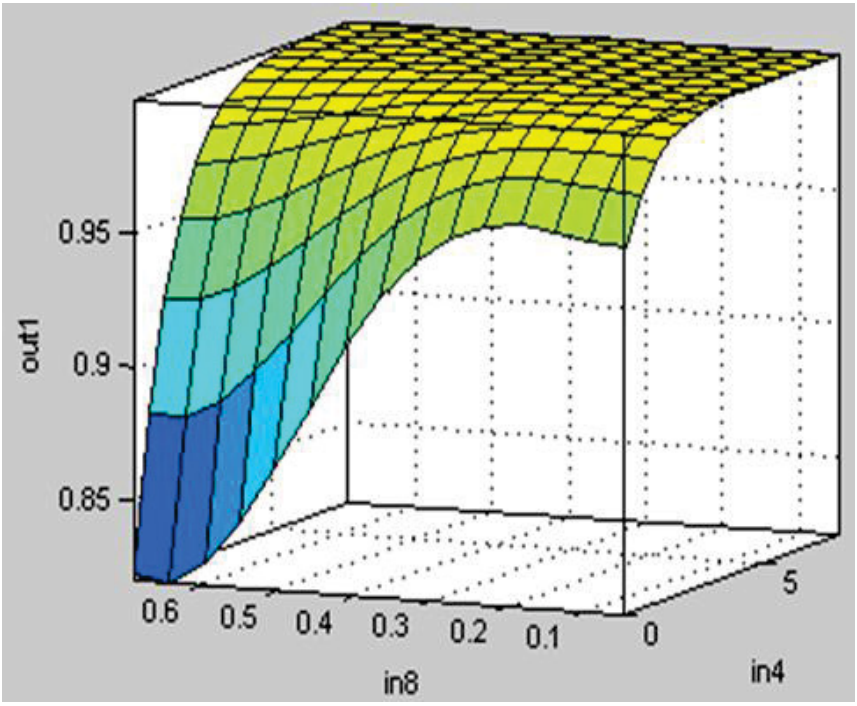

Figure 3.33 Surface between Soil fines content and cyclic stress ratio

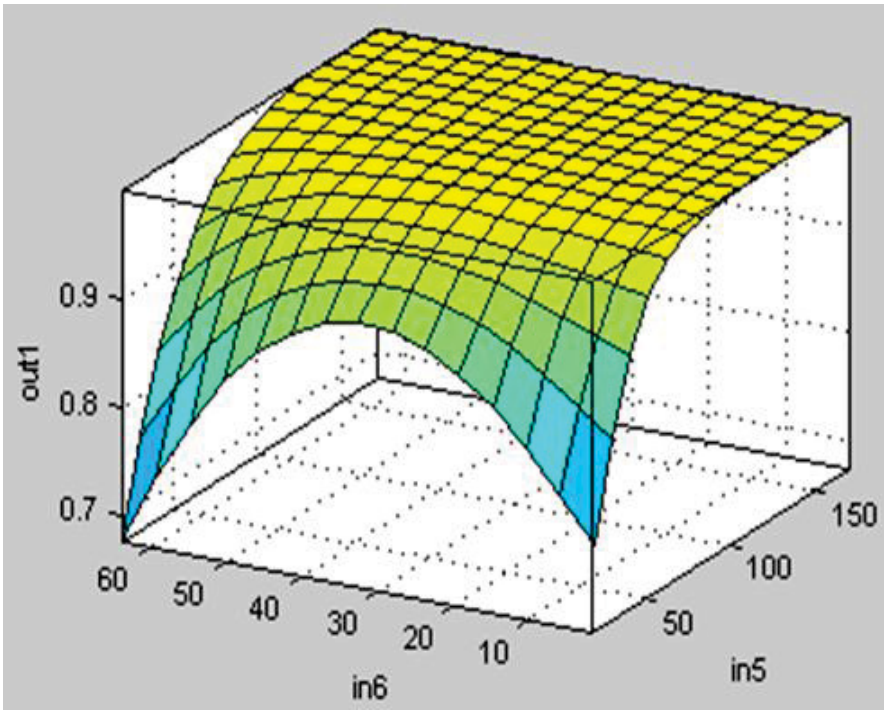

Figure 3.34 Surface between Peak ground acceleration and Depth of water

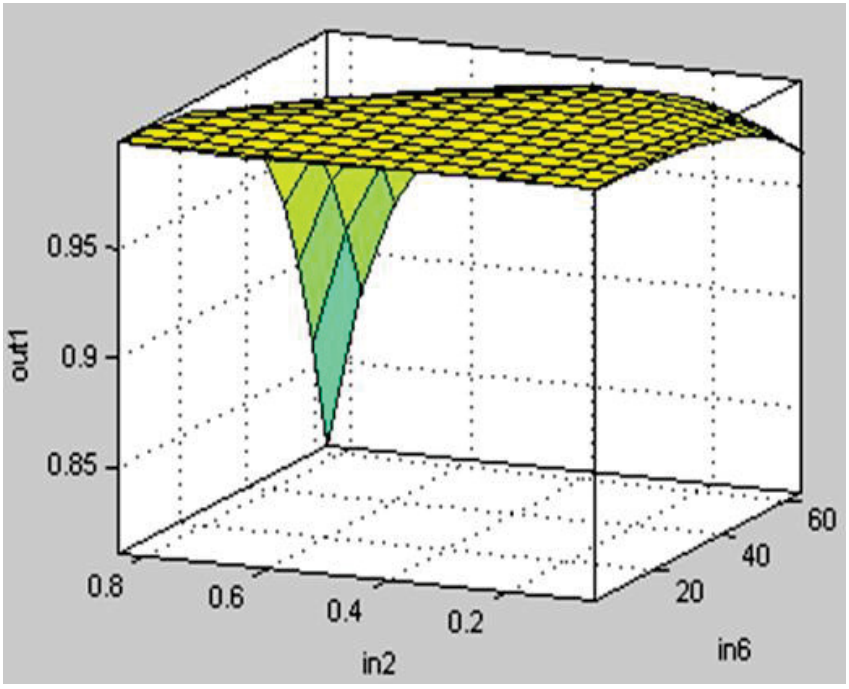

Figure 3.35 Surface between Depth of water and Standard penetration test

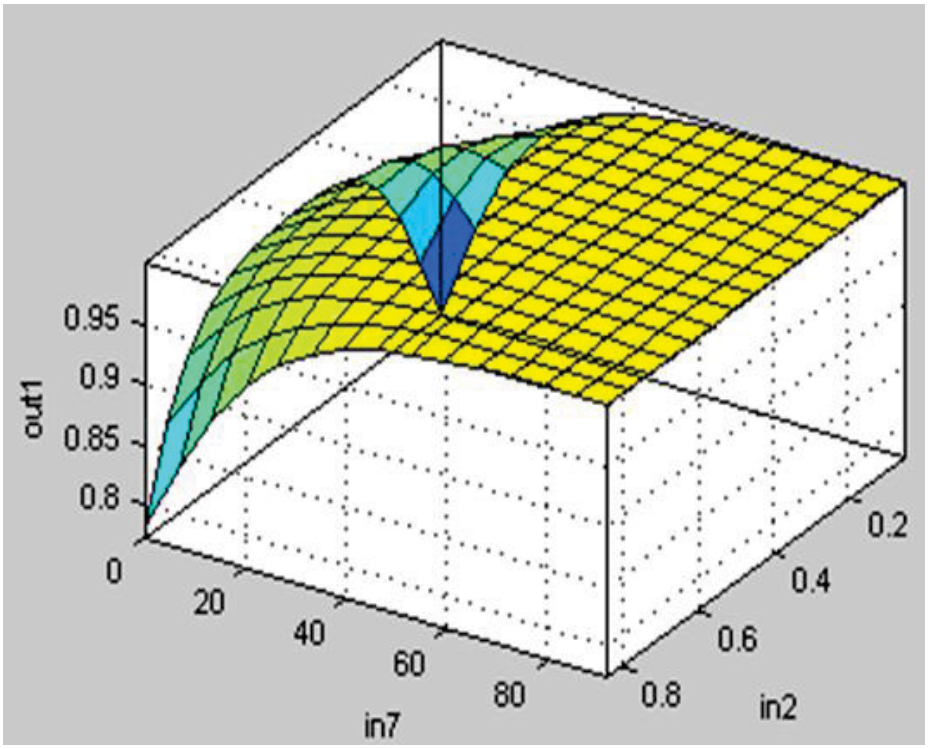

Figure 3.36 Surface between Depth of soil layer and Standard penetration test

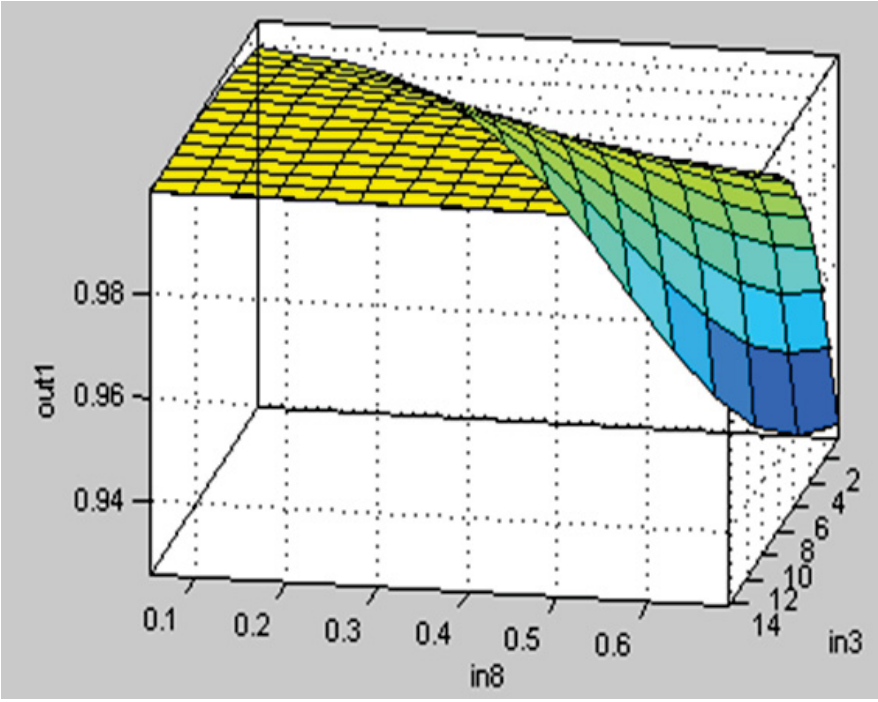

Figure 3.37 Surface between Cyclic stress ratio and Effective overburden pressure

Finally, the probability of soil liquefaction in Wildlife site for 4 piezometers was predicted with NFLP. These piezometers were determined based on their depths. The results of prediction were shown in figure 3.38.

The happenings of liquefaction have signed with blue stars (*), and the probability of liquefaction based on NFLP have signed with red stars (*). The NFLP has predicted probability of liquefaction accruing for P1, P2, P3 and P5 equals to 0.97, 0.80, 1.0 and 0.92 respectively.

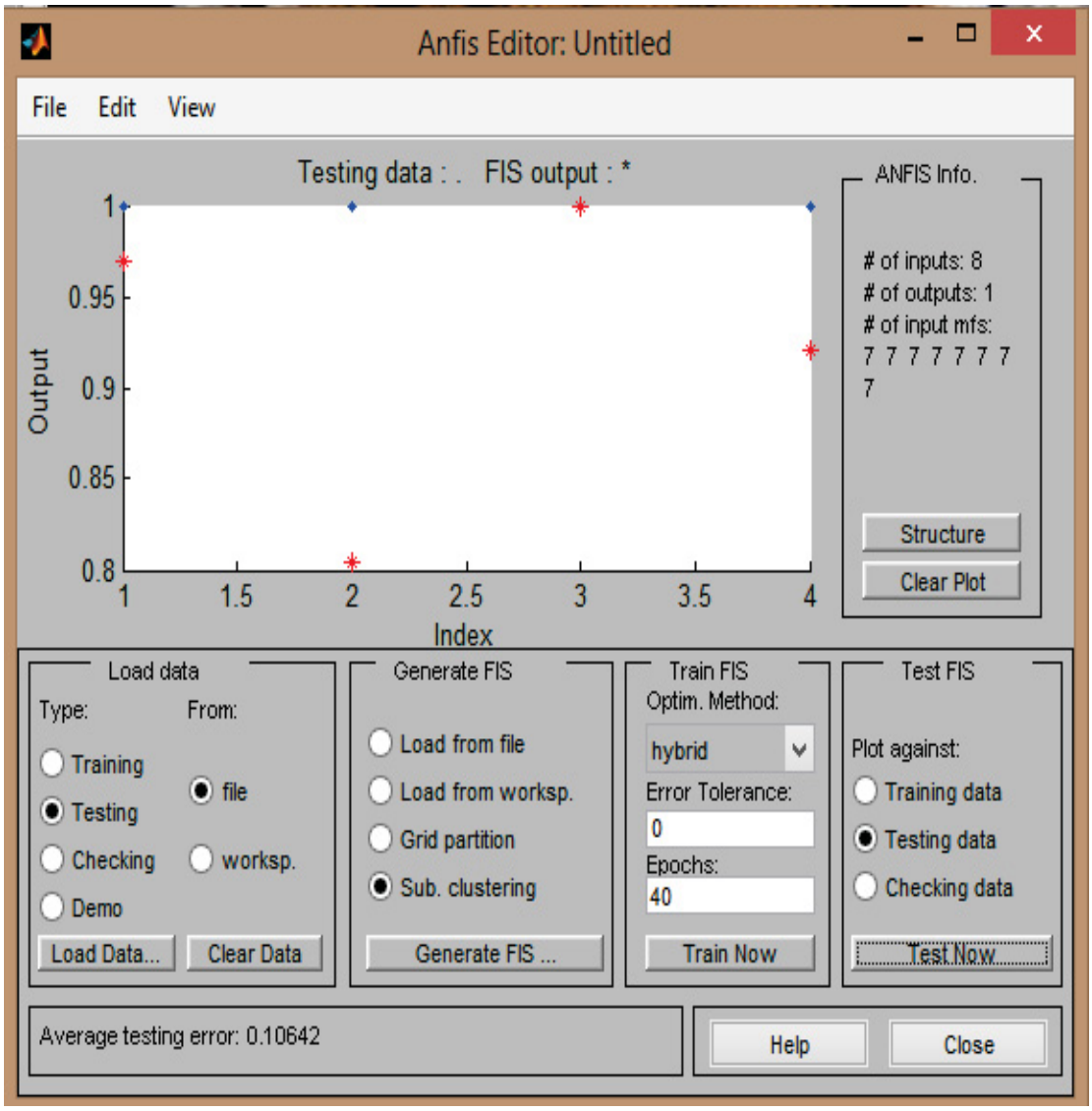

Figure 3.38 Prediction of NFLP for P1, P2, P3 and P5 in Wildlife site

1. Overview

Based on literatures, the liquefaction occurrence of soil deposits can be defined as the decline of shear strength due to pore pressure build-up in the soil skeleton. When saturated loose sands are subjected to earthquake or cyclic loading, primarily induced by upward extension of shear waves from bedrock, they tend to settle and densify. However, the duration of the cyclic stress application is so short compared to the time required for water to drain, that the soil volume contraction cannot occur immediately and excess pore pressure will progressively build up.

When the pore pressure equals the total stress, thereby reducing the effective stress to zero, sands will, at least provisionally, completely lose their stiffness and shear strength. Such a state is referred to as "initial liquefaction". At the onset of initial liquefaction, loose sands will undergo unlimited deformations or flow without mobilizing significant resistance to deformation. As a result, structures supported above or within the liquefied deposit undergo significant settlements and tilting; water flows upward to the surface creating sand boils. This phenomenon is referred to as "liquefaction" and is obviously a condition to be avoided in any type of major construction.

This phenomenon has caused lots of damages and financial losses. For example, in 1995 Hykogen Nambu Earthquake in Japan caused 100 billion dollars damage, mostly by liquefaction and lateral spreading (Soroush & Koohi, 2004).

Various procedures for evaluating the liquefaction potential of saturated soil deposits have been proposed in the past years. One of the most important methods is numeral modelling. FLAC and PLAXIS are useful software which uses this technique.

Nowadays, pattern of calculation in Computers were changed. This change caused to create new methods in data mining. Mixture of new data mining rules and intelligent mathematical methods had good and more acceptable results in scientific research. Neural network and Fuzzy logic are the two of these intelligent methods.

In this research by using the data of Superstation Hills Earthquake in 1987, ability and capability of Finn-Byrne formulation in FLAC and UBC3D-PLM formulation in PLAXIS were considerate. This compression will be presented in next parts.

Moreover, in this thesis, in order to achieve a better prediction algorithm with lowest errors, methods of Fuzzy logic and neural network have mixed in MATLAB software. The result of this Combination was NFLP (Neuro Fuzzy Liquefaction Prediction). In continue, the results of these methods will be analysed.

2. Trend diagram review of excess pore-water pressure from numerical models

In FLAC software, the wildlife liquefaction array based on Finn-Byrne formulation was modelled. The excess pore water pressure in 4 piezometers (P_1, P_2, P_3 and P_5), were calculated under superstition hills earthquake effect.

UBC3D-PLM pattern was used for modelling of this area in PLAXIS. Same to FLAC‘s model, 4 piezometers (P_1, P_2, P_3 and P_5) for calculation excess pore water pressure were simulated. The diagram of these two models will be compared with the real measured diagram in Wildlife site.

2.1. Diagrams of Piezometer P_1

The combination of these three diagrams was presented in figure 4.1. In this figure green line shows the results of Finn-Byrne model in FLAC, and red line presents the results of UBC-PLM model in PLAXIS. The blue line is measured excess pore pressure in site. It should be noted that E.O.S is the Effective Overburden Stress.

The Superstition earthquake on P1 in Wildlife site has caused the rising of E.P.P (Excess pre pressure) until 56 kPa. The trend shows the stable EPP in 10 first second of earthquake. After that

the EPP in P1 rising gradually until around 56 kPa. This EPP is the equivalent to EOS. So the measured trend shows the liquefaction in P_1.

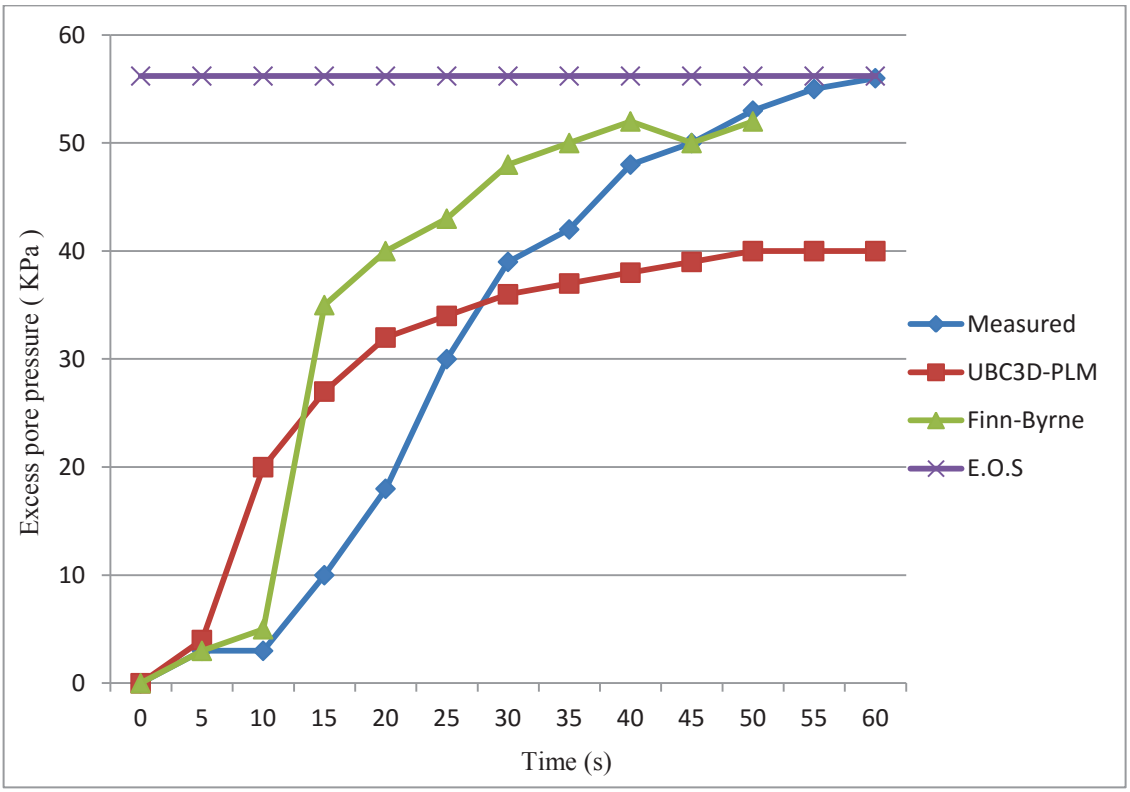

Figure 4.1 results of Excess pore pressure in P1.

FLAC result shows the same reaction in 10 first second. In this period the EPP was stable approximately. But after this period, EPP raised until 40 kPa in second 20 sharply. After this time the trend increased but so slower than before until 55 kPa. This EPP is so near to EOS, so the Finn-Byrne can predict liquefaction in $P_{1.}$

The trend of EPP from PLAXIS started the rising in 10 first second. This period lifted the EPP to 20 kPa. But after that the trend shows slow increasing until 40 kPa. Base on this trend UBC3D-PLM could not show any liquefaction effect.

2.2. Diagrams of Piezometer P_2

Figure 4.2 consist of the results of FLAC, PLAXIS and measured trends. Same as last diagram green points show the results of Finn-Byrne prediction, and red points present the results of UBC-

PLM prediction. The blue points are measured excess pore pressure in site; and E.O.S is the Effective Overburden Stress.

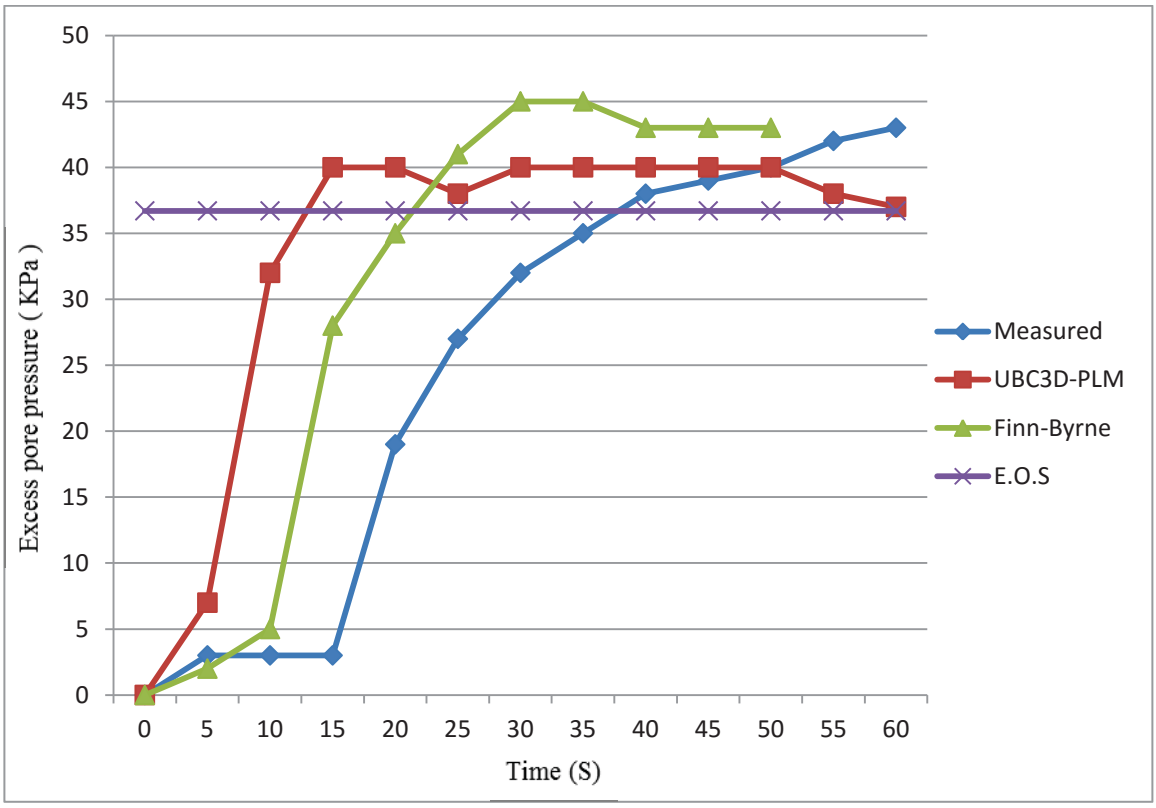

Figure 4.2 results of Excess pore pressure in P2.

In piezometer 2, the superstition earthquake has made any special effect until 15 first seconds. After that EPP has raised until 43 kPa uniformly. By attention to EOS line, the EPP in P2 exceed EOS in 40 second.

The results of Finn model in P2 show the stable EPP only until 10 first second, after that grew up until 30 kPa in 15 second. This trend went up to 45 kPa in 35 second. In these last seconds, EPP decreased a little until 43 kPa. Confluence of EPP and EOS in 22 seconds shows the ability of Finn model to predict liquefaction in P2.

Based on figure 4.2, UBC3D-PLM shows fast increase in P2. The EPP reach the 40 kPa in 15 seconds. In fact, trend before 15 seconds reach to EOS line. After 15 second, trend has remained relatively constant.

2.3. Diagrams of Piezometer P_3

EPP in Piezometer 3, unlike before, start rising at first of earthquake. This raising was not so high, only to 8 kPa in Second 10. After this time, the trend increased until 63 kPa. Based on literatures, the EPP had reached to 71.2 kPa after 90 second (Figure 4.3).

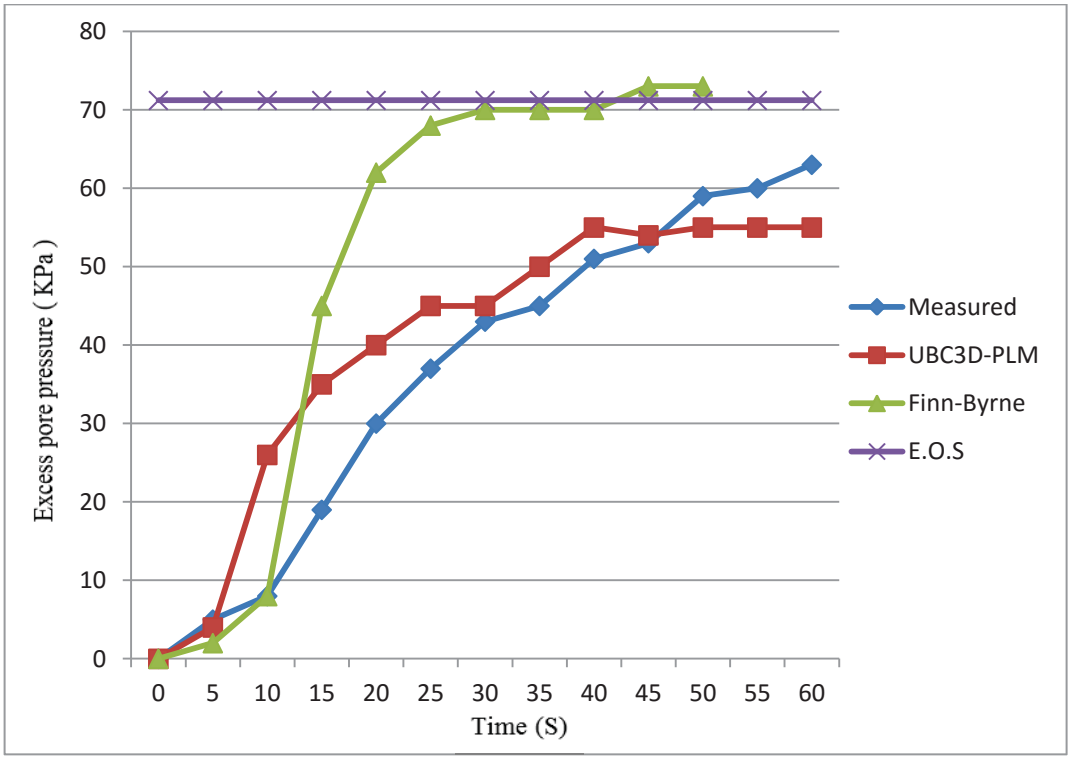

Figure 4.3 results of Excess pre pressure in P3.

Finn formulation had same reaction in 10 seconds after earthquake. After this period, EPP raise very fast to 68 kPa on 25 second. EPP had slow rising until 73 kPa in 50 second. Finn formulation could build EPP in P3 until EOS quantity.

Plaxis has same reaction with measured trend results until 54 kPa in 45 second. But after that the trend stable and remain constant. So UBC3D-PLM could not build EPP until EOS in P3.

2.4. Diagrams of Piezometer P_5

In 10 seconds of Superstition earthquake, EPP in P5 has remain constant same as P1 and P2. After this moment, EPP raised uniformly until 50 kPa. The line crossed with EOS line in 27 second.

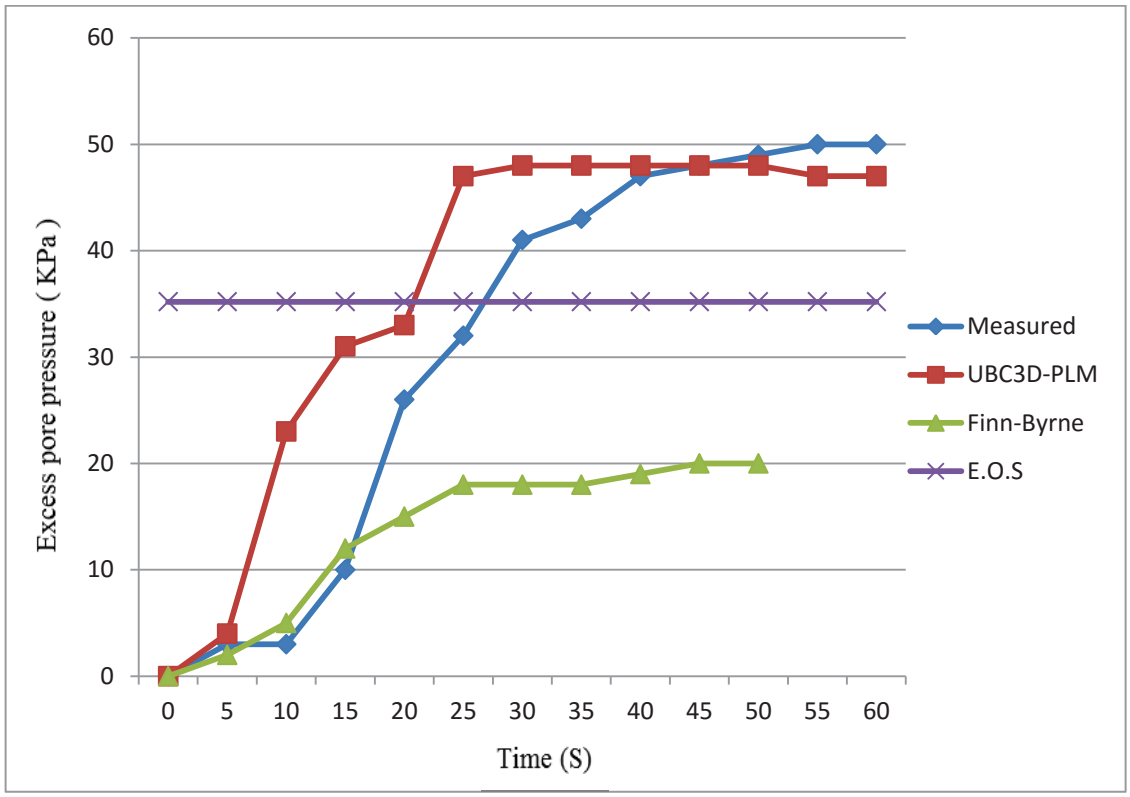

Figure 4.4 results of Excess pre pressure in P5.

Based on figure 4.4 the result of Finn-Byrne is not interesting. The level of EPP was too low. After 50 seconds, the EPP reached to 20 KPa. So there should not be any conflict between EPP from FLAC and EOS in P5.

PLAXIS had good result for this piezometer. After 22 second, EPP crossed with EOS line, and after 25 second in 47 KPa remained approximately constant.

3. Comparison between the prediction of Finn-Byrne, UBC3d-PLM and NFLP

The modelling of every phenomenon has special conditions. This condition and its usage depend to user and tools. Every user can use different methods. But the main goal of them is the same: Better simulation of reality. Based on this goal, in this research it was tried to make better liquefaction simulating with 2 available patterns and one new algorithm.

In Piezometer 1:

- Flac software by using Finn-Byrne formulation was almost able to predict liquefaction.
- Plaxis software by using UBC3d-PLM model could not predict liquefaction.
- NFLP model has predicted the liquefaction in this piezometer with 92% probability.

In Piezometer 2:

- Both of Finn-Byrne and UBC3D-PLM models could predict liquefaction happening in this piezometer.
- 80% was the probability of liquefaction occurrence, which NFLP has predicted for P2.

In Piezometer P3:

- The Flac software, by using the Finn-Byrne formulation, has clearly predicted the liquefaction in this part.

- The Plaxis software, by using the UBC3D-PLM model, has good overlapping with measured EPP.

- The "Neuro-Fuzzy-Liquefaction-Prediction" model has estimated the occurrence of liquefaction in this piezometer equivalent 100%.

In piezometer P5:

- Only in this piezometer FLAC software with Finn-Byrne model was not able to estimate liquefaction.
- The Plaxis has reasonable overlapping with measured EPP in this piezometer, and it has predicted liquefaction happening in this piezometer.
- The NFLP model could predict, the liquefaction happening for this piezometer with 92% probability. Table 4.1 shows the summary of this ability.

Table 4.1 ability of liquefaction occurrence prediction

	Finn-Byrne	**UBC3D-PLM**	**NLFP**
P1	Yes	No	97%
P2	Yes	Yes	80%
P3	Yes	Yes	100%
P5	No	Yes	92%

4. Conclusion

In this research the abilities of Finn-Byrne model and UBC3D-PLM model were considered. In order to this goal advantages and disadvantages of FLAC and PLAXIS software were compared too. After introduction of NFLP model in this thesis, its level of confidence for liquefaction prediction was examined.

This thesis shows some hidden aspects of soil liquefaction in Wildlife area after Superstition earthquake (1987). Comparing the results of numerical modelling of pore water pressure and observation of pore water pressure in Wildlife area lead to some differences which can depend on consolidation processes and special soil behaviour in this area.

In this research the generation of excess pore water pressure on wildlife site was considered by using Finn-Byrne- and UBC3D-PLM model. The calculation of excess pore water pressure shows that these constitutive models can reproduce the main mechanism of liquefaction. In spite of the first relax period in Finn-Byrne model the pore water pressure generation is not smooth, but in UBC3D-PLM modelling pore water-pressure generation is gradual rising. The sharp generation problem in Finn-Byrne model was improved in UBC3D-PLM model by using two yields surface in hardening process.

The generation of excess pore water pressure in Finn-Byrne model depends on cyclic irrecoverable volume increment. So this model cannot work in static or monotonic loading. However the UBC3D-PLM model has modeling ability of excess pore water pressure in monotonic and cyclic conditions.

The Finn-Byrne has a simple formulation. The model was introduced based on irrecoverable volume increment. The software connects this increment and pore water pressure based on Biot - Skempton theory. On the other hand the UBC3D-PLM has a lot of parameters, which need more field and laboratory testing. The definition of controlling parameters in UBC3D-PLM is based on curve fitting of cyclic direct shear test. This kind of data does not exist in a lot of cases. The

correlation and calibration of UBC3D-PLM parameters are useful, but not comprehensive. Therefore the result trends of this model are extremely dependent on model parameters.

The generated results of pore-water pressure in Wildlife area with Finn-Byrne- and UBC3D-PLM model are resembled each other. Nevertheless, some calculation results with UBC3D-PLM model have better overlapping with measured data. Furthermore UBC3D-PLM model by using flow rules can predict post liquefaction condition, while Finn-Byrne model is disabled to predict this situation after shaking. That means generation of pore water pressure will stop exactly after shaking.

The new pattern for prediction of soil liquefaction is designed based on a mixture of Fuzzy logic and neural network. "Neuro- Fuzzy- Liquefaction- prediction" (NFLP) pattern has reliable results in this area. This new pattern could predict liquefaction happening in four Piezometers at wildlife site. "NFLP" is designed based on eight input parameters. The results of this pattern by using these input parameters show a reasonable effect on liquefaction accuracy. The ability of this pattern to predict liquefaction occurrence makes this pattern as a proper tool for pre-feasibility or feasibility studies. In addition the fast and simple application of NFLP introduces this pattern very helpful for mapping and next study planning.

5. Recommendations for Future

The following future studies are recommended:

In this research, by apply the FLAC and PLAXIS software the liquefaction of Wildlife area were considerate. By attention to reaction of soils and layers, study on microscopic behavior of soil is inevitable. So modelling of this area by using the Particle Flow Code (PFC) is recommended.

In this research, the new version of UBC3D-PLM calibration was applied. Consideration of the results, show the procedure of pre-water pressure working truly, but the results is not approved. For this reason, more study and testing to prepare better calibration for UBC3D-PLM parameters is recommended.

In Finn-Byrne the pore-water pressure update occurs when a half-cycle is completed. The result of this persuader is rapid changing in pore water quantity and steep curves. To solve this defect, modification of the code for this model in FLAC is suggested.

Data mining and learning algorithms have direct relation by amount and accuracy of data. NFLP model was based on specified number of data. Validation of this pattern such as other scientific research is essential.

NFLP has specific methods for fuzzification, learning algorithm and defuzzification. It is possible, changing of this methods lead to better estimates and results.

References:

Aboim, C.A., Roth, W.H., Bounding surface plasticity applied to cyclic loading of sand [Conference] // international symposiom on Numerical Models in Geomechanics. - Zurich : [s.n.], 1982. - pp. 65-72.

Andrus, R.D., Stokoe, K.H., Lquefaction resistance of soils from shear-wave velocity [Journal] // Journal of geotechnical and geoenvironmental engineering, ASCE. - 2000. - 11 : Vol. 126. - pp. 1015-1025.

Bardet, J.P., A bounding surface model for sands [Journal] // Journal of engineering mechanics, ASCE. - 1986a. - 11 : Vol. 112. - pp. 1198-1217.

Bardet, J.P., Application of plasticity theory to sand behavior: A new sand model [Report]. - Pasadena : california university(Doctor thesis), 1983. - p.93.

Bardet, J.P., Lode dependences of isotropic pressure sensitive elastoplastic materials [Journal] // Journal of applied mechanics. - 1990a. - pp.746-760.

Bardet, J.P., Modeling of sand behavior with bounding surface plasticity [Conference] // 2nd international conference on Numerical Models in Geomechanics. - Ghent : [s.n.], 1986b. - pp. 79-90.

Bardet, J.P., Prediction of deformation of Hostun and Reid Bedford sands with a simple bounding surface plasticity model [Conference] // international Workshop on Constitutive Equations for Granular Non-Cohesive Soils. - Ohio : [s.n.], 1987. - pp. 31-148.

Bartlee, S.F., Youd, T.L., Emperical prediction of lateral spread displacement [Report]. - [s.l.] : NCEER, 1992a. - pp. 351-365.

Bartlee, S.F., Youd, T.L., Emperical analysis of jorizontal ground displacement generated by liquefaction-induced lateral spreads [Report]. - New York : NCEER, 1992b. - p. 114.

Bartlee, S.F., Youd, T.L., Emperical prediction of liquefaction-induced lateral spread [Journal] // Journal of geotechnics engineering, ASCE. - 1995. - 4 : Vol. 121. - pp. 316-329.

Bauer, E., Calibration of comprehensive hypoplastic model for granular materials [Journal] // Soil foundation journal. - 1996. - Vol. 36. - pp. 13-26.

Bauer, E., Wu, W., Hypoplastic constitutive model for cohesive powders [Journal] // Journal of powder technology. - 1995. - Vol. 85. - pp. 1-9.

Baykasoglu, A., Gullu, A., Canakci, H., Ozbakir, L.L., Prediction of compressive and tensile strength of limestone via genetic programming [Journal] // journal of Expert Systems with Applications. - 2008. - Vol. 35. - pp. 111-123.

Baziar, M.H., Dobry, R., Elgamal, M., Engineering evaluation of permanent ground deformation due to seismically induced liquefaction [Report]. - Buffali : NCEER, 1992. - p. 148.

Beaty, M., Summary of UBCSand constitutive model: Versions 904a and 904aR [Report]. - [s.l.] : Beaty Engineering LLC, 2009. - p. 79.

Beaty, M.H., Byrne, P.M., Ubcsand constitutive model version 904ar [Report]. - [s.l.] : Itasca UDM Web Site,, 2011. - p. 69.

Beca, C., Liquefaction Study, Waimakariri District [Report]. - [s.l.] : Beca, Carter, Hollings, Ferner, Christchurch., 2000.

Beca, C., Christchurch Liquefaction Study Update 2012 [Report]. - [s.l.] : Beca Infrastructure Ltd, 2012.

Bennett, M.J., McLaughlin, P.V., Sarmient, J.S., Youd, T.L., Geological investigation of liquefaction sites, Imoerial valley, California [Report]. - California : US Geological Survey, 1984. - p.109.

Boulanger, R.W., High overburden stress effects in liquefaction analyses [Journal] // Journal of Geotechnical and Geoenvironmental engineering, ASCE. - 2003. - 12 : Vol. 129. - pp. 1071-1082.

Brinkgreve, R.B.J., Selection of soil models and parameters for geotechnical engineering application [Report]. - Virginia : American society of civil engineers, 2005. - pp. 69-98.

Brinkgreve, R.B.J., Selection of soil models and parameters for geotechnical engineering application [Journal] // Geotechnical Special Publication, ASCE. - 2005. - Vol. 128. - pp. 69-98.

Brown, L.J., Weeber, J.H., Geology of the Christchurch urban area. 1:25,000 geological map and booklet [Report]. - Wellington : Institute of Geological and Nuclear Sciences,, 1992. - p. 104.

Burland, J.B., The teaching of soil mechanics- a personal view [Conference] // ECSMFE. - Dublin : [s.n.], 1987. - Vol. 3. - pp. 1427-1447.

Byrne, P.M., A cyclic Shear-Volume Coupling and Pore Pressure Model for Sand Proceeding [Conference] // Second International Conference on Recent Advances in Geotechnical Earthquake Engineering and Soil Dynamics. - Missouri : [s.n.], 1991. - pp. 340-358.

Byrne, P.M., Cheung, H., Yan, L., Soil parameters for deformation analysis of sand masses [Journal] // Canadian Geotechnical Journal. - 1987. - 3 : Vol. 24. - pp. 366-376.

Castro, G., Liquefaction of sands [Journal] // Harvard Soil Mechanics Series. - [s.l.] : Pierce hall, 1969. - Vol. 81. - p. 120.

Castro, G., Poulos, S.J., France, J.W., Enos, J.L., Liquefaction induced by cyclic loading [Report]. - Washington D.C : Geotechnical engineers inc, 1982. - p. 80.

Castro, G., Poulos, S.J., Factors affecting liquefaction and cyclic mobility [Journal] // Journal of geotecnical engineering division. - 1977. - Vol. 103. - pp. 501-516.

Cetin, K.O., Seed, R.B., Nonlinear shear mass participation factor (rd) for cyclic shear stress ratio evaluation [Journal] // Journal of " Soil Dynamics and Earthquake Engineering. - 2004. - Vol. 24. - pp. 103-113.

Chen, X.M., Luo, X.C., Indeterminate gray prediction method of possibility of sand liquefaction during earthquake [Journal] // Journal of Guilin university of technology. - 1997. - 2 : Vol. 17. - pp. 106-109.

Chiou, B.S.J., Youngs, R.R., An NGA model for the average horizontal component of peak ground motion and response spectra [Journal] // Jornal of Earthquake Spectra. - 2008. - 1 : Vol. 24. - pp. 173-215.

Christchurch Engineering Lifelines Risks and Realities: A Multi-disciplinary Approach to the Vulnerability of Lifelines to Natural Hazards [Report]. - [s.l.] : Christchurch Engineering Lifelines Group, 1997. - p. 80.

Christian, J. T., Swiger, W.F., Statistics of liquefaction and SPT results [Journal] // Journal of Geotechnical Engineering Division, ASCE. - 1975. - 11 : Vol. 101. - pp. 1135-1150.

Clough, R.W., The finite element method in plane stress analysis [Conference] // 2nd Conference on Electronic Computation, ASCE. - Pittsburgh. : [s.n.], 1960. - pp. 756-771.

Courant, R., Variational methods for the solution of problems of equilibrium and vibrations [Journal] // Bulletin of American Mathematics Society. - 1943. - Vol. 49. - pp. 234-242.

Dafalias, Y.F., Bounding surface plasticity: I. Mathematical foundation and hypoplasticity [Journal] // Mechanical engineering journal, ASCE. - 1986. - 9 : Vol. 112. - pp. 966-987.

Dafalias, Y.F. Hermann, L.R., Bounding surface plasticity: II. Application to isotropic cohesive soils [Journal] // Mechanical engineering journal, ASCE. - 1985. - 12 : Vol. 112. - pp. 1263-1291.

Dafalias, Y.F., Popov, E., A model of nonlinearly hardening materials for complex loading [Journal] // Acta mechanics journal. - 1975. - 3 : Vol. 21. - pp. 173-192.

Daftari, A., Kudla, W., Prediction of soil liquefaction by using UBC3D-PLM model in PLAXIS [Conference] // ICCESE. - Barcelona : [s.n.], 2014. - pp. 1168-1173.

Daftaribesheli, A., Ataei, M., Sereshki, F., Assessment of rock slope stability using the fuzzy slope mass rating(FSMR) system [Journal] // Journal of applied soft computing. - 2011. - Vol. 11. - pp. 4465-4473.

Davis, R.O., Berrill, J.B., Liquefaction at the Imperial Valley Wildlife Site [Journal] // Bulletin of the New Zealand society for earthquake engineering. - 2001. - 2 : Vol. 34. - pp. 91-106.

Elder, D.M.G., McCahon, I. F., Yetton, M.D., The Earthquake Hazard in Christchurch: A Detailed Evaluation [Report]. - [s.l.] : Soils & Foundations Ltd, Christchurch, 1991. - p. 65.

ElZahaby, K.M., Rahman, M.S., Non-Statistical Uncertainties in Liquefaction Risk Assessment [Book Section] // Uncertanity in the geologic environment: from theory to practice / book auth. al C.D. Shackelford et. - 1996. - Vol. 2. - pp. 130-175.

Enghdal, E.R., Villasenor, A., Global seismicity: 1900-1999 [Book Section] // International Handbook of Earthquake and Engineering Seismology. - 2002. - Vol. 81A. – pp. 430-484.

Finn, W.D.L., Aspects of Constant Volume Cyclic Simple Shear [Journal] // Advanced in the Art of Testing Soil Under Cyclic Conditions. - New York : [s.n.], 1985. - pp. 74-98.

Finn, W.D.L., Pickering, D.J., Bransby, P.L., Sand Liquefaction in Triaxial and Simple Shear Tests [Journal] // Journal of the Soil Mechanics and Foundations. - 1971. - SM4 : Vol. 97. - pp. 639-659.

Flood, I., Kartman, N., Neural networks in civil engineering. I. Principles and understanding [Journal] // Journal of computer and civil engineering, ASCE. - 1994. - 2 : Vol. 4. - pp. 131-148.

Geotechnical seismic hazards [Report]. - [s.l.] : SCDOT Geotechnical disigh manual, 2010. - pp. 83.

Goh, A.T.C., Seismic liquefaction potential assessed by neural networks [Journal] // Journal of Geotechnical and Geoenvironmental Engineering, ASCE. - 1995. - 9 : Vol. 120. - pp. 1467-1480.

Grima, M.A., Bruines, P.A., Verhoef, P.N.W., Modeling tunnel boring machine performance by Neuro-Fuzzy methods [Journal] // Journal of tunelling and underground space technology. - 2000259-269. - Vol. 15. - pp. 349-362.

Groot, M.B., Bolton, M.B., Foray, P., ... , Physics of liquefaction phenomena around marine structures [Journal] // Journal of Water port coastal ocean engineering. - 2006. - 4 : Vol. 132. - pp. 227-243.

Gudehus, G., A comprehensive constitutive equation for granular materials [Journal] // journal of soils foundation. - 1996. - Vol. 36. - pp. 1-12.

Gu, W.H., Morgenstern, N.R., Robertson, P.K., Post earthquake deformation analysis of Wildlife site [Journal] // Journal of geotecnical engineering. - 1994. - 2 : Vol. 120. - pp. 274-289.

Hamada, M., Yasouda, S., Isoyama, R., Emoto, K., Study on liquefaction induced permanent ground displacements [Report]. - [s.l.] : Assiciation for the development of erthquake prediction in Japan, 1986. - p. 87.

Hardin, B.O., The nature of stress-strain behaviour of soils [Conference] // Earthquake Engineering and Soil Dynamics Proceedings of the ASCE Geotechnical Engineering Division Specialty Conference. - California : [s.n.], 1978. - Vol. 1. - pp. 3-90.

Hashiguchi, M., Constitutive equations of elastoplastic materials with elasticplastic transition [Journal] // journal of applied mechanics, ASME. - 1980. - Vol. 47. - pp. 266-272.

Hatanaka, M., Uchida, A., Suzuki, Y., Correlation between undrained cyclic shear strength and shear wave velocity for gravely soils [Journal] // Soils and foundation journal. - 1997. - 4 : Vol. 37. - pp. 85-92.

Holtzer, T.L., Youd, T.L., Hanks, T.C., Dynamic of liquefaction during the superstation hills earthquake of november 24,1987 [Journal] // Journal of science. - 1989. - Vol. 244. - pp. 56-59.

Hushmand, B., Sctt, R.F., Crouse, C.B., In-Place calibration of USGS transducers at Wildlife site, California, USA [Conference] // 10th world conference on earthquake engineering. - Rotterdam : [s.n.], 1992. - pp. 1263-1268.

Idriss, I.M., Boulanger, R.W., Semi-emperical procedures for evaluating liquefaction potential during earthquakes [Conference] // 11th Internatioanl conference on earthquake geotechnical engineering. - [s.l.] : Stallion press, 2004. - Vol. 1. - pp. 32-56.

Idriss, I.M., Boulanger, R.W., Soil liquefaction during earthquakes. Monograph MNO-12 [Report]. - Oakland : Earthquake Engineering Research Institute, 2008. - p. 261.

Idriss, I.M., Boulanger, R.W., SPT-Based liquefaction triggring procedures [Book]. - California : UNIVERSITY OF CALIFORNIA AT DAVIS, 2010. - p. 259.

Inc Itasca Consulting Group FLAC manual [Report]. - Minneapolis : Itasca Consulting Group Inc, 2008. - p. 1749.

Iwasaki, T., Tatsuoka, F., Tokida, K., Yasuda, S., A Practical method for assessing soil liquefaction potential based on case studies at various sites in Japan [Conference] // 2nd International conference on Microzonation. - 1978. - pp. 885-896.

Iwaski, T., Tokida, K., Tatsuoka, F., ... , Microzonation for soil liquefaction potential using simplified methods [Conference] // 2n International conference on microzonation. - Seattle : [s.n.], 1982. - pp. 1319-1330.

Jaksa, M.B., The influence of spatial variability on the geotechncial design properties of a stiff,overconsolidated clay [Report]. - Adelaide : University of Adelaid(PhD thesis), 1995. – p. 157.

Jang, J.S.R., ANFIS: Adaptive network-based fuzzy inference systems [Conference] // IEEE. - 1993. - Vol. 23. - pp. 665-685.

Jang, S.R., Sun, T., Mizutani, E., Neuro-Fuzzy and Soft Computing [Book]. - [s.l.] : Prentice Hall, 1997. - p. 390.

Jibson, R.W., Prediction earthquake-induced landslide displacements using Newmark's sliding block analysis [Journal] // Journal of transportation reasearch record. - 1993. - pp. 9-17.

Juang, C.H. Chen, C.J., Jiang, T., Andrus, R.D., Risk-based liquefaction potential evaluation using standard penetration tests [Journal] // Canadian Geotechnical journal. - 2000. - Vol. 37. - pp. 1195-1208.

Kayadelen, C., Estimation of effective stress parameter of unsaturated soils by using artificial neural networks [Journal] // International Journal for Numerical and. - 2008. - Vol. 32. - pp. 1087-1106.

Kayadelen, C., Gunaydin, O., Fener, M., Demir, A., Ozvan, A., Modeling of the angle of shearing resistance of soils using soft computing systems [Journal] // journal of Expert Systems with Applications. - 2009. - Vol. 36. - pp. 11814-11826.

Kayen, R.E., Mitchell. J.K., Seed, R.B., ..., Evaluation of SPT and CPT and shear wave-based methods for liquefaction potetial using Loma Prieta data [Conference] // 4th Japan-US workshop on earthquake resistant design of lifeline facilities and countermeasures for soil liquefaction. - [s.l.] : NCEER, 1992. - pp. 177-204.

Kokusho, T., In-Situ dynamic soil properties and their evaluation [Conference] // 8th Asian conference on soil mechancs and foundation engineering. - 1987. - p. 489- 501.

Kolymbas, D., An outline of hypoplasticity [Journal] // Archive of applied mechanics. - 1991. - Vol. 61. - pp. 143-151.

Konrad, J.M., Wang, T., Undrained Cyclic Loading of Anisotropically Consolidated Clayer Silts [Journal] // Journal of geotechnical engineering. - 1993. - 5 : Vol. 119. - pp. 929-947.

Kramer, S.L., Geotechnical earthquake engineering. Prentice Hall, Upper Saddle river. [Report]. - New Jersey : [s.n.], 1996. - p. 258.

Lee, C.C., Fuzzy logic in control systems: fuzzy logic controllers parts 1 and 2 [Conference] // IEEE. - 1990. - Vol. 20. - pp. 404-435.

Lee, K.L., Seed, H.B., "Cyclic Stress Conditions Causing Liquefaction Of sand [Journal] // Journal of the Soil Mechanics and Foundations Division, ASCE. - 1967a. - SM1 : Vol. 93. - pp. 47-70.

Lee, K.L., Seed, H.B., Dynamic Strength Of Anisotropically Consolidated sand [Journal] // Journal of the Soil Mechanics and Foundations Division, ASCE. - 1967b. - SM5 : Vol. 93. - pp. 169-190.

Lippmann, RP., An introduction to computing with neural nets [Conference] // IEEE. - 1987. - pp. 4-22.

McVay, M., Taesiri, Y., Cyclic behavior of pavement base materials [Journal] // Journal of geotechnics engineering division, ASCE. - 1985. - 1 : Vol. 111. - pp. 399-416.

Makra, A., Evaluation of the UBC3D-PLM constitutive model for prediction of earthquake induced liquefaction on embankment [Report]. - Delft : Delft university(M.Sc thesis), 2013. - p. 112.

Martin, G.R., Finn, W.D.L., Seed, H.B., Fundamentals of Liquefaction under cyclic loading [Journal] // Journal of the Geotechnical Engineering. - 1975. - GT5 : Vol. 101. - pp. 423-437.

Mohammad, R., Dobry, R., Undrained monotonic and cyclic triaxial strength of sand [Journal] // Journal of geotechnical engineering. - 1986. - 10 : Vol. 112. - pp. 941-958.

Mohanraj, M., Jayaraj, S., Muraleedharan, C., Applications of artificial neural networks for refrigeration, air-conditioning and heat pump systems, A review [Journal] // Journal of Renewable and Sustainable Energy Reviews. - 2012. - Vol. 16. - pp. 1340-1358.

Moss, R.E.S., CPT-based probabilistic assessment of seismic soils liquefaction initiation [Journal]. - Berkeley, California : Ph.D. Dissertation, University of California, 2003. - p. 528.

Moss, R.E.S., Cetin, K.O., Seed, R.B., Seismic liquefaction triggering correlations within a bayesian framework [Conference] // ICASP. - 2003. –pp. 1019-1034.

Naaz, S., Alam, A., Biswas, R., Effect of different defuzzification methods in fuzzy based load blancing application [Journal] // International journal of computer science. - 2011. - 5 : Vol. 8. - pp. 261-267.

Negussey, D., Vaid, Y.P., A critical assessment of membrane penetration in the triaxial test [Journal] // Journal of ASTM Geotechnics. - 1984a. - Vol. 2. - pp. 70-76.

Negussey, D., Vaid, Y.P., Relative density of air and water pluviated sand [Journal] // Journal of soils and foundation. - 1984b. - 2 : Vol. 4. - pp. 101-105.

Peacock, W.H., Seed, H.B., "Sand Liquefaction Under Cyclic Loading Simple Shear Conditions [Journal] // Journal of the Soil Mechanics and Foundations. - 1968. - SM3 : Vol. 94. - pp. 689-708.

Pickering, D.J., Drained liquefaction testing in simple shear [Journal] // Journal of the soil mechanics and foundations. - 1973. - SM12 : Vol. 99. - pp. 1179-1184.

Ptalas, A., Galvi, V., PLAXIS Liquefaction Model: UBC3D-PLM [Report]. - Delft : Delft university, 2013. - p. 93.

Pyke, R., Nonlinear soil models for irregular cyclic loadings [Journal] // Journal of Geotechnical Engineering. - 1979. - 2 : Vol. 87. - pp. 715-726.

Rahman, M.S., Wang, J., Fuzzy neural network models for liquefaction prediction [Journal] // journal of Soil Dynamics and Earthquake Engineering. - 2002. - pp. 243- 256.

Rauch, A.F., EPOLLS: An empirical method for predicting surface displacement due to liquefaction – induced lateral spreading in earthquakes [Report]. - [s.l.] : Ph.D. dissertation, Virginia Polytechnic Institution, 1997. - p. 247.

Robertson, P.K., Wride, C.E., Evaluating cyclic liquefaction potential using the cone penetration test [Journal] // Canadian geotechnical journal. - 1998. - Vol. 35. - pp. 442-459.

Rose, T.J., Fuzzy Logic with Engineering Applications [Book]. - New York : McGraw Hill Co, 1995. - p.536.

Rowe, P.W., The stress-dilatancy relation for static equilibrium of an [Conference] // Proceedings of the Royal Society of London. - [s.l.] : Mathematical and Physical Sciences, 1962. - pp. 500-557.

Rumelhart,D.E, McClelland, J.L., Parallel distributed processing explorations in the micro-structure of cognition [Journal] // Massachusetts Institute of Technology Press. - 1986. - 2 : Vol. 1. - pp. 67-80.

Schnitman, L., Yoneyama, T., A method for learning membership functions in Mamdani fuzzy models [Conference] // 9nd Brasilian Congress on Automation. - 2000. - pp. 840-851.

Schweiger, H.F., The Role of Advanced Constitutive Models in geotechnical engineering [Journal] // Journal of Geomechanics and Tunneling. - 2008. - 5 : Vol. 1. - pp. 336-344.

Seed, H.B., Earthquake-resistant design of earth dams [Conference] // Seismic of earth dams and caverns, ACSE. - New york : [s.n.], 1983. - pp. 41-64.

Seed, H.B., Idriss, I.M., Simplified procedure for evaluating soil liquefaction potential [Journal]. - [s.l.] : Journal of soil mechanics and foundation division, ASCE, 1971. - SM9 : Vol. 97. - pp. 1249-1273.

Seed, H.B., Lee, K.L., Liquefaction Of Saturated Sands During Cyclic [Journal] // Journal of the Soil Mechanics and Foundations Division, ASCE. - 1966. - SM6 : Vol. 92. - pp. 105-134.

Seed, H.B., Peacock, W.H., Test procedures for measuring soil liquefaction [Journal] // Journal of Geotechnical engineering division, ASCE. - 1971. - 8 : Vol. 97. - pp. 1099-1119.

Seed, H.B., Peacock, W.H., Test Procedures for Measuring Soil Liquefaction Characteristics [Journal] // Journal of Geotechnical Engineering. - 1971. - SM8 : Vol. 97. - pp. 1099-1119.

Seed, H.B., Tokimatsu, K., Harder, L.F., Chung, R., Influence of SPT procedures in soil liquefaction resistance evaluation [Journal] // Journal of geotechnical engineering, ASCE. - 1985. - 12 : Vol. 111. - pp. 1425-1445.

Seed, H.B., Tokimatsu, K., Harder, L.F., Chung, R., The influence of SPT procedures in soil liquefaction resistance evaluations [Report]. - Berkley : University of California, 1984. - p. 50.

Sereshki, F., Ataei, M., Daftaribesheli, A., A Mamadani inference system for rock mass rating(RMR) and it's use in rock mass parameters estimation [Journal] // journal of Archive mining science. - 2010. - 4 : Vol. 55. - pp. 947-960.

Shahin, M.A., Maier, H.R., Jaksa, M.B., Settlement prediction of shallow foundations on granular soils using B-spline neurofuzzy models [Journal] // Journal of Computers and Geotechnics. - 2003. - Vol. 30. - pp. 637-647.

Shibata, T., Teparaksa, W., Evaluation of liquefaction potential of soils using cone penetration tests [Journal] // Soil and Foundation Journal. - 1988. - 2 : Vol. 28. - pp. 49-60.

Sladen, J.A., D'Hollander, R.D., Krahn, J., The liquefaction of sand, a collapse surface approach [Journal] // Canadian Geotechnics Journal. - 1985. - Vol. 22. - pp. 564-578.

Soroush, A., Koohi, S., Numerical analysis of liquefaction induced lateral spreading [Conference] // 13th World Conference on Earthquake Engineering. - Vancouver : [s.n.], 2004. - p. 1275-1283.

Tsegay, A.B., PLAXIS liquefaction model [Report]. - Delft : Delft university, 2010. - p. 45.

Tokimatsu, K., Yamazaki, T. Yoshimi, Y., Soil liquefaction evaluation by elastic shear moduli [Journal] // Soil foundation Journal. - 1986. - 1 : Vol. 26. - pp. 25-35.

Towhata, L., Kogai, Y., Amimoto, K., Putra, H.G., Theory and model tests on mitigation measures against lateral flow of liquefied ground [Conference] // NCEER. - 1996. - pp. 403-417.

Tsurumaki, K.N., Yuichi, K., Babasaki, R., Study on the Simplified procedure for evaluating the undraind cyclic strength for gravelly soils [Conference] // 17th International Conference on Structural Mechanics in Reactor Technology. - Prague : [s.n.], 2003. - p. 658-674.

Tutmez, A., Tercan, A.E., Spatial estimation of some mechanical properties of rocks by fuzzy modelling [Journal] // Journal of Computers and Geotechnics. - 2007. - Vol. 34. - pp. 10-18.

Vaid, Y.P. Chern, J.C., Effects of static shear on resistance to liquefaction [Journal] // Soils and Foundation journal. - 1983. - 1 : Vol. 23. - pp. 47-60.

Vasquez-Herrera, A., Dobry, R., Re-evaluation of the Lower San Fernando Dam: Report 3 [Journal] // US. Army Corps of Engineers Contract report. - 1989. - p. 90.

Wang, W., Liquefaction in california desert, An unexpected geological hazad [Report]. - [s.l.] : Department of conservation, 1996. - p.106.

Wolffersdorff, P.A., A hypoplastic relation for granular materials with a predifined limit state surface [Journal] // Journal of mechanical cohesesive-frictional materials. - 1996. - Vol. 1. - pp. 251-271.

Wu, W. Bauer, E., A simple hypoplastic constitutive model for sand [Journal] // International journal of numerical analysis methods in geomechanics. - 1994. - Vol. 18. - pp. 833-862.

Wu, W., Bauer, W., Kolymbas, D., Hypoplastic constitutive model with critical state for granular materials [Journal] // Journal of mechanics and materials. - 1996. - Vol. 23. - pp. 45-69.

www.bindichen.co.uk/post/AI/tsukamoto-fuzzy-models.html.

www.ce.washington.edu/liquefaction.

www.codeproject.com/Articles/477689/JavaScript-Machine-Learning-and-Neural-Networks-wi.

www.demlateralearthpressure.weebly.com/week-1.html.

www.eeg.geoscienceworld.org.

www.gsl.erdc.usace.army.mil/gl-history/Chap11.htm.

www.homepages.rpi.edu/~dobryr/sketch.html.

www.neuralnetworksanddeeplearning.com/chap6.html.

www.onlinemanuals.txdot.gov/txdotmanuals/pdm/information_needed_for_pavement_design.htm.

www.quanser.blogspot.de/2013/02/how-quanser-shake-tables-are-shaking-up.html.

www.ucl-sites.uclouvain.be/gce/infos/jfvdb3_res-en.html

Yang, B.L., Dafalias, Y.F., Hermann, L. R., A bounding surface plasticity model for concrete [Journal] // Mechanical engineering journal, ASCE. - 1985. - 3 : Vol. 111. - pp. 359-380.

Yegian, M.K., Marciano, E.A., Ghahraman, V.G., Earthquake-induced permannent deformations [Journal] // Journal of geotechnics engineering, ASCE. - 1991. - 1 : Vol. 117. - pp. 35-50.

Yetton, M., McCahon, I., Selwyn District Engineering Lifelines Project: Earthquake Hazard Assessment [Report]. - Christchurch : Geotech Consulting Ltd, 2006. - p.140.

Youd, T.L., Gilstrap, S.D., Liquefaction and deformation of silty and finegrained soils [Conference] // 2nd international conference on earthquake geotechnical engineering. - 1999. - Vol. 3. - pp. 1013-1020.

Youd, T.L., Gilstrap, S.D., Liquefaction and Deformation of Silty and Fine-Grained Soils [Conference] // 2nd International Conference in Earthquake Geotechnical Engineering. - 1999. - Vol. 3. - pp. 1013-1020.

Youd, T.L., Holzer, T.L., Piezometer performance at Wildlife liquefaction site, California [Journal] // Journal of Geotechnical engineering. - 1994. - Vol. 120. - pp. 975-995.

Youd, T.L., Idriss, I.M., Evaluation of liquefaction resistanc of soils [Conference] // NCEER Workshop. - New York : State university of New York, 1997. - p. 167-180.

Youd, T.L., Idriss, I.M., Liquefaction resistance of soils: Summary report from the 1996 NCEER and 1998 NCEER/NSF workshops on evaluation of liquefaction resistance of soils [Journal] // Journal of geotechnical and geoenvironmental engineering. - 2001. - pp. 297-313.

Youd, T.L., Idriss, I.M., Andrus, R.D.,… Liquefaction resistance of soils: summary report from the 1996 NCEER and 1998 NCEER/NSF [Journal] // Journal of Geotechnical and Geoenvironmental engineering, ASCE. - 2001. - 10 : Vol. 127. - pp. 817-833.

Youd, T.L., Perkuns, D.M., Mapping of liquefaction severity index [Journal] // Journal of geotechnics engineering, ASCE. - 1987. - 11 : Vol. 113. - pp. 1374-1392.

Yotton, M., McCahon, I., Earthquake Hazard Assessment for Waimakariri District [Report]. - Christchurch : Geotech Consulting Ltd, 2009. - p. 193.

Zadeh, L., Fuzzy sets [Journal] // Information und control system. - 1965. - Vol. 8. - pp. 338-353.